D-MEM
PhD-UNIMI

Doctorate program
Milan
EXPERIMENTAL
MEDICINE

UNIVERSITÀ DEGLI STUDI DI MILANO

PhD Course in Experimental Medicine

CYCLE XXXVIII
PhD thesis

IGF2R: a new player in the insulin like growth factor 2 (IGF2) pathway sustaining adrenocortical tumours cell growth

Candidate: **Dr. Emma Nozza**
Matr.ID R13844
ORCID ID 0000-0002-1573-036X

Tutor: Prof. Erika Maria Peverelli

Supervisor: Dr. Rosa Catalano

Director: Prof. Nicoletta Landsberger

Academic Year 2024-2025

TABLE OF CONTENTS

ABSTRACT

Adrenocortical tumours (ACT) are a highly heterogeneous class of endocrine cancers, ranging from the common adrenocortical adenoma (ACA) to the rare and aggressive adrenocortical carcinoma (ACC). ACT management is currently relying on the surgical approach; however, the identification of novel therapeutic strategies constitutes an urgent need especially in the management of advanced and metastatic ACC.

During the years, several approaches directed at different overexpressed target have constituted the core of clinical and preclinical studies. Of particular interest, the insulin-like growth factor 2 (IGF2), overexpressed in the majority of ACC, is a growth factor responsible for the autocrine proliferative loop that sustains ACC growth. In the IGF2 system, two well addressed tyrosine-kinase receptors, IGF1R and IR, were found responsible for the IGF2 pro-mitotic signal transduction. Unfortunately, even if promising in *in vitro* settings, the inhibition of these receptors was not successful in prolonging the overall survival of ACC patients in clinical trial.

Furthermore, in the IGF2 system is involved another specific IGF2 receptor, IGF2R, which was historically addressed as anti-oncogenic, due to its role in promoting IGF2 lysosomal degradation. However, recent studies in other cancers determined a possible tumorigenic action of IGF2R. Thus, the main aim of this PhD project was to uncover the presence, role, and mechanism of action of the IGF2R in the ACT context.

The project was conducted *in vitro*, using 4 different ACC cell lines, derived from either primary or metastatic tumours, to better reflect ACC heterogeneity. Moreover, data were corroborated using several ACA, uncertain malignant potential tumours (UMP), and ACC primary cultures.

Firstly, IGF2R was found overexpressed in ACT compared to normal adrenal tissue (NA), and we confirmed IGF2 overexpression in ACC versus ACA. Then we proceeded to assess whether the role of IGF2R was pro or anti-oncogenic, both on stabilized models and primary cultured cells. Knockdown and inhibition of IGF2R at its IGF2-binding site confirmed a reduction of proliferative activity and coherently, IGF2R transient transfection promoted both proliferation and viability increase.

This evidence of a pro-tumorigenic role for IGF2R was a complete novelty in ACT context, thus it needed a supporting mechanism of action. Indeed, we investigated the IGF2-IGF2R binding as well as the possible downstream effectors of IGF2R.

The evaluation of the IGF2 impact on IGF2R mitogenic action was conducted in the only cell line, H295R, where IGF2 extracellular levels were affected by IGF2R presence. Indeed, we administer retinoic acid (RA), another IGF2R ligand, known to facilitate IGF2 internalization and stimulate apoptosis. Surprisingly, RA treatment increased IGF2 extracellular levels, and even though this accumulation was potentially able to promote cellular proliferation via IGF1R and IR, we observed a decrease in cellular proliferation. This anti-mitotic effect was confirmed to be mediated by IGF2R and due to the increase of IGF binding proteins (IGFBP2 and 6) induced by RA, that determined the extracellular sequestering of IGF2. We also confirmed the pro-apoptotic effect of RA, even though it was not attributable only to IGF2R.

The downstream mechanism of IGF2R was object of study in other cellular models, mainly by the group of El Shewy, who identified two enzymes, the sphingosine kinases (SphKs), and their product S1P, as responsible for the activation of PI-3K/Akt and MAPK pathways. Indeed, we confirmed the overexpression of SphK, mainly the isoform SphK1, in ACT compared to NA. Moreover, this was the first project to correlate IGF2R with SphK in ACT, proving that in case of IGF2R knockdown or inhibition the activity of SphK is hampered.

The identification of these novel actors in the ACT pathogenesis opened the possibility to investigate SphKs as therapeutic targets. Indeed, we tested two different inhibitors, safingol and fingolimod. The two drugs were able to impair cell proliferation, viability, and cortisol secretion, both on ACC cell lines and primary cultures. Moreover, we compared their antitumoral activity with the current therapeutic strategy for advanced ACC, the EDP-M scheme, and the combination of safingol or fingolimod with EDP-M resulted additive in controlling cell viability.

Overall, in this PhD project a novel pro-oncogenic role of IGF2R in the ACT context was demonstrated. In particular, we proved its connection with IGF2 and most importantly with SphK, able to activate a downstream proliferative cascade sustaining tumorigenesis. Remarkably, we successfully tested two SphK inhibitors *in vitro*, laying the foundations of new preclinical pharmacological studies.

DISCLOSURE FOR RESEARCH INTEGRITY

I hereby declare that the research presented in this PhD thesis has been carried out in accordance with the principles of research integrity outlined by the European Code of Conduct for Research Integrity.

LIST OF ABBREVIATIONS

ACA	Adrenocortical adenoma
ACC	Adrenocortical carcinoma
Ach	Acetylcholine
ACTH	Adrenocorticotropic hormone
APA	Aldosterone-producing adenoma
BrdU	5-bromo-2′-deoxyuridine
CPA	Cortisol-producing adenoma
DHEA	Dehydroepiandrosterone
DHS	Dihydroxysphingosine
DMF	N'N'-dimethylformamide
DMS	N,N-Dimethylsphingosine
DMSO	Dimethyl sulfoxide
DTT	Dichlorodiphenyltrichloroethane
EDP-M	Etoposide, doxorubicin, cisplatin, mitotane
EGF	Epidermal growth factor
ELISA	Enzyme-linked immunosorbent assay
ENSAT	European Network for the Study of Adrenal Tumours
FAP	Familial adenomatous polyposis
FDG-PET	Positron emission tomography with 18F-2-fluoro-2-deoxy-D-glucose
FTY	Fingolimod
HRP	Horseradish peroxidase
IGFBP	Insulin-like growth factor binding protein
IGF1R	Insulin-like growth factor 1 receptor
IGF2	Insulin-like growth factor 2
IGF2R	Insulin-like growth factor 2 receptor
IR	Insulin receptor

IRS1 Insulin receptor substrate 1

LH/hCG Luteinizing hormone and chorionic gonadotropin

MEN1 Multiple endocrine neoplasia 1

MTT 3-(4,5-dimethylthiazol-2-yl)-2,5-diphenyltetrazolium bromide solution

M6P Mannose-6-phosphate

NA Normal adrenal gland

NFDM Non-fat dry milk

OS Overall survival

PACAP Pituitary adenylate cyclase-activating polypeptide

PCC Pheochromocytoma

PI-3K Phosphatidylinositol 3-kinase

RA Retinoic acid

RTK Tyrosine-kinase receptor

SAF Safingol

SF-1 Steroidogenic factor 1

siRNA small interfering RNA

SphK Sphingosine kinase

StAR Steroid acute regulatory protein

STR Short tandem repeats

S1P Sphingosine 1 phosphate

$S1P_{1-5}$ Sphingosine 1 phosphate receptor

TFGβ Transforming growth factor β

TMB Tetramethylbenzidine

TNM Tumour-Node-Metastasis score

UMP Uncertain malignant potential tumours

INTRODUCTION

1. Adrenal gland physiology overview

Adrenal or suprarenal glands are two distinct organs located above the medial side of the upper pole of each kidney and firmly attached to it. Adult adrenal glands have a peculiar shape: the right gland is pyramidal, while the left one, larger than the other, is elongated or lunate. Either healthy gland weighs around 4g and measures 2cm in width, 5cm in length, and 1cm in thickness and it presents as golden/yellow in colour due to the rich lipidic content of the cortical region (1).

Adrenal glands are extensively vascularized and innervated compared to their small volume. Main blood supply derives from the inferior phrenic arteria, the aorta, and the renal arteria, who branches in as many as 50 arterioles into each adrenal gland. For the outtake, blood converged into the corticomedullary junction is drained from the central adrenal vein directly into the inferior vena cava for the right gland, or indirectly via the renal vein for the left gland. Innervation of each gland is mainly deriving from the thoracic splanchnic nerve (1–3).

Adrenal glands are composed of three separate and well-differentiated regions: an outer layer of fibrotic capsule, often merged with the perinephric capsule; the cortex, accounting for 85% of the whole adrenal gland, which is the major source of steroid hormones, and the internal medulla, red/brown in colour and representing only 10% of the total glandular volume, which is responsible for the production of catecholamines. The defined organization within the organ reflects the substantial differences between the two main adrenal regions (3,4).

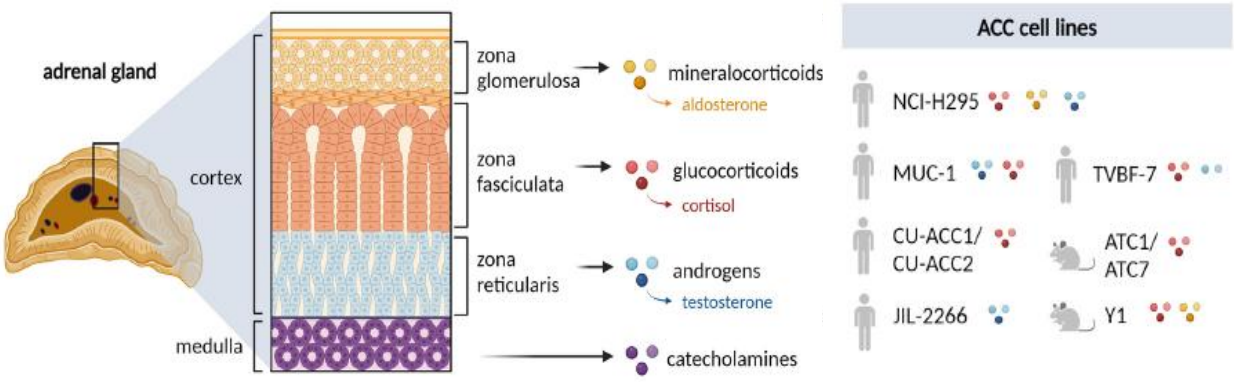

Figure 1. Adrenal cortex overview: zonation and hormonal production. Adapted from Luca et al., 2024

1.1. Adrenal medulla

Adrenal medullary region is the most internal one. It arises from neuroectodermic cells migrating from the neural crest and disposing along the developing foetal cortex, to finally differentiate into chromaffin cells (5). Its main function is the secretion of catecholamines, which are contained in large granules within the chromaffin cells.

Chromaffin cells are modified post-ganglionic sympathetic neurons, organized in clusters, that upon splanchnic nerve stimulation via the neurotransmitter acetylcholine (Ach), synthetize, store, and secrete a precise set of catecholamines: epinephrine for adrenergic cells and norepinephrine for noradrenergic cells, both directed to the adrenergic receptors throughout the body. The adrenal medulla is involved in the fight-or-flight response, in stress, and in metabolic pathways, thus its signalling influences numerous systems, such as respiratory, neuroinflammatory, and cardiovascular (6,7).

1.1.1. Hormone production in the adrenal medulla

The catecholamines secretion process arises mostly from Ach stimulation, able to trigger a calcium-dependent stimulus-secretion that induces the release of epinephrine and norepinephrine. In case of stress or hypoxia, pituitary adenylate cyclase-activating polypeptide (PACAP) and low oxygen pressure, respectively, contribute to Ach to stimulate catecholamines production (7,8). Catecholamine secretion into the bloodstream is a fast process, thus the vast majority of chromaffin cell cytosol is occupied by 12 to 20 thousand chromaffin vesicles specialized in the secretion of either epinephrine or norepinephrine.

Catecholamine synthesis starts from L-tyrosine, a non-essential amino acid, that is converted into L-DOPA from tyrosine hydroxylase into the cytoplasm of chromaffin cells. Subsequently L-DOPA is decarboxylated to dopamine by aromatic L-amino acid decarboxylase in the presence of vitamin B6. Upon translocation in chromaffin vesicles, dopamine can be transformed into norepinephrine by dopamine β-hydroxylase. Furthermore, only in epinephrine-secreting cells, norepinephrine returns to the cytoplasm via passive diffusion and is finally converted into epinephrine by the enzyme phenylethanolamine-N-methyl transferase (9).

1.2. Adrenal cortex

The cortical region, developing from the fifth week of gestation from the coelomic mesoderm of the urogenital ridge, is the predominant part of the adrenal gland. The development of the adrenal cortex from foetal to adult is one of the most relevant processes during human gestation: foetal adrenal gland is mainly composed of foetal zone cells, that are lost in favour

of definitive zone cells from the eighth week of gestation. SF-1-positive definitive zone cells originate underneath the capsule and during the first years of life organize into three functionally and histologically specialized zones, as displayed in Fig. 1, to compose the adult adrenal cortex (10,11).

The innermost is *zona reticularis*, organized in densely packed cells, is directly in touch with the adrenal medulla and is deputed to the synthesis and secretion of androgens, as dehydroepiandrosterone (DHEA) and testosterone, that are released into the bloodstream to be further transformed into active hormones in the gonads. This zone is the last to be completed, around 5 years of age, and androgens secretion pathways are activated upon stimulation of the pituitary adrenocorticotropic hormone (ACTH) and other endocrine and paracrine factors, as luteinizing hormone and chorionic gonadotropin (LH/hCG), whose receptors are present on the surface of zona reticularis cells (10,12).

The intermediate region is the *zona fasciculata*, with glucocorticoid secreting cells structured into fascicles. *Zona fasciculata* has the biggest adrenal cells, termed “clear cells” and accounts for the vast majority of adrenal cortex. Its secretory profile consists mainly of cortisol, thus it is rich in lipid vacuoles. Glucocorticoid secretion, dependent from the hypothalamic-pituitary-adrenal axis via ACTH stimulation, impacts a wide range of organs, mainly regulating glucose metabolism and suppressing inflammation and immunity (4,13).

The outermost is *zona glomerulosa*, composed of ovoidal mineralocorticoids producing cells. It accounts for 5 to 10% of the cortex and its main product is aldosterone, involved in the regulation of blood pressure and electrolyte balance. *Zona glomerulosa* hormone synthesis depends both on the renin-angiotensin system, potassium concentration, and ACTH (8,11,14).

1.2.1. Hormone production in the adrenal cortex

The whole synthesis of adrenal cortex steroids, defined steroidogenesis, initiates from cholesterol, which is transformed into free cholesterol through the hydroxylation of LDL cholesterol, taken up from LDL receptors on the adrenal cells (12). Steroidogenesis takes place in the inner mitochondrial membrane, where cholesterol is transported by the steroid acute regulatory protein (StAR) (15).

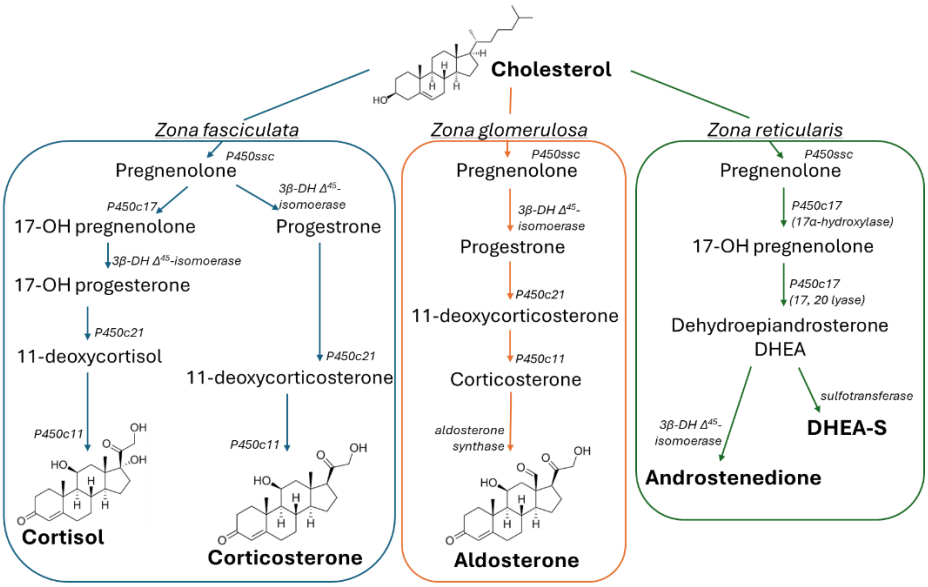

Figure 2. Schematic pathway of adrenal steroidogenesis. Adapted from Ortstater et al., 2012

Zona reticularis is deputed to the biosynthesis of androgens, as shown in Fig. 2, where cholesterol is transformed into pregnenolone by P450scc, a cytochrome acting to cleave cholesterol to obtain a 21-carbon molecule. Subsequently, the action of another cytochrome P450, P450c17, initially acts hydroxylating pregnenolone into 17-OH pregnenolone, then acts as a lyase and splits the bond between C17 and C20 to produce DHEA. Ultimately, DHEA can be converted into DHEA-S by a sulfotransferase; this subproduct is pivotal during embryonic development for the placental synthesis of oestrogens, while in adult life it is useful in controlling DHEA production to avoid androgen excess (11). Both DHEA and DHEA-S are normally released into the bloodstream to reach the gonads and can be transformed into active androgens (10). DHEA can also be converted into androstenedione, by the enzyme 3-β-hydroxysteroid dehydrogenase. Androstenedione is the last precursor of testosterone, whose synthesis is minimal in the adrenal cortex and takes place mainly in the gonads.

Glucocorticoid production is mainly localized in *zona fasciculata,* and their biosynthesis starts from the synthesis of pregnenolone. In this adrenal region, the production of cortisol is the most predominant pathway of steroidogenesis: after pregnenolone is converted to 17-OH pregnenolone as described earlier, this is transformed into 17-OH progesterone via 3-β-hydroxysteroid dehydrogenase, who becomes the substrate of the cytochrome P450c21 that generates 11-deoxycortisol (16). The ultimate conversion of 11-deoxycortisol into cortisol is done inside the mitochondria by P450c11β, an enzyme specifically belonging to *zona fasciculata*. The parallel pathway of corticosterone production arises in case

pregnenolone is converted into progesterone from 3-β-hydroxysteroid dehydrogenase, bypassing the action of P450c17. Progesterone is then converted to 11-deoxycorticosterone and ultimately to corticosterone (17,18).

In *zona glomerulosa*, steroidogenesis replicates the pathway of corticosterone production seen in *zona fasciculata*, with an additional hydroxylation of corticosterone generating aldosterone by the action of aldosterone synthase (17). This mitochondrial enzyme is closely similar to cytochrome P450c11β and is located only in *zona glomerulosa* cells (18).

2. Pathology of the adrenal glands

As aforementioned, adrenals are involved through hormone synthesis in the physiology of various systems in the human body, regulating homeostasis, immunity, and stress response (19,20).

2.1. Adrenal disorders

Alterations of normal adrenal cortex development can generate a variety of disorders: adrenal insufficiency, also referred to as Addison's disease, is commonly caused by an autoimmune destruction of adrenal cortex, in the means of atrophy, which hampers steroids production. Secondary adrenal insufficiency can happen in case of ACTH impairment that leads to a similar atrophy of the adrenal cortex, despite the androgen production is maintained (13).

On the contrary, Cushing's syndrome is an excess in glucocorticoids production that can be dependent on ACTH, in case of a pituitary or neuroendocrine tumour that increases ACTH production which ultimately overstimulates the adrenals. However, ACTH-independent Cushing's syndrome frequently happens in case of adrenocortical adenomas determining autonomous cortisol hypersecretion (CPA) (13). Cushing's syndrome manifestations include obesity, hypertension, and immunosuppression (20).

Hyperaldosteronism is characterized by alterations in the cardiovascular system, promoting hypertension and renal repercussions as fluid retention. This condition can be imputed to aldosterone-producing adenomas (APA), familiar hyperaldosteronism, or adrenal cortical hyperplasia (21).

Adrenal cortical hyperplasia is a genetic disorder caused by the inactivation of one or more steroidogenic enzymes. This condition causes the partial suppression of the enzymes due to inactivating mutations that induce a reduced steroid production that is rescued by the

increase of steroidogenic cells (13), resulting in a thicken and wider adrenal cortex. Depending on which enzyme is defective, adrenal cortical hyperplasia can be milder, as in case of non-classical variants, or severe, as in case of StAR detriment (21).

Among adrenal lesions, medullary or cortical tumours are common and well addressed pathologies, in either case they can bear a benign or, rarely, malignant connotation. They are often identified through imaging and defined as “incidentalomas” (22).

2.2. Medullary lesions: pheochromocytomas (PCC)

Pheochromocytomas, are the most common type of medullary tumours in adult patients, with an incidence of 0.005-0.1% in the general population, notably increased among hypertensive people (up to 0.6%) (22,23). PCC are defined as adrenal paragangliomas, since they have a similar origin, paragangliomas derive from neural crest progenitors, while pheochromocytomas originate from mature chromaffin cells. Chromaffin cells determine also their secretory profile, since pheochromocytomas are featured in 90% of cases by the hypersecretion of epinephrine or norepinephrine, depending on their cell of origin (23). As a result of catecholamines hypersecretion, PCC can be associated with tremors, anxiety/panic, palpitations, or nausea.

PCC are mostly benign tumours, only 10-15% of PCC retain a metastatic potential, but highly heterogeneous in their clinical presentation as well as in their genetic subset. Around 70% of PCC can be typecast into one of three molecular clusters, since both PCC and paragangliomas are tumours with a high hereditability rate. Each cluster retains peculiar features: cluster 1 tumours are characterized by high metastatic potential and are featured by mutations in genes related to the Krebs cycle (as succinate dehydrogenase) or in the hypoxia pathway (as HIF-2α), determining an additive subset of cluster 1A and 1B. Cluster 2 mutations are associated with tyrosine kinase signalling, with gain of function mutations of RET, NF1, or Met, promoting pro-mitotic and anti-apoptotic pathways; these tumours are rarely aggressive and often arise in a syndromic context, as MEN2A or NF1. Cluster 3 tumours, altered in the Wnt/βcatenin pathway, are the rarest subset of PCC (24).

Pheochromocytomas management is commonly through laparoscopic surgery, whenever applicable, associated with α-adrenoreceptor and β-adrenoreceptor antagonists (22). Otherwise, as in case of metastatic or inoperable tumours, systemic therapies as chemotherapy, inhibition of tyrosine kinase receptors, and radionuclide therapy can be useful in PCC treatment (23,24).

2.3. Adrenocortical tumours: adrenocortical adenomas (ACA), tumours of uncertain malignant potential (UMP), and carcinomas (ACC)

As stated earlier, adrenal incidentalomas are often encountered in the general population, with a prevalence of 1 to 10% depending on the age group. In most cases, these adrenal masses are benign adenomas (80-85%), but rarely (0.4-4%) also adrenocortical carcinomas are diagnosed as incidentalomas (25). ACA incidence is very common, >3% in adults over the age of 50 (26), while ACC are rare tumours, with an incidence of 0.5-2% worldwide. These carcinomas are mostly arising in females, and when divided by age present a bimodal distribution, with peaks around the first and the fourth-fifth life decades (22,27). Rarely, pathologists can encounter tumours that are difficult to diagnose, referred to as uncertain malignant potential tumours (UMP) (28).

2.3.1. Clinical presentation

Adrenocortical tumours are non-functional for the vast majority, indeed most of the adenomas are non-symptomatic. On the contrary, functional ACA, only 30% of the total, and ACC, up to 75%, can be characterized by an excess of cortisol secretion, often related to Cushing's Syndrome, or hyperandrogenism, or hyperaldosteronism. Notably, ACC often show a concurrency of cortisol and androgens hypersecretion (26). Symptoms can be nonspecific, as abdominal, flank or gastrointestinal pain, or associated to the tumoral secretory profile: hypercortisolism can cause muscle weakness, osteoporosis, diabetes mellitus, and hypertension; androgen excess induces virilization, hirsutism, and menstrual abnormalities; hyperaldosteronism causes hyperkalaemia and hypertension (27,29).

Typically, these masses are solid tumours of yellow to brown colour, with haemorrhagic and cystic changes and can present calcifications (29). Adenomas are smaller in size, homogeneous and can be distinguished between lipid-rich or lipid-poor tumours; while ACC have typically greater volumes (>6cm), often palpable, and are featured by heterogeneity, irregular margins, and necrotic areas (27,29,30).

2.3.2. Diagnosis

The diagnostic work-up of adrenocortical tumours is mainly aimed at identifying a potential malignancy and distinguishing between ACC and ACA. The European Network for the Study of Adrenal Tumours (ENSAT) has established a routinary assessment of hormones (i.e. cortisol, ACTH, DHEA-S, 17-OH progesterone, androstenedione, testosterone, and oestradiol, plus dexamethasone suppression test and free urinary cortisol) (30).

Tumour imaging is usually performed via computed tomography (CT), on the abdomen for the primary tumour, and on the chest to exclude the presence of metastases. The functional assessment with the positron emission tomography with 18F-2-fluoro-2-deoxy-D-glucose (FDG-PET) is particularly relevant for ACC (25,26).

Since pre-operatory biopsies are uncommon in the case of ACT, post-surgical histological analysis is fundamental to obtain a diagnosis. One of the first markers to be assessed is the steroidogenic factor 1 (SF-1), that implies the adrenocortical origin of the tumour (30). The microscopical analysis of the pathologist is commonly guided by the nine Weiss criteria that altogether define the Weiss scoring system (31). Specifically, presence of capsular, venous, or lymphatic invasion, necrosis, atypical mitosis, Furman nuclear grade of 3/4, mitotic count >5 over 50 high-power fields, diffuse architecture in >30%, and clear cells in <25%, are all the criteria, worth one point each, that summed represent the Weiss score. ACA have a Weiss score ranging from 0 to 2, while a Weiss score higher than 3 is indicative of ACC (32). The original Weiss system, established in 1984, has been modified and integrated to better reflect patients diagnosis: a modified Weiss was proposed in 1989, the Lin-Weiss-Bisceglia score is used for the oncocytic ACC variant, and the new Helsinki scoring system integrates the mitotic index and necrosis, already present in the Weiss score, to the value of Ki67 labelling index, which reflects the proliferation of cells. This score is useful to discriminate between ACA and ACC, and to predict the metastatic outcome (33). However, clinicians report a gray zone of diagnosis, tumours with a Weiss score of 2 or 3 can be considered UMP, but no in-depth study of this tumour category is available at the present (28,34).

2.3.3. ACC staging and prognosis

The most used ACC staging system is the ENSAT score, also called tumour-node-metastasis score (TNM), established from the European Network for the Study of Adrenal Tumours. This system, reported in Table 1, comprises several criteria to better reflect patient's clinical parameters: primary tumour (T) can vary from 1, size smaller than 5cm, to 2, larger than 5cm, to 3, ACC that infiltrate surrounding the periadrenal adipose tissue, and 4, tumours that infiltrate adjacent organs as kidney, liver, pancreas, vessels, and diaphragm. Regional lymph nodal invasion (N) is another crucial parameter of ENSAT staging, N0 means absence of metastasis in the lymph nodes of the adrenal region, while N1 highlights the presence of at least one metastasis. The last feature is the presence of distant metastases (M), which are absent (M0) in stage I to III, and present only in stage IV tumours (27,35,36).

ENSAT STAGE	FEATURES
I	T1 N0 M0
II	T2 N0 M0
III	T1-2 N1 M0
	T3-4 N0-1 M0
IV	T1-4 N0-1 M1

Table 1. ENSAT staging system. Adapted from Lughezzani et al., 2010

The main value of a staging system is its prognostic role: for the ENSAT classification, patients with ACC at stage I have a five-year survival rate of 66-82%, at stage II of 58-64%, at stage III of 24-50%, and at stage IV of 0-17% (30). Moreover, other factors are associated with survival rates, as cortisol secretion, often related to worsened prognosis, or young age, which is typically predictive of a better clinical outcome (22). Metastases are the most diffused cause of death in ACC patients, they are commonly located in the liver, lungs, lymph nodes, and bones (27).

Recently, some changes to the ENSAT classification, aimed at giving better prognostication, have been proposed: a modified ENSAT stage, that includes the number of metastases in lymph nodes and distant organs; the GRAS and S-GRAS scoring systems, with the first comprising histological grading, resection status, age at presentation, and symptoms, and the latter including also the ENSAT stage (37).

2.3.4. Treatment: surgery and therapy

The standard approach to the treatment of ACT is the complete surgical resection of the mass. However, the surgical approach can be challenging from different points of view: adenomas and ACC at early stages, mostly ENSAT I to III, can effectively benefit from surgery, while removal of the mass must be considered case by case for metastatic patients (30). There is no unanimous consensus in the approach of tumour resection, which can be managed via open or laparoscopic adrenalectomy, with the first being a more invasive procedure, but the latter bearing some disputable downsides, as the highest risk of recurrency. However, in the current clinical practice, for both adenomas and localized and small ACC, laparoscopic adrenalectomy is preferred (22,38). Moreover, in case of metastatic or recurrent disease, surgery can be considered as an option for reducing steroid excess and favouring the action of other therapies (26,27).

While in case of adenomas surgery is mostly the only necessary approach, ACC bear high recurrency rates, thus adjuvant therapies can help in the management of post-operatory disease control. Radiotherapy can be used as adjuvant therapy after the resection and it was proved to be effective in preventing local recurrences, even if multiple studies did not find differences with untreated patients in terms of overall survival (26,30,38). The most used drug in ACC adjuvant therapy is mitotane, a derivative of dichlorodiphenyltrichloroethane (DTT), which exerts adrenolytic and cytotoxic action, as demonstrated in preclinical models. The real action mechanism of mitotane is still not completely identified, but it is involved in endoplasmic reticulum stress, leading to the impairment of steroidogenic processes, as the action of P450scc. Mitotane use was widely accepted since the result of some retrospective studies, thus the ADIUVO clinical trial was set to establish the efficiency of mitotane adjuvant therapy. Unluckily, mitotane proved beneficial only in a limited number of patients and only in case of standard or high risk of recurrence, while the sole post-operatory surveillance was considered enough for low-recurrence risk ACC (39). Mitotane, altogether with chemotherapeutics (etoposide, doxorubicin, and cisplatin) can also be used in clinical practice as first- or second-line therapy of inoperable, advanced, and metastatic tumours, as in the FIRM-ACT study, where it was demonstrated that this combination, referred to as EDP-M scheme, was efficient in increasing the progression free survival of patients (40).

3. ACT molecular features

Although ACC and ACA share some similarities and it is not completely cleared out if adenomas can turn into ACC over time, their molecular background can be analysed to distinguish one from the other (26).

3.1. ACA genetics

Adenomas can arise sporadically or in the context of syndromes as in case of multiple endocrine neoplasia 1 (MEN1) or familial adenomatous polyposis (FAP) (41).

Mutations, either germinal or somatic, are strictly correlated to the endocrine function of the tumour: APA are mostly featured by mutations in *KCNJ5*, a gene coding for the protein GIRK4 whose impairment causes calcium-dependent increase of *CYP11B2* transcription and thus aldosterone production. Other diffused APA mutations target CACNA*1D*, *ATP1A1*, and *ATP2B3*, which are all genes encoding for proteins involved in the fine regulation of $Na^+/K^+/Ca^{2+}$ fluxes that are upstream of aldosterone biosynthesis (42).

Cortisol producing adenomas molecular pathogenesis is mainly to be addressed to mutations in *PRKACA* or *GNAS* which cause an increase in the catalytic subunit activity of PKA, compared to the regulatory subunit, and eventually implies an over-activation of PKA even in absence of ACTH stimulation. Activation of PKA induces CREB activation with a downstream increased transcription of its target genes, as CYP11B1, increasing cortisol production. A small subgroup of protein altering mutations in *TP53* and *RB1* was identified via whole exome sequencing as well, and this constitutes either a more malignant subset or an early-step in ACC tumorigenesis (42).

3.2. ACC genetics

ACC can bear germline or somatic mutations that may represent drivers in tumorigenesis or contribute to disease progression. Among germline mutations, alterations of *TP53* are highly common, as they characterize 50% of child ACC and arise in the context of Li Fraumeni Syndrome. Other syndromes can be associated to ACC onset, as Lynch syndrome, whose mutated genes are involved in mismatch repair pathways, or MEN1 (41).

Transcriptomic studies have characterized ACC genetic background, distinct from ACA, and highlighted two clusters of ACC according to their altered genes. In general, ACC are featured by overexpression of growth factors and receptor pathways, DNA replication, and cell cycle, while downregulated in steroidogenesis and metabolism/transport genes. ACC differential clusterization depending on transcriptomics was then related to patient prognosis, with the first group, defined C1A, which bore higher metastatic risk, had alterations in transcription and cell-cycle genes, while enrichment in metabolism, apoptosis, and cell differentiation genes was found typical of the low-risk group, C1B. More specifically, the combination of overexpressed *PINK1* and *BUB1B* could be associated with reduced overall survival (43,44).

Among ACC dysregulated pathways, the most relevant are the abnormal activation of Wnt/β-catenin, impairment of cell cycle regulators, overexpression of the insulin-like growth factor 2 (IGF2), and the loss of steroidogenic properties (45). The Wnt/β-catenin pathway is frequently altered in ACC though gain of function mutations in *CTNNB1* gene or loss of function mutations in the negative regulator *ZNRF3*.

3.3. The IGF system

The IGF system is a commonly upregulated ensemble in ACC, whose predominant role in tumour growth has made it a well-known and investigated target. This system is composed

of IGF1, insulin, and IGF2, their receptors: IGF1 receptor (IGF1R), IGF2 receptor (IGF2R), and the insulin receptor (IR), and their binding proteins (IGFBP1-6) (46,47).

IGF1 and IGF2 are highly similar single chain polypeptides deputed to mitogenic functions. IGF1 is physiologically produced in the liver under stimulation of the growth hormone and is necessary during both post-natal and adult life to maintain skeletal and muscular mass (48). Similarly, IGF2 is devoted to promoting cell growth and differentiation; this 7.5kDa protein is not only produced in the liver, but also in other tissues where its secretion can impact in autocrine or paracrine manner. Despite the major role of IGF2 during foetal adrenal development, both *IGF1* and *IGF2* are expressed in the adult adrenal gland. However, *IGF2*, not *IGF1*, alterations are involved in ACC tumorigenesis: *IGF2* locus alterations are commonly found in the context of Beckwith-Wiedmann syndrome where the duplication of the paternal allele implies an overexpression of *IGF2* and also in sporadic ACC. Interestingly, *IGF2* is rarely altered in ACA; indeed, several studies pointed out that IGF2 expression measured via immunohistochemistry could be a useful diagnostic marker for discriminating between ACA and ACC (47). Therefore, IGF2 has been considered a promising therapeutic target, however, IGF2 levels were not found to be correlated with ACC aggressiveness, thus it is not a useful prognostic marker (49).

3.3.1. IGF1R and IR

IGF2 pro-mitotic action was demonstrated *in vitro* on the immortalized cell line H295R, however its capability of initiating ACC tumorigenesis is still debated (49). To exert its proliferative action, IGF2 binds either one of two transmembrane tyrosine kinase receptors, IGF1R and IR, in their extracellular domain. Interestingly, IGF1R is able to bind not only IGF2 but also IGF1, while the IR, is subject to a peculiar alternative splicing process, generating the mitogenic isoform IR-A, able to bind IGF2, and the metabolic isoform IR-B, whose affinity is strong for insulin and very low for IGF2 (47). These receptors, composed of one α and one β subunits, are capable of binding their ligand after dimerization, and since they have a high degree of sequence homology, they can also combine into a hybrid receptor. Once the homo or heterodimers are bound to IGF2, the RTK-domain activates through autophosphorylation and recruits insulin receptor substrate 1 (IRS1) (48,50). Downstream activation of two different pathways can be initiated from IRS1: anti-apoptotic signal starts with the recruitment of phosphatidylinositol 3-kinase (PI-3K), which is activated by IRS1 and in turn activates Akt. Akt can function inactivating BAD and contemporarily activating MDM2 that ultimately inhibits apoptosis. On the other hand, IRS1 phosphorylation

can recruit other elements to the IGF1R-complex, as the adaptor protein Shc, that in turn recruits Grb2 and SOS, able to activate the MAPK pathway starting from Ras, which phosphorylates Raf-1, then MEK and ERK1/2, who finally transduce a pro-mitotic signal inside the nucleus (48).

3.3.1.1 Targeted drugs

Due to their proliferative and anti-apoptotic roles IGF1R and IR have been considered potential pharmacological targets. IGF1R was considered particularly promising in the ACC context, thus both a specific small molecule inhibitor, NVP-AEW541, and a monoclonal antibody, IMC-A12, have been developed. *In vitro,* on the reference cell line H295R, and *in vivo,* on mice xenografts, studies have shown promising results of both drugs. However, the only drug to reach clinical trial stage was linsitinib, a dual inhibitor of IGF1R and IR. Its promising effects in preclinical models, even tolerated at high dosages, have led to different clinical trials on solid tumours and on ACC (51–53). Unfortunately, the randomized multicentric phase III trial on ACC conducted between 2009 and 2011 did not reach the expected results, with no observed difference between linsitinib and placebo in terms of overall survival (51).

3.3.2. IGF2R

Alongside the RTKs, the IGF system comprises a specific IGF2-receptor, IGF2R. This type-1 280kDa transmembrane receptor is composed of a large N-terminal extracellular domain, a small transmembrane portion, and a C-terminal intracellular domain. A soluble IGF2R isoform can be found in the circulation (0.7µg/mL). The extracellular region is made of 15 homologous units with high similarity, able to bind several ligands, implying a multifunctional role of IGF2R (54,55). Indeed, the receptor, also referred to as M6P-receptor has high affinity for mannose-6-phosphate (M6P), thus it can be bound by several M6P-containing complexes, such as transforming growth factor β (TGFβ), proliferin, or cathepsin D (56,57). M6P-proteins interact with IGF2R at domain 3, 5 and 9, while among the non-M6P-ligands, the most relevant one is certainly IGF2, that binds at domain 11 and whose affinity is increased by domain 13 interaction (58,59).

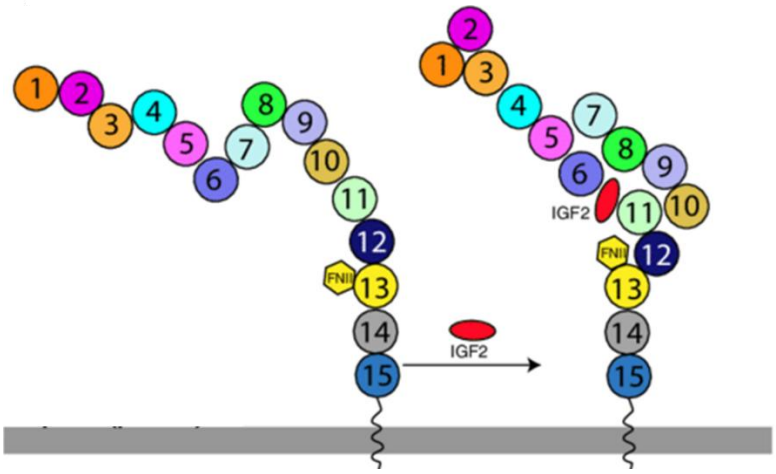

Figure 3. IGF2R conformational change after IGF2 binding. Adapted from Wang et al., 2020.

Upon IGF2 binding, IGF2R, whose intracellular domain does not bear any signal transduction function, triggers its scavenging role: the IGF2-IGF2R complex is internalized and delivered to the Golgi apparatus, to be later directed to the lysosomes for IGF2 degradation. IGF2R is particularly important during foetal life, where it controls overgrowth by contrasting IGF2 action (56). *In vitro* studies have demonstrated that increasing IGF2R affinity towards IGF2 resulted in a detriment of cancer cell proliferation, while *in vivo* studies confirmed that *IGF2R* stable transfection can delay breast cancer onset and spread (57). Moreover, in different cancer models and also in ACT, loss-of-heterozygosity at IGF2R locus has been described, correlating the IGF2R inactivation with tumour progression (60). Since these premises, *IGF2R* has been addressed as a tumour suppressor gene.

Nevertheless, in the latest years, the involvement of IGF2R in tumorigenesis has been proved (61). Overexpression of IGF2R has been reported in hepatocellular and gastric carcinomas (62). In cervical cancer, IGF2R was correlated to a poor prognosis, and *in vitro* *IGF2R*-knockdown induced cancer cell death (55). Moreover, IGF2R has a double pro-mitotic and anti-apoptotic function in haemangioma cells, where both *in vitro* and *in vivo*, IGF2R knockdown was effective in hampering tumour growth (54).

In ACT, only few studies focused on the expression and tumorigenic potential of IGF2R. In 2005, Velazquez-Fernandez and colleagues demonstrated that IGF2R, along with some other genes of the IGF2 pathway (as *IGF2, IGFBP3,* and *IGFBP6*), is overexpressed in ACC compared to ACA (62). Furthermore, the study of De Martino et al. evaluated the mRNA expression of several ACC and found *IGF2R* overexpressed in more than 40% of tumours and a strong-positive IHC staining in all tumours evaluated (52). However, IGF2R mRNA

level was positively correlated with IGF1R, suggesting an active involvement in ACT tumorigenesis (52).

Since IGF2R is not an RTK, some studies have aimed at finding its downstream mechanism of action. It was observed that the small cytoplasmic domain can be phosphorylated and some of its sequence motifs can serve as protein kinases substrates (63). El Shewy et al. demonstrated that IGF2R is strictly connected to sphingosine kinases (SphK) pathway. Indeed, after IGF2 stimulation, IGF2R recruits SphK to the plasma membrane, which act on the phosphorylation of sphingosine into sphingosine-1-phosphate. This product is latter extracellularly secreted and directed at its receptors that lead to a pro-mitotic signal via a heterotrimeric G protein dependent ERK1/2 activation (64–66).

Apart from IGF2, IGF2R is bound by numerous ligands, that can also influence its affinity for IGF2. Interestingly, the binding of the retinoic acid (RA) to IGF2R can increase IGF2R-mediated IGF2 internalization. Up to now, the binding site of RA to IGF2R is still unknown. Moreover, it was *in vitro* demonstrated that RA can stimulate cell apoptosis by activating cathepsin B when bound to IGF2R (67,68).

3.3.3. IGFBP1-6

Other relevant proteins of the IGF2 pathway are the IGFBPs, these 6 proteins are able to regulate the bioactivity of IGF1 and IGF2 both in the extracellular environment and in the circulation. IGFBPs are differentially expressed between ACC and normal adrenal (NA) as their function can be opposite. IGFBP1 and 4 are regulated by ACTH, IGFBP3 and 5 are regulated by IGF2, while no regulation of IGFBP2 and 6 has been observed (69). Even though no difference among ACC or ACA patients were found in IGFBP2 circulating levels, ACC patients with high IGFBP2 levels had a better OS and abdominal progression-free survival (70). On the contrary, IGFBP2 overexpression often correlated with the volume of the tumour mass (45), and most importantly it was able to increase *in vitro* cell proliferation even though the mechanism is still unclear (69). Apart from IGFBP2, the investigation of the other IGFBP resulted in conflicting data: mRNA of both *IGFBP3* and *6* was quantified in ACC and NA in several independent studies, but they were not coherent in their findings (46,52).

4. Sphingosine kinase pathway

Sphingosine kinases (SphKs) are lipidic kinases involved in the process of ceramides transformation. This mechanism, known as sphingolipid rheostat, can have an oncogenic connotation when, starting from ceramide, then deacylated by ceramidases into

sphingosine, is then transformed into sphingosine-1-phosphate (S1P) by SphKs. S1P is then released in the extracellular environment, where it binds its receptors S1P-receptors 1-5 ($S1P_{1-5}$), a range of G protein-coupled receptors able to increase cell trafficking, promote vascular integrity and transduce a pro-survival and pro-mitotic downstream signal, ultimately leading to cancer or inflammatory diseases (71). This pathway can be reverted, S1P can be dephosphorylated into sphingosine by S1P phosphatases, and sphingosine can be turned into ceramide by ceramide synthase enzyme. The accumulation of either ceramide or sphingosine in tumoral cells leads cancer cells to anti-survival signals, through apoptosis, autophagy and cell cycle arrest (72–74).

SphKs are the only enzymes able to phosphorylate sphingosine into S1P. These enzymes are composed of 5 domains, N-terminal domains C1-3 constitute the catalytic region, C4 region is exclusive of SphKs and represents the only domain able to induce the ATP-dependent sphingosine phosphorylation, while C5 is the C-terminal region (73). Human SphKs are mainly two isoforms, 42kDa SphK1 and 63kDa SphK2: the first is commonly found in cytosol and translocate to the plasma membrane when active, while the latter has nuclear and mitochondrial localization (72,75). The two isoforms slightly differ in the N-terminal domain and in the central one, where SphK2 presents a pro-apoptotic 9-aminoacid motif with high homology to the one found in BH3-only proteins, a subgroup of the Bcl-2 family (76,77). SphKs are ubiquitously expressed in human tissues, but SphK1 has higher expression levels in leukocytes, lungs and spleen, while SphK2 is consistently expressed in kidneys and liver tissues.

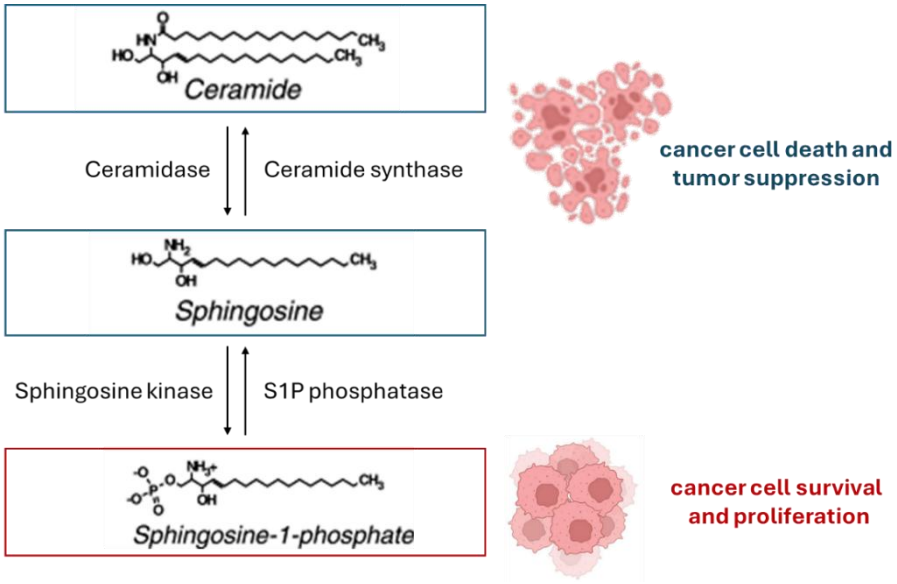

Figure 4. The sphingosine rheostat. Adapted from L.W. Hii et al., 2021.

SphK1 increased expression and/or activation is subjected to external stimuli, such as growth factors, cytokines and hormones: some of them are well-known, as transforming growth factor β, tumour necrosis factor α, prolactin, or 17β-oestradiol. These agonists are known to act promoting SphK1 phosphorylation (via ERK1/2), which results in a 14-fold increase of catalytic activity and contextually phospho-SphK1 is translocated to the plasmalemma where it can act on phosphorylating sphingosine into S1P (78). S1P can either interact with intracellular effectors as TRAF2/NFkβ or secreted in the extracellular environment where it can bind $S1P_{1-5}$ and later activate cell proliferation, via ERK1/2, anti-apoptotic signals, via PI-3K/Akt, or migration, via Rac/PLC. These downstream signalling pathways are common mechanism of different cancer types, indeed SphK1 upregulation was found involved in the onset and progression of breast, ovarian, liver, lung, kidney, and various other tumours (79). In 2015, Xu and colleagues reported SphK1 overexpression in ACC, both at transcript and protein levels, compared to adenomas, highlighting a role in malignancy. Moreover, they correlated SphK1 levels with patient's overall survival, describing that higher levels of SphK1 denotate more aggressive malignancies (80). Furthermore, an indirect demonstration of SphK1 role on ACC is given by Lucki et al., who demonstrated that S1P can increase cortisol production by H295R cells, a known marker of ACC aggressiveness (81).

SphK2 functions are only partially overlapping SphK1 ones, SphK2 is stimulated by fewer external agonists, such as TNFα, epidermal growth factor (EGF), and interleukin-1β. SphK2 activation could trigger different pathways with opposite fate. The presence of the BHL domain is deemed responsible for the pro-apoptotic role of SphK2, and the nuclear S1P produced by SphK2 specifically contributes to cell cycle arrest (78). On the opposite, it was demonstrated that in case of serum deprivation SphK2 was able to initiate pro-survival signalling (77). Furthermore, SphK2 active role in both stimulating cancer cell growth, proliferation and metastasis, and promoting resistance to chemotherapy was demonstrated in different tumours: kidney, breast, pancreatic, and prostate cancers were all described to be negatively affected by SphK2 expression and activity (82).

4.1 Sphingosine Kinase inhibitors

Since SphKs are widely recognized as oncogenes, driving crucial processes as angiogenesis, lymph-angiogenesis and cell migration, and can also be responsible for DNA damage response (DDR), a process that induces chemoresistance, they are considered new interesting therapeutic targets (77,79).

Among the inhibitors of the two kinases, various small molecules have been tested. The first compounds to be identified were SKI I-IV, a group of compounds with different IC50 and bioavailability. SKI I is potent and specific for SphK1, while SKI II targets both SphKs and was efficient in controlling xenograft growth of different cancers. Derivatives of these compounds have been designed to increase their bioavailability and stability.

Another class of inhibitors are the sphingosine analogues N,N-Dimethylsphingosine (DMS) and Dihydroxysphingosine (DHS, safingol). These unspecific inhibitors, with an IC50 of 5-10μM, have been tested in preclinical models of both solid and hematic cancers, giving positive feedback on their pro-apoptotic and anti-mitotic action. Interestingly, safingol has peculiar inhibitory behaviour, being a substrate for SphK2 and a competitive inhibitor for SphK1. Due to its successful *in vitro* response, safingol has been involved in several phase I clinical trials, in combination with different agents: Schwartz et al. reported a mild response to safingol combined with doxorubicin in patients with pancreatic cancer and angiosarcoma (83); Dickson et al. lead a trial on advanced solid tumours combining safingol with cisplatin and concluded that the best response was the stabilization of disease for an average of 3 months (84). Interestingly, safingol was proposed as optimal treatment for cisplatin resistant cancers, since resistance mechanisms to this chemotherapy was proven to correlate with increased SphK1 levels (85). Among the patients of the Dickson trial, 7 had ACC, and, notably, one of them experienced lung and liver metastases regression and another had prolonged stable disease. The most recent clinical trial on safingol, including also one ACC patient, was conducted in 2023 by Boulter et al., who administered it in combination with fenretide, another interactor of the ceramides pathway, on patients with advanced malignancies, and obtained only a minimal therapeutic activity (86). However, phase I studies highlighted the possible hepatotoxicity of this drug, thus no phase II trial has been approved (85).

FTY720 (fingolimod) is a structural analogue of sphingosine bearing a double role of inhibiting SphK1 and being a functional antagonist of $S1P_1$, indeed different action mechanisms were proposed: a direct inhibition of Sphk1 that blocks the downstream PI-3K/AKT/mTOR activation, or the generation of ROS that stimulates apoptosis, or the arrest of cell cycle through increase of p21 and p27 levels. Moreover, FTY720 has a structure that confers it an immunosuppressant activity, thus it is commercially approved for the treatment of multiple sclerosis. In cancer treatment, fingolimod showed a strong anti-proliferative and anti-metastatic effect in preclinical studies on different cancer models, such as ovarian,

breast, liver tumours, and glioblastoma (72,85). Among preclinical studies, Xu et al. demonstrated that FTY720 was able to reduce cell proliferation and invasion of ACC-derived H295R cell line while stimulating apoptosis. Furthermore, fingolimod resulted efficient in controlling H295R-derived xenograft growth (80), however, to date no clinical trial with fingolimod on ACC nor on other solid cancers has been initiated.

Various other interactors of the sphingosine rheostat have been developed, and their efficacy has been assessed *in vitro* or *in vivo*, but none of these has been tested on ACC models nor in clinical trials on ACC patients.

AIM OF THE THESIS

Adrenocortical tumours (ACT) are common and heterogeneous adrenal malignancies. Currently, the preferred management of ACT is adrenalectomy for localized masses, while in case of advanced carcinomas (ACC) the only therapeutic option is the adrenolytic agent mitotane, alone or in combination with EDP chemotherapeutics (EDP-M), thus the challenge of discovering novel drugs remains open. Molecular studies aimed at highlighting ACC-overexpressed features have identified the insulin-like growth factor 2 (IGF2) and its receptors as potential new druggable candidates.

The main aim of this study is to uncover the role of the IGF2 receptor, IGF2R, which has been proposed as anti-oncogenic, due to its IGF2 degrading function, but never been deeply investigated in the ACT context.

This project begun evaluating and comparing IGF2R presence in ACC, adenomas (ACA), normal adrenal tissues, and ACC lines, and will proceed with the identification of IGF2R role, as promoter or inhibitor of ACT tumorigenesis. *In vitro* methodologies, as IGF2R silencing, neutralizing antibody incubation, and transient transfection of IGF2R, were applied to evaluate the effect of IGF2R on two main endpoints, cell proliferation and viability, in ACC lines and ACT primary cell cultures.

A second part of the PhD project was aimed at testing the IGF2 scavenging role of IGF2R, to understand the underlying mechanism of action of the receptor. To do this, retinoic acid (RA) was used, as it is known to facilitate IGF2 internalization via IGF2R.

The latter section of this work was focused on the hypothesis of an IGF2R-downstream mitogenic cascade, that in other cell models is mediated by sphingosine kinase enzymes (SphKs). To this aim, SphK activity, upon IGF2R modifications, were assessed. Moreover, since the recent interest in SphK as therapeutic target in other pathologies and the positive results obtained in ACT clinical and preclinical studies, we proceeded to test the efficacy of two different SphK inhibitors, safingol and fingolimod. In particular, cellular proliferation, viability, apoptotic stimulation, and cortisol secretion were assessed in our *in vitro* models after treatment. Moreover, the antitumoral action of each drug was evaluated in monotherapy or in combination with the standard treatment EDP-M, in order to prove a possible synergism.

MATERIALS AND METHODS

1. Cell culture and reagents

In vitro culturing of 4 different human ACC cell lines was carried out at 37°C, 5% CO_2, and 95% humidity. NCI-H295R (H295R), deriving from a primary ACC tumour of an adult female patient, were bought from American Type Culture Collection (ATCC, Manassas, VA USA). H295R were cultured in DMEM F-12 1:1 (Merck KGaA, Darmstadt, Germany) supplemented with 5% Nu Serum IV (Corning®, NY USA), 1% ITS+Premix (Corning®, NY USA), and 1% penicillin-streptomycin (Gibco, Waltham, MA USA). JIL-2266, isolated from a primary ACC of an adult female patient, were kindly gifted by Dr. Laura Sophie Landwher, and cultured according to a previously established protocol (87). Briefly, they were cultured in a peculiar media composed of Ham's F12 Nutrient Mix (Gibco, Waltham, MA USA) 3:1 with pyruvate-enriched DMEM (Gibco, Waltham, MA USA) supplemented with 10% Fetal Bovine Serum (FBS, Gibco, Waltham, MA USA), 1% penicillin-streptomycin (Gibco, Waltham, MA USA), 5µg/mL insulin (Merck KGaA, Darmstadt, Germany), 0.4µg/mL hydrocortisone (Sigma-Aldrich Merck KGaA, Darmstadt, Germany), 8.4ng/mL cholera toxin (Merck KGaA, Darmstadt, Germany), 24µg/mL adenine (Sigma-Aldrich Merck KGaA, Darmstadt, Germany), and 10ng/mL epidermal growth factor (EGF, Invitrogen, Thermo Fisher Scientific, Waltham, MA USA). Two metastatic ACC cell lines were cultured as well, MUC-1 cells (88), established from a male patient's neck metastasis, gifted by Professor Constanze Hantel and TVBF-7 cells (89), obtained from the lymph nodal metastasis of a male patient, donated by Professor Sandra Sigala. These two cell lines were cultured in Advanced DMEM/F12 medium (Gibco, Waltham, MA USA) added with 10% FBS, 1% penicillin-streptomycin and, only for TVBF-7 cells, with supplementation of 2mM L-glutamine (Merck KGaA, Darmstadt, Germany). All cell lines were harvested and seeded for experiments only within a range of 20 passages, moreover they were authenticated by genetic profiling with the polymorphic short tandem repeat (STR) technique (Promega, BMR Genomics Cell Profile service, Italy) in May 2024.

2. Primary cell cultures

This study was approved by the Ethical Committee of CE-AVEC (105/2017/U/Tess) and by Milano Area 2 Ethical Committee (554_2022bis). All patients who underwent adrenalectomy gave informed consent to the use of their clinical information (Table 1) and tumour samples.

Patient number	Tumour	Gender	Age	Tumour size	Weiss score	Hormone secretion
#1	ACA	F	23	3 m	-	Hypercortisolism
#2	ACA	M	73	3.2 cm	0	Hypercortisolism
#3	ACA	M	71	1.6 + 1.9 cm	2	Inactive
#4	ACA	F	59	8 cm	1	Hypercortisolism
#5	ACA	F	52	2.5	2	Hyperaldosteronism
#6	ACA	M	48	2.1 + 0.8 cm	1	Hyperaldosteronism
#7	ACA	F	49	4 cm	1	Hypercortisolism
#8	ACA	M	59	-	0	Hypercortisolism
#9	ACA	F	58	5.4 cm	1	Hypercortisolism
#10	ACA	F	32	3.8 cm	2	Hypercortisolism
#11	ACA	M	46	1.6 cm	1	Hyperaldosteronism
#12	ACA	M	55	1.6 cm	1	Hyperaldosteronism
#13	ACA	M	59	1.6 cm	0	Hyperaldosteronism
#14	ACA	M	53	2.2+ 1.1 cm	2	Hyperaldosteronism
#15	ACA	F	80	3.2+ 0.9 cm	0	Hypercortisolism
#16	ACA	M	63	-	2	Hypercortisolism
#17	ACA	M	55	1.6+ 0.7 cm	0	Hyperaldosteronism
#18	ACA	M	71	2.6 cm	0	Hyperaldosteronism
#19	ACA	F	70	2.5 cm	2	Hyperaldosteronism
#20	ACA	F	16	3.2 cm	0 paediatric	Hypercortisolism
#21	ACA	F	64	1.8 cm	1	Hypercortisolism
#22	ACA	F	41	4 cm	1	Hypercortisolism
#23	ACA	F	73	2.8 cm	1	Hypercortisolism
#24	ACA	F	69	4 cm	1	Hyperaldosteronism
#25	ACA	M	60	6 cm	1	Hypercortisolism
#1	UMP	F	49	6.5 cm	-	Hypercortisolism
#2	UMP	F	64	7.5 cm	0	Hyperaldosteronism
#3	UMP	F	51	3.2 cm	3	Inactive
#1	ACC	M	67	11 cm	7	Inactive
#2	ACC	M	57	4.5 cm	3	Hypercortisolism
#3	ACC	F	30	20 cm	7 (oncocytic)	Hypercortisolism, Hyperandrogenism
#4	ACC	M	54	7.5 cm	> 3	Hypercortisolism
#5	ACC	F	31	4.5 cm	2	Hypercortisolism

Table 1. Clinical data of patients with ACA, UMP, and ACC whose tissues were collected for primary cell culture establishment and experiments.

ACC, UMP, and ACA tissues were collected after adrenalectomy and stored temporarily in MACS® Tissue Storage Solution (Miltenyi Biotec, Bergisch Gladbach, Germany). Under sterile conditions, tissues were approximately divided into halves to be partially stored at -80°C for RNA and protein extraction and partially devoted to establishing primary cultures. Each tissue was primarily mechanically dissected, using a scalpel, and subsequently it was

enzymatically dissociated through a 2-hour incubation at 37°C in 2mg/mL collagenase IA (Merck KGaA, Darmstadt, Germany) solution in DMEM. After the incubation, the cell suspension was passed through a 100μM strainer to eliminate undigested material as cell aggregates and extracellular matrix conglomerates, and ultimately, to obtain single cells. To ensure adipocytes elimination, 1000rpm centrifugation for 10min allowed the formation of a lipidic ring above the supernatant and the pellet, enabling its remotion. Cells were harvested in Advanced DMEM/F12 medium supplemented with 20% FBS, 2mM L-glutamine, and 1% penicillin-streptomycin. ACC, UMP, and ACA primary cells grew in adherent monolayers; thus, erythrocytes were removed by PBS (EuroClone SPA, Pero, Italy) washing, while fibroblast contamination was monitored daily to ensure there was not overgrowth.
Whenever possible, both tumoral and peritumoral tissue of the adrenal gland were collected, the latter were entirely stored at -80°C and used only for RNA and protein extraction as representative of normal adrenal gland tissue (NA).

3. IGF2R genetic silencing and transfection

IGF2R was genetically silenced through small interfering RNA (siRNA) technology: this technique allows the formation of lipid micelles containing the siRNA, able to fuse to the cellular membrane and release the siRNA into the cytoplasm. Once in the cells, siRNA will be incorporated into RISC complex and, after the degradation of the sense strand, this ssRNA-RISC complex will bind to the target mRNA and degrade it, de facto preventing transduction into protein. In detail, ON-TARGETplus human IGF2R siRNA (Dharmacon Inc., Ge Healthcare, Lafayette, CO USA), containing a mix of 4 different siRNAs targeting IGF2R, was incubated for 5min with the transfection reagent Lipofectamine 2000 RNAiMax (ThermoFisher Scientific, Waltham, MA USA) in OptiMEM transfection medium (Gibco, Waltham, MA USA), to form lipid micelles. After the incubation, the mixture was inserted drop-by-drop on seeded cells in complete media. IGF2R or scramble siRNA (used as control because of its feature of not targeting any transcript) was used between 25 and 50nM concentrations for 3 to 6 days incubation, depending on cell line. To verify knockdown efficiency, protein expression was evaluated through Western blot technique. Only experiments with IGF2R knockdown higher than 60% were considered silenced and included in further statistical analysis.
IGF2R transient transfection was performed through lipofection to obtain IGF2R overexpression. In particular, IGF2R-EGFP DNA plasmid (pRP[Exp]-EGFP/Puro-CAG>hIGF2R[NM_000876.4], VectorBuilder Inc., Chicago USA) was transfected at 1μg/μL concentration for 48-hour incubation time. Transfection was optimized using Lipofectamine

2000 (ThermoFisher Scientific, Waltham, MA USA) and OptiMEM transfection medium: at first, two separate mixes of Lipofectamine or DNA plasmid in OptiMEM were incubated for 5 minutes at RT and subsequently the plasmid-containing mixture was inserted into the Lipofectamine solution for 20 minutes at RT, to be eventually inserted drop-by-drop onto pre-seeded cells in complete growth medium. An empty-EGFP plasmid was transfected in control samples maintaining the same experimental conditions as the IGF2R-EGFP plasmid. To ensure efficient transfection, fluorescence of both control and IGF2R transfected samples was verified via microscope.

4. IGF2R pharmacological inhibition

IGF2R downstream effect was inhibited through a human anti-IGF2R antibody (Biotechne, Minneapolis, MN USA) targeting the extracellular binding site of IGF2R with its ligand IGF2. Incubation with the neutralizing antibody was performed at 4µg/mL concentration for ACC cell lines and at 20µg/mL for primary cell cultures, in serum-deprived media. Anti-IGF2R antibody incubation was performed for 24, 48, and 72 hours to assess a time course of inhibition.

5. Retinoic acid (RA) treatment

All-trans retinoic acid (Merck, KGaA, Darmstadt, Germany), a known ligand of IGF2R and pro-apoptotic agent, was purchased as powder and solubilized in DMSO at a starting concentration of 50mM. A range of RA concentrations from 0.5 to 50µM was tested in apoptosis on different cell lines and primary cultures to establish efficient dosage. All concentrations tested had DMSO concentration lower than 0.5%, thus the effects evaluated strictly depended on RA. 1µM concentration was used to evaluate alterations in mRNA expression of targeted genes after 3-6h treatment, IGF2 secretion after 24h treatment, and cell proliferation after 24h treatment.

6. Sphingosine kinases pharmacological inhibition: safingol (SAF) and fingolimod (FTY)

Inhibition of sphingosine kinases was achieved via SAF, a dual inhibitor of sphingosine kinase 1 (SphK1) and 2 (SphK2) and FTY, an inhibitor of SphK1. SAF powder (Abcam Inc., Waltham, MA USA) was solubilized in DMSO at a starting concentration of 2.5 mM. FTY720 powder (Abcam Inc., Waltham, MA USA) was solubilized in DMSO at a starting concentration of 50mM, then a range of concentrations (determined from clinical trials plasmatic concentrations, (86)) was tested to determine the IC50 via MTT assay. All

concentrations tested had DMSO concentration lower than 0.5%, thus the effects evaluated strictly depended on SphK inhibitors.

7. EDP-M scheme for *in vitro* treatment

EDP-M scheme, currently used in ACC patients, was adapted for *in vitro* treatment by Hantel et al. (90). Mitotane, etoposide, and cisplatin powders were purchased from Target Mol Chemicals Inc. (Boston, MA USA), the first two were dissolved in DMSO, while the latter was dissolved in N'N'-dimethylformamide (DMF). Doxorubicin was dissolved in DMSO as well (RayBiotech, Peachtree Corners, GA USA). IC50 for each drug of the EDP-M scheme was retrieved from Hantel: 15.9 μM mitotane, 1.2 μM etoposide, 9.6 μM cisplatin, and 11 μM doxorubicin (90); treatment in complete medium lasted for 24h, after 2h starvation.

8. mRNA expression: quantitative real time PCR (RT-qPCR)

To evaluate the transcript expression of target genes, RT-qPCR was used. The first step, RNA extraction, was performed differently according to the origin sample: RNA from tumour tissues was obtained via Trizol extraction protocol, while cell pellet-derived RNA was extracted using the RNeasy Mini Kit (Qiagen, Hilden, Germany). The starting material for an optimized Trizol extraction was 5 to 50mg of tissue, to be dissociated through a potter in Trizol reagent. The following step of phase separation allowed to isolate the RNA from DNA and other cell material of each sample. RNA was subsequently precipitated by isopropyl alcohol, then washed in ethanol to further dissolve the obtained pellet in water. RNA obtained from either protocol was quantified at NanoDrop Lite (Thermo Fisher Scientific, Waltham, MA USA) and 1ng of each sample was reverse transcribed using the RevertAid H Minus First Strand cDNA Synthesis Kit (Thermo Fisher Scientific, Waltham, MA, USA). Upon this step, cDNA was diluted at 1:10 to perform RT-qPCR.

RT-qPCR was performed to obtain RNA expression of *IGF2, IGF2R, IGFBP2, IGFBP6, SPHK1, SPHK2*, and *GAPDH* genes. Ad hoc forward and reverse primers were synthesized by Thermo Fisher Scientific (Waltham, MA USA). Sybr Green chemistry was used, thus an appropriate master-mix for each gene of interest was prepared: 1.6μL of 1:1 mix of forward and reverse primers, 2.4μL of H2O, in 8μL of SsoFast EvaGreen™Supermix (Bio-Rad Laboratories Inc., Hercules, CA USA). For each sample 4μL of diluted cDNA were added to the 12μL of master-mix and loaded in triplicate. Comparative ΔCT analysis method was used for retrieving results, normalize on *GAPDH* expression of each sample, and ultimately quantify RNA expression.

9. Protein expression: Western blot

Protein expression was evaluated from both tumour tissues and seeded cells. In ice, small portions of frozen tumour tissues were minced with a scalpel and lysed using a 1X Lysis buffer (Cell Signaling Technology Inc., Danvers, MA USA), supplemented with a protease inhibitor (Roche, Basel, Swi). Tissues were incubated with the lysis solution for 15 to 30 minutes, vortexing repeatedly to obtain an homogeneous mixture, then were centrifuged at 13000 rpm for 15minutes at 4°C. The supernatant of each sample, containing proteins, was collected and pellets were discarded. A similar procedure was performed for seeded cells: cells were either detached with trypsin and pellets were lysed as described above or directly scraped from 6-well plates with the lysis solution, then collected and processed as stated earlier. Proteins were quantified following the Pierce BCA method (Invitrogen, Thermo Fisher Scientific, Waltham, MA, USA), and 30 to 45µg of proteins (or 100µg for tissue deriving proteins) were loaded on pre-casted 4-12% SDS gels (Invitrogen, Thermo Fisher Scientific, Waltham, MA, USA). 40minutes of electrophoretic run in Bolt solution (Invitrogen, Thermo Fisher Scientific, Waltham, MA USA) set at 200V allowed protein separation on the gel, then proteins were transferred on a 0.2µm pore size nitrocellulose membrane through 90min of electrophoretic transfer in 20% methanol and 10% Tris/Glycine solution (Bio-Rad Laboratories Inc., Hercules, CA USA). Ponceau S solution (Sigma-Aldrich, Merck KGaA, Darmstadt, Germany) was added to reveal correct transfer of proteins on the membrane. Membranes were incubated for 1 hour in 5% non-fat dry milk (NFDM) solution to block unspecific binding sites and then incubated overnight at 4°C with the primary antibody diluted according to manufacturer's instructions: IGF2R 1:1000 in 5% NFDM (Cell Signaling Technology Inc., Danvers, MA USA), SphK1 1:500 in 5% BSA (Abcam Inc., Waltham, MA USA), SphK2 1:1000 in 5% NFDM (Cell Signaling Technology Inc., Danvers, MA USA). The following morning, membranes were washed 3 times and incubated for 1hour at RT with appropriate secondary antibodies diluted 1:2000 in 5% NFDM. GAPDH (Invitrogen, Thermo Fisher Scientific, Waltham, MA USA) was used to normalize protein expression among different samples, incubation with 1:4000 primary antibody in 5% NFDM lasted 1hour at RT and was followed by secondary antibody incubation as described above. ChemiDoc (Bio-Rad Laboratories Inc., Hercules, CA USA) was used to capture chemiluminescence after ECL incubation. ImageJ software (91) was used to quantify chemiluminescent signals measuring the pixel intensity of each band: background signal was subtracted from sample signal, then for each protein GAPDH normalization was performed. Ultimately, samples were compared with basal or reference samples of each experiment.

10. ELISA technique for the quantification of secreted-IGF2

The Enzyme-Linked ImmunoSorbent Assay (ELISA) is used to quantify a certain protein of interest in a complex mixture. Herein, the Human IGF2 ELISA kit (LSBio, Shirley, MA USA) was employed to quantify the IGF2 secreted from cells and accumulated in the supernatant.

According to the manufacturer's instructions, cell supernatants were collected after treatment and centrifuged at 1000g for 20min prior freezing at -80°C, in order to eliminate cell debris. On the day of the kit all reagents were brought at room temperature. A curve of standard IGF2 was prepared, at concentrations ranging from 0 to 10ng/mL, and was loaded on a pre-coated 96-well plate, along with samples (assessed in duplicate), to be further incubated for 2h at 37°C. After the incubation, the liquid was removed and 100µL of detection reagent A (a primary antibody against-IGF2) were added for 1h at 37°C. 3-times wash with 350µL of 1X Washing solution were carried out before a 1h incubation at 37°C with 100µL of detection reagent B (a secondary antibody directed against the primary and conjugated with HRP). At the end of this incubation, 5-times wash with 350µL of 1X Washing solution were performed. Then 90µL of TMB were added to each well and incubated until the reaction developed into a blue-green colour (10-20min); once the correct colour intensity was reached, 50µL of Stop Solution were added to avoid saturation. The plate absorbance was read at 450nm wavelength via Victor Nivo™ plate reader (Perkin-Elmer, Waltham MA USA).

To obtain IGF2 quantity of each sample, absorbance results were interpolated within the standard IGF2 curve. Only samples with a concentration within the curve span were considered reliable and used in further statistical analyses.

11. Cell proliferation: 5-bromo-2′-deoxyuridine (BrdU) incorporation

Prior to proliferation assessment, cells were seeded in transparent 96-well plates at a density of: 12 to 14*10^3 H295R and primary ACC and ACA cells/well, 4 to 4.5*10^3 JIL-2266 and MUC-1 cells/well, 12 to 15*10^3 TVBF-7 cells/well, then silenced, transfected, or treated according to time and concentrations stated in Sections 3-4-5-6. 3 to 5 wells were seeded for each experimental condition and a non-specific binding (NSB) well was included on each plate along with the samples. At the end of each treatment, to quantify actively proliferating cells, BrdU internalization was assessed via Cell proliferation ELISA colorimetric kit (Roche, Manheim, Germany). Following manufacturers' instructions, cell lines were incubated at 37°C for 2 hours with 1µM BrdU in DMEM, while for primary cultures, incubation time was prolonged to 24 hours. NSB wells were not supplemented with BrdU, to further reflect the

unspecific signal of the cells. Subsequently, at RT, BrdU mixture was removed and 200µL of Fix/Denat solution, necessary to immobilize the cells on the plate bottom and at the same time allow DNA denaturation for facilitating BrdU label accessibility, was added for 30 minutes. Removal of Fix/Denat was followed by 60-90 minutes of incubation with 100µL of anti-BrdU antibody, able to recognize BrdU in the newly synthetized DNA and tagged with peroxidase (HRP). The following step of washing with 200µL of 1:10 diluted washing solution was repeated 3 times before 2-20 minutes incubation with 100µL of tetramethylbenzidine (TMB), able to bind to the peroxidase-conjugated anti-BrdU antibody. Colorimetric reaction happened only in case of immune complexes formation, thus only when BrdU was incorporated into the DNA. The reaction was stopped before reaching a plateau by 25uL of 1M sulfuric acid. VICTOR® Nivo™ plate reader (Perkin-Elmer, Waltham MA USA) was set at 450nm wavelength to obtain single-wells absorbance values. The mean absorbance value of each condition was calculated, then NSB was subtracted, and the percentage of the ratio between each treatment and the control sample was used as result and included in the statistical analysis.

12. Viability assay: MTT

Cell viability was assessed via MTT assay. Cells were seeded in 96-well plates as stated in Section 11 and silenced, transfected, or treated according to Sections 3, 6, and 7. At the end of the experimental treatment, culture medium was removed from the wells and cells were incubated at 37°C for 3 to 4 hours in a 1:10 solution of 5mg/mL 3-(4,5-dimethylthiazol-2-yl)-2,5-diphenyltetrazolium bromide solution (MTT, Sigma-Aldrich Merck KGaA, Darmstadt, Germany) in DMEM without Phenol Red (Merck KGaA, Darmstadt, Germany). This step allowed the formation of purple formazan crystals in cells with active mitochondria that were able to convert MTT into formazan through the action of succinate dehydrogenase. After visual observation of formazan presence, MTT medium was carefully removed and 100µL of dimethyl sulfoxide (DMSO) were added to allow the solubilization of the salt into a homogeneous solution. After mixing, the absorbance was quantified by VICTOR® Nivo™ plate reader (Perkin-Elmer, Waltham MA USA) at 560nm wavelength. Mean value of each condition was calculated and results were expressed as the percentage of the ratio between each treatment and the control sample.

13. Apoptosis assay: caspase 3/7 activity quantification

Quantitative analysis of the apoptotic pathway activation was assessed through the measurement of the amount of active caspases 3 and 7 in the samples, via ApoONE®

Homogeneous Caspase-3/7 Assay (Promega Corporation, Madison, WI USA). Briefly, cells were seeded on black 96-well plates, to avoid interference of fluorescence between wells, at the same density as in Section 11 and treated as described in Sections 5 and 6. Following manufacturer's instructions, after treatment, a working reagent composed of 1:100 of ApoONE® substrate in ApoONE® buffer was added in equal volume to the plate wells for a 2hour incubation at RT in the dark. The working reagent contains lytic enzymes and other components to facilitate caspase activity and a pro-fluorescent caspase substrate that upon cleavage by caspases present in the samples reveals a fluorescent signal that can be detected. Plate fluorescence was detected by VICTOR® Nivo™ plate reader (Perkin-Elmer, Waltham MA USA) at 485nm excitation wavelength. For each experiment, a blank well, containing only culture medium and no cells, was included and its fluorescence value after incubation with the working reagent was subtracted to the mean value of each experimental sample triplicate. The result was expressed as the percentage of the ratio between treated and control samples.

14. Sphingosine kinases activity quantification

To measure the activity of both sphingosine kinases after cell treatments, an enzymatic activity assay, able to detect the amount of ATP consumed after sphingosine conversion into S1P, was performed. Cells were seeded into 6-wells plates at a density of: $3*10^5$ H295R or primary cells/well, $1.5*10^5$ JIL-2266 or MUC-1 cells/well and $5*10^5$ TVBF-7 cells/well and silenced, transfected, or treated as stated in Sections 3-4-6. After treatment, cell pellets were collected and lysed using a specific Mammalian Cell Lysis Kit (Merck KGaA, Darmstadt, Germany), then quantified via Pierce BCA assay (Invitrogen, Thermo Fisher Scientific, Waltham, MA, USA). Preliminary experiments on basal cell conditions were used to determine the best protein quantity to test on the assay: 5 to 15ng of protein were required for primary cultures, 40ng for MUC-1, and 20ng of protein were needed for TVBF-7. The assay was performed following instructions from the manufacturer (Echelon Biosciences Inc., Salt Lake City, UT USA): the Reaction Buffer containing 1mM DTT, to maintain proteins in their active state, was used to prepare the 400µM sphingosine and the 20µM ATP solutions. Sample wells, assayed in duplicate, were prepared by adding 10µL of sample lysate, 10µL of ATP solution, and 20µL of sphingosine solution. Moreover, standard wells were prepared by adding 10µL of reaction buffer, 10µL of ATP standard curve, and 20µL of sphingosine solution. Subsequently, 2 hours incubation at RT are needed for the sphingosine kinase in the samples to convert sphingosine into S1P, consuming the supplemented ATP. At last, 40µL of K-LUMa, an ATP detector, were added to sample and

standard wells and incubated for 10 minutes in the dark prior to reveal its luminescent signal using VICTOR® Nivo™ plate reader (Perkin-Elmer, Waltham MA USA). The signal recorded is inversely proportional to the active sphingosine kinases present in the sample, thus the mean signal of each sample was interpolated on the ATP standard curve to calculate the remaining amount of ATP; finally, the opposite of this value was calculated to quantify the sphingosine kinase activity.

15. Cortisol production quantification

Cortisol levels were measured on samples of supernatant media of cells derived from cortisol-producing tumours after 72h treatment with antiIGF2R antibody or SphK inhibitors SAF and FTY. After collection, supernatant samples were centrifuged for 10min at 13000rpm at 10°C to eliminate debris, then measured with the specific immunoassay Elecsys Cortisol II (Cobas, Roche, Basel, Swi).

16. Synergy evaluation and statistical analysis

Synergy of drug combinations was calculated via SynergyFinder+ online software (92). Synergy scores were obtained from both Bliss and HSA mathematic models: a synergistic effect of treatments was confirmed by a synergy score higher than +10, an agonist effect was indicated by a synergy score between -10 and +10, and antagonism was determined by synergy scores lower than -10. GraphPad Prism 10.5.0 software (GraphPad Software Inc., San Diego, CA, USA) was used to perform the statistical analyses of the project. Statistical analyses were listed in the corresponding legend for each graph, results were plotted as median ±IQR.

RESULTS

1. IGF2 and IGF2R expression in different ACT models

To properly investigate the role of IGF2R in adrenocortical carcinoma pathogenesis, a preliminary assessment of the expression level of IGF2R and its ligand IGF2 among ACC, ACA, and normal adrenal tissue was conducted.

IGF2 mRNA expression, displayed in Fig.1A, was assessed through RT-qPCR. IGF2 resulted overexpressed in ACC (1.002 (4.893) *p<0.05 vs ACA) compared to ACA (0.028 (0.0351)). The IGF2R transcript expression resulted in similar levels among the three groups (Fig.1B). However, as shown in Fig.1C, IGF2R protein quantification resulted significantly higher in both tumour types (1.15-fold vs H295R cells (1.5) in ACC, ***p<0.001; 1.54-fold vs H295R cells (2.8) in ACA, **p<0.01 vs NA) than in NA tissue (0.31-fold vs H295R cells (0.49)). These findings suggest the relevance of the IGF2-IGF2R axis in ACC more than ACA or NA, since only ACC overexpressed both the ligand and the receptor.

To corroborate the previous data, IGF2 and IGF2R were quantified both at transcript and protein level on four different ACC cell lines: H295R and JIL-2266, derived from primary tumours, and MUC-1 and TVBF-7, derived from metastatic ACC.

As shown in Fig.2A, IGF2 mRNA resulted significantly overexpressed in H295R and TVBF-7 cells (1.043 (1.1) and 1.296 (1.3) respectively), compared to MUC-1 and JIL-2266 (0.003 (0.0027) and 0.012 (0.018) respectively). However, all cell lines are able to secrete IGF2 in cell culture media at similar concentrations (Fig. 2B).

Interestingly, IGF2R mRNA levels (Fig.2C) reflected those of IGF2, showing a significant overexpression in H295R (0.03 (0.025)) and TVBF-7 (0.036 (0.035)) cells, almost 10 times higher than in MUC-1 (0.0037 (0.008)) and JIL-2266 (0.0028 (0.002)).

Since these data were never investigated by previous literature in adrenocortical carcinoma cell lines, we further investigated the protein expression of the IGF2 receptor, as illustrated in Fig 2D. We observed similar levels of IGF2R in H295R and MUC-1 (0.79 (0.47) and 0.84 (0.74) respectively), while TVBF-7 were featured by a significant overexpression compared to all other cell lines (2.04 (1.86), **p<0.01 vs H295R and MUC-1, ****p<0.0001 vs JIL-2266). Conversely, IGF2R levels of JIL-2266 resulted significantly lower than in the other cell lines (0.22 (0.41), *p<0.05 vs H295R and MUC-1, ****p<0.0001 vs TVBF-7), with a protein

expression 10-times inferior to TVBF-7. These results are clearly depicted in the representative immunoblot shown in Fig. 2D.

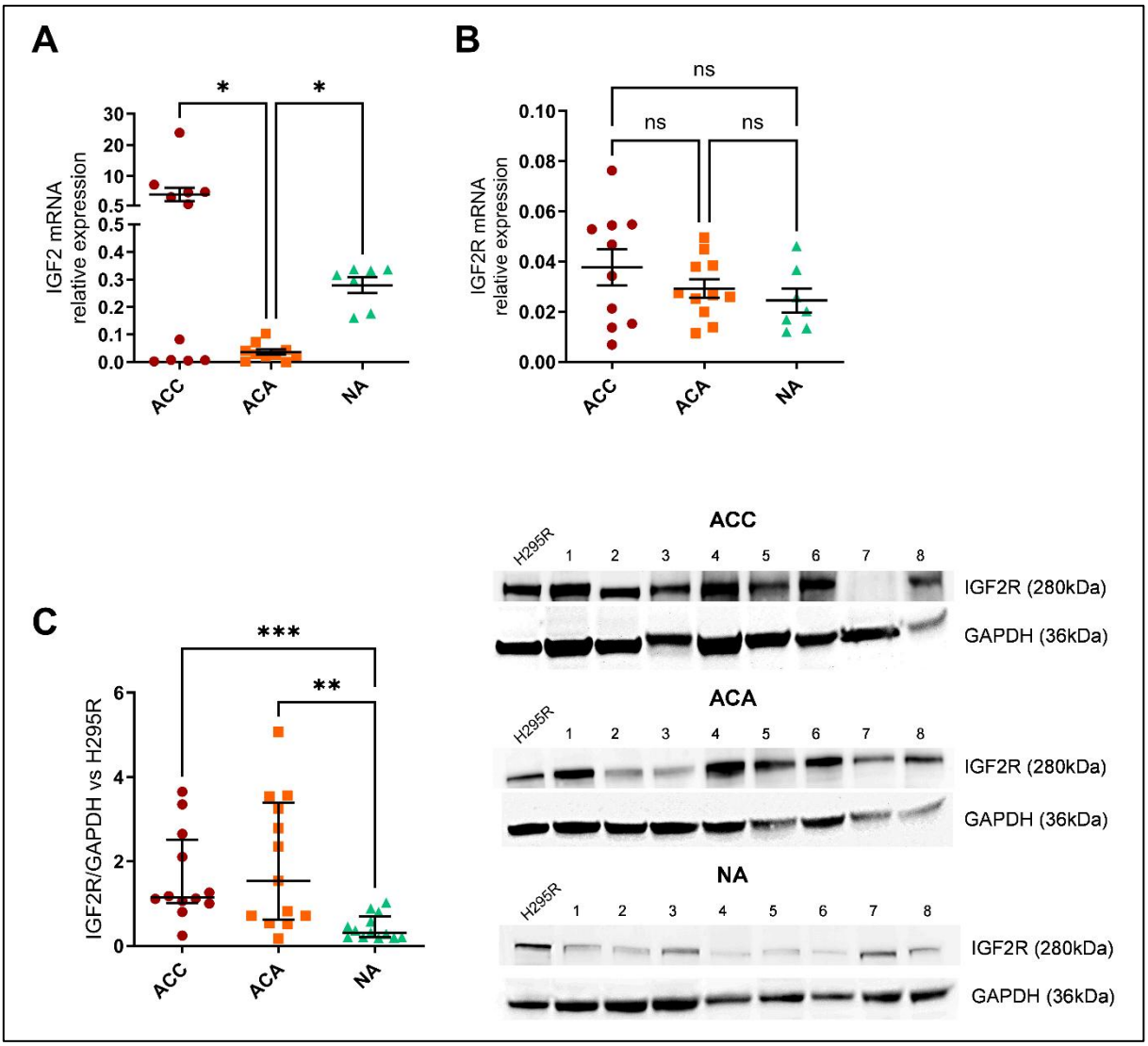

Figure 1. IGF2 and IGF2R differential expression in ACC, ACA, and NA tissues. **A**) IGF2 mRNA relative expression evaluated through RT-qPCR on tumoral tissue. n=11 ACC, 10 ACA, 7 NA. Results were plotted as individual dots, plus median ±IQR. **B**) IGF2R mRNA relative expression evaluated through RT-qPCR on tumoral tissue. n=10 ACC, 11 ACA, 7 NA. Results were plotted as single dots, plus median ±IQR. **C**) Western blot analysis of IGF2R protein levels of tumoral tissue of ACC, ACA, and NA, normalized on GAPDH housekeeping levels, alongside representative immunoblot of 8 tumours of each type showing corresponding IGF2R and GAPDH bands. n=12 ACC, 13 ACA, 13 NA. Results were plotted as single dots, plus median ±IQR of IGF2R/GAPDH ratio normalized on H295R expression levels. Statistical analysis was performed via GraphPad Prism software, using Kruskal-Wallis test coupled with Uncorrected Dunn's post hoc analysis. *p<0.05, **p<0.01, ***p<0.001.

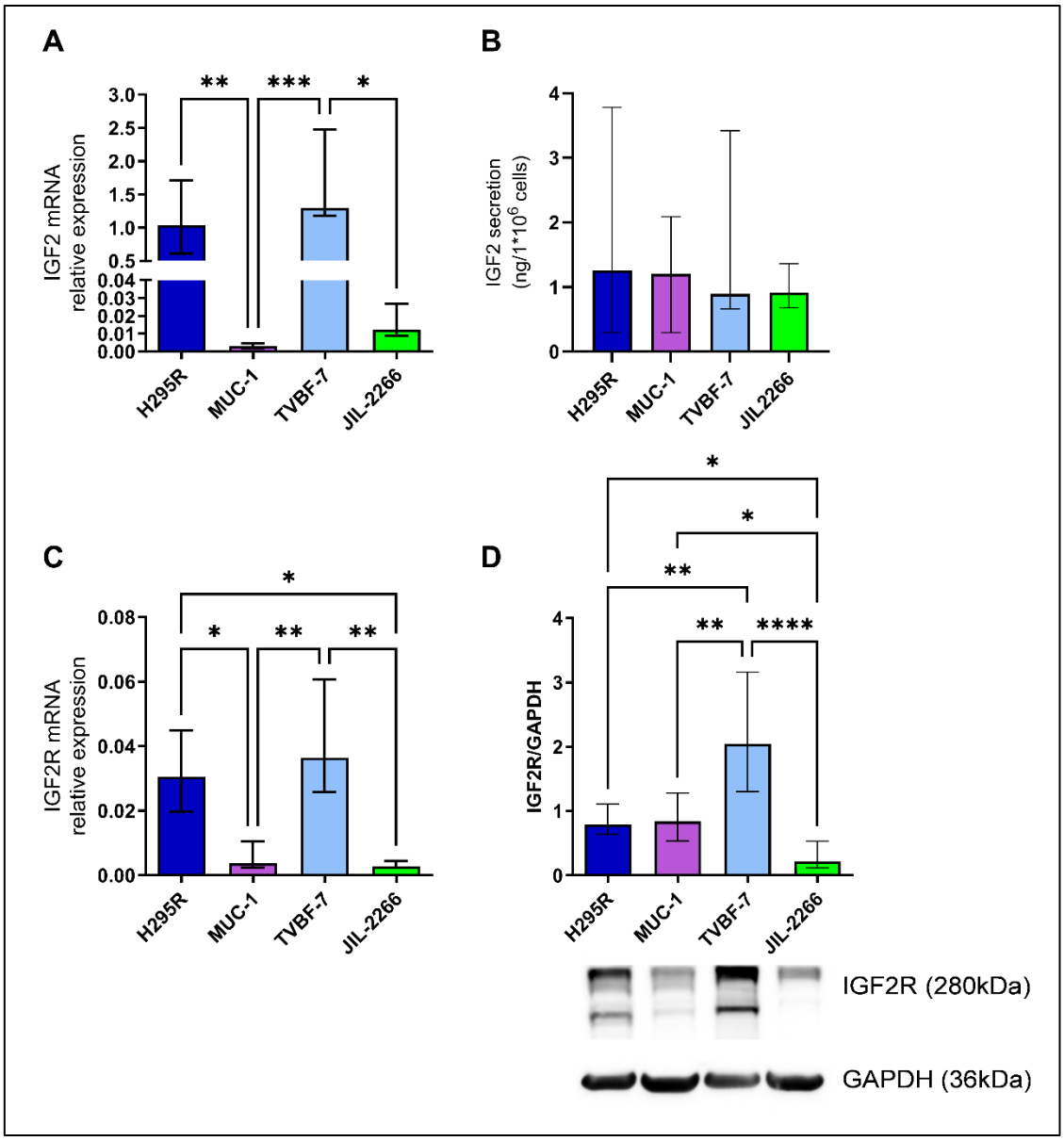

Figure 2. IGF2 and IGF2R differential expression in 4 ACC cell lines. **A**) IGF2 mRNA relative expression evaluated through RT-qPCR on H295R, MUC-1, TVBF-7, and JIL-2266 cells. n>4. Results were plotted as median ±IQR. **B**) IGF2 secretion, quantified via ELISA on cell supernatants of H295R, MUC-1, TVBF-7, and JIL-2266 after 2h serum starvation. Results of n>3 experiments were plotted as median ±IQR of IGF2 ng/1*10^6 cells. **C**) IGF2R mRNA relative expression evaluated through RT-qPCR on H295R, MUC-1, TVBF-7, and JIL-2266 cells. n>4. Results were plotted as median ±IQR. **D**) Western blot analysis of IGF2R protein levels of H295R, MUC-1, TVBF-7, and JIL-2266, normalized on GAPDH housekeeping levels. n>5. IGF2R/GAPDH ratio data were plotted as median ±IQR alongside representative immunoblot showing IGF2R and GAPDH levels. Statistical analysis was performed via GraphPad Prism software, using Kruskal-Wallis test coupled with Uncorrected Dunn's post hoc analysis. *p<0.05, **p<0.01, ***p<0.001, ****p<0.0001.

2. IGF2R modifications: silencing or inhibiting IGF2R reduces ACT cell proliferation

IGF2R was strongly addressed as anti-mitotic, due to its IGF2-degrading function. Nevertheless, its overexpression in ACC compared to normal adrenal tissue, rose the hypothesis of a possible contribution of IGF2R in ACC growth.

The investigation of the previous hypothesis was conducted by silencing (via siRNA) or inhibiting IGF2R binding site for IGF2 with a neutralizing antibody (Ab antiIGF2R).

IGF2R knock-down significantly impacted cell proliferation, measured as BrdU incorporation. As shown in Fig. 3, H295R (3A), MUC-1 (3B), and TVBF-7 (3C), had a reduced proliferative activity after silencing (-10.25% (8.4), -12.55% (17.23), -16.28% (26.42) respectively). This effect was restricted to the sole pro-mitotic activity whereas no reduction of cell viability was observed after IGF2R-silencing (Fig.3E-G).

Interestingly, JIL-2266, the cell line with the lowest IGF2R protein level, was not affected by IGF2R silencing, nor in terms of proliferation or viability (Fig. 3D, H), suggesting that IGF2R pathway in this cell line does not contribute significantly to cell growth.

Fig.4 displays a time-course treatment with 4µg/mL of antiIGF2R neutralizing antibody, the first concentration that significantly altered cell proliferation. We observed a significant reduction of cell proliferation in H295R (-28.24% (20.89), *p<0.05 vs bas), MUC-1 (-25.77% (12.89), *p<0.05 vs bas), and TVBF-7 (-26.44% (17.93),*p<0.05 vs bas) after 72h incubation. In agreement with IGF2R silencing results, JIL-2266 (Fig. 4D) were unaltered by antiIGF2R antibody incubation.

To corroborate the findings presented above, both the silencing and the inhibitory strategy were experimentally assessed on primary cell cultures of ACA, UMP, and ACC. ACA are easily accessible, since the incidence of adrenal adenomas is 2-8% of the population, thus more than 10 tumours were collected and successfully silenced for IGF2R. As shown in Fig.5A, IGF2R knock-down confirmed the result obtained in ACC cell lines, with a significant reduction of cell proliferation (-15.82% (30.41), **p<0.01 vs bas).

Unlike ACA, UMP and ACC are rare malignancies, therefore only a small number of tumours were collected and presented here. Only one uncertain malignancy was silenced and tested for alterations in pro-mitotic activity (Fig. 5B), finding a trend of reduction (-40%) after IGF2R knock-down. On two different ACC, displayed in Fig. 5C, IGF2R silencing had similar results, a reduction of around 20% of cell proliferation, which did not result significant in either case, due to the technical impossibility to repeat the experiments

Effects of treatment with antiIGF2R neutralizing antibody on primary cell cultures proliferation are presented in Fig.6. On primary cultures, the antibody was administered at 20µg/mL, 5-times higher than on immortalized ACC cell cultures, allowing more than 90%

inhibition of IGF2R binding site. Assessment of alterations in ACA cell proliferation after treatment did not result in any significant change (Fig. 6A$_1$); however, stratification according to tumour secretion, aldosterone (APA) against cortisol producing adenomas (CPA), unmasked the anti-mitotic effect of the antiIGF2R antibody in CPA tumours, as illustrated in Fig.6A$_2$ (-9.84% (26.85), *p<0.05 vs bas). Coherently, cortisol secretion showed a trend towards reduction after the antiIGF2R treatment, as shown in Fig. 6B, even though no significant difference was evaluated.

One cortisol-secreting uncertain malignancy was treated with antiIGF2R, resulting in a significant decrease of cell proliferation, Fig. 6C (*p<0.05 vs bas). Interestingly, two ACC primary cultures treated with the neutralizing antibody had different responses, ACC#1 was unaltered by IGF2R inhibition (Fig.6D), while a marked reduction of cell proliferation can be observed in ACC#2 (-28.13, p=0.0571 vs bas). Similar to previous data, ACC#2 was featured by cortisol secretion, while ACC#1 culture derived from a non-functioning tumour.

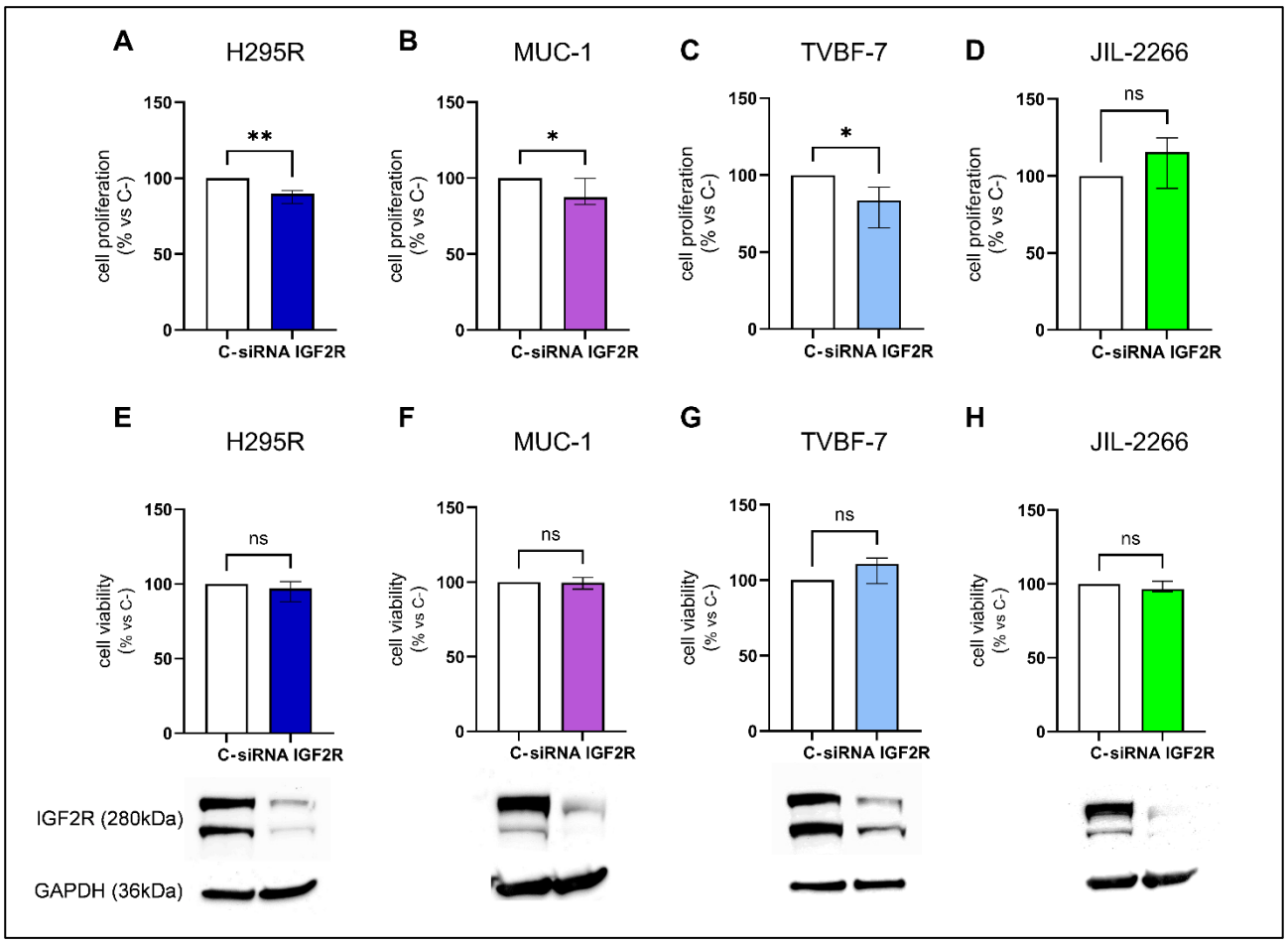

Figure 3. IGF2R silencing: effect on cell proliferation and viability of ACC cell lines. **A-D**) % of cell proliferation measured as BrdU incorporation after 3 (A-B-D) or 6 days (C) of IGF2R genetic silencing at 25 (A) or 37.5nM (B-C-D). Silencing efficiency >60% was considered for further analysis. Results of n>5 experiments, plotted as median ±IQR. **E-H**) % of cell viability, assessed via MTT test, after 3 (E-F-H) or 6 days (G) of IGF2R genetic silencing at 25 (E) or 37.5nM (F-G-H). Silencing efficiency >60% was considered for further analysis. Results of n>4 experiments, plotted as median ±IQR. A-H)

Representative immunoblots of silencing control (C- siRNA) and IGF2R (siRNA IGF2R) samples, showing IGF2R and corresponding GAPDH bands. Statistical analysis was performed via GraphPad Prism software, using Wilcoxon test. *p<0.05, **p<0.01 vs C- siRNA.

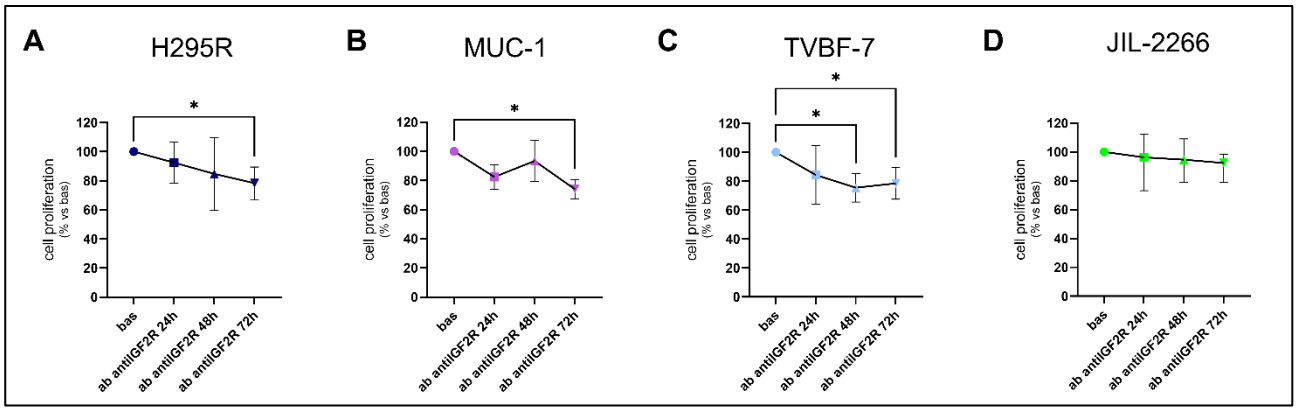

Figure 4. IGF2R inhibition: effect on cell proliferation of ACC cell lines. % of cell proliferation measured as BrdU incorporation after 24, 48, or 72h of 4µg/mL antiIGF2R antibody in starved medium. Results of n>4 experiments were plotted as median ±IQR. Statistical analysis was performed via GraphPad Prism software, using Kruskal-Wallis test coupled with Dunn's post hoc analysis. *p<0.05 vs bas.

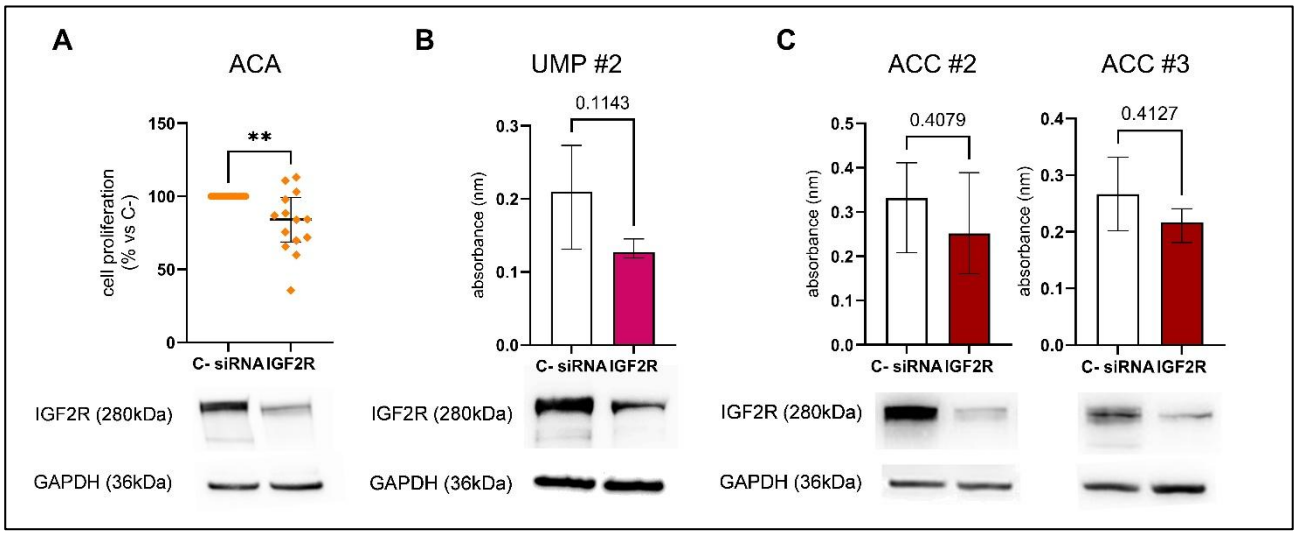

Figure 5. IGF2R silencing: effect on cell proliferation of ACA, UMP, and ACC primary cultures. **A**) % of ACA cell proliferation measured as BrdU incorporation after 3 days of IGF2R genetic silencing at 50nM. Silencing efficiency >60% was considered for further analysis. Results of n=14 primary cultures, plotted as individual dots with median ±IQR. Statistical analysis was performed via GraphPad Prism software, using Wilcoxon test. **p<0.01 vs C- siRNA. **B-C**) Cell proliferation measured as BrdU incorporation after 3 days of IGF2R genetic silencing at 50nM of UMP (B) or ACC (C). Silencing efficiency >60% was considered for further analysis. Absorbance values of a single experiment (5 technical replicates) were plotted as median ±IQR. Statistical analysis was performed via GraphPad Prism software, using Mann-Whitney test. A-C) Representative immunoblots of each tumour type for silencing control (C- siRNA) and IGF2R (siRNA IGF2R) samples, showing IGF2R and corresponding GAPDH bands.

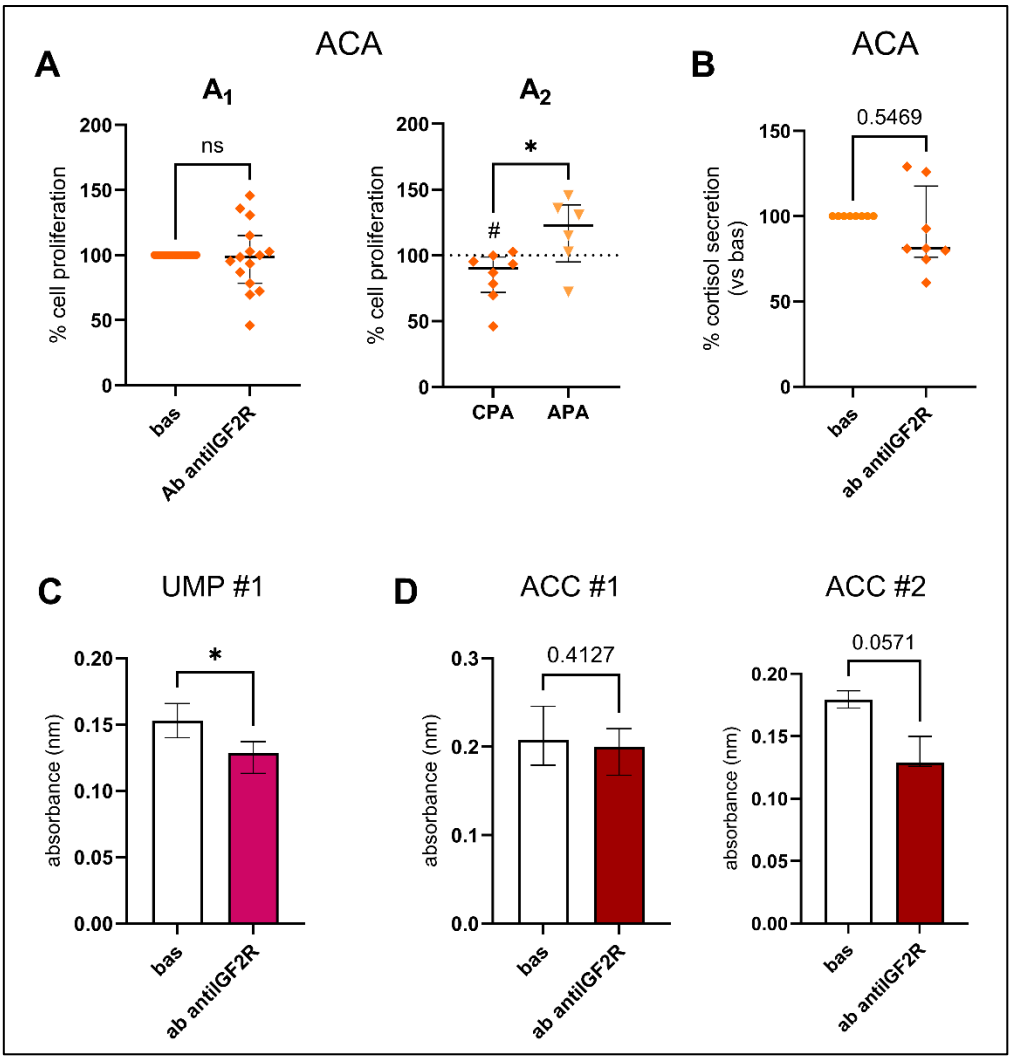

Figure 6. IGF2R inhibition: effect on cell proliferation and cortisol secretion of ACA, UMP, and ACC primary cultures. **A**) % of ACA cell proliferation measured as BrdU incorporation after 72h of 20µg/mL antiIGF2R antibody in starved medium. **A_1**) Results of n=15 primary cultures plotted as individual dots with median ±IQR. **A_2**) Stratification according to hormone secretion: 8 CPA and 6 APA plotted as individual dots with median ±IQR. Statistical analysis was performed via GraphPad Prism software, using Mann-Whitney test, *p<0.05 vs APA, #p<0.05 vs bas. **B**) % of CPA cortisol secretion after 72h of 20µg/mL antiIGF2R antibody in starved medium. 8 CPA plotted as individual dots with median ±IQR. Statistical analysis was performed via GraphPad Prism software, using Kruskal-Wallis test. **C-D**) Cell proliferation measured as BrdU incorporation after 72h of 20µg/mL antiIGF2R antibody in starved medium of UMP (C) or ACC (D). Absorbance values of a single experiment (5 technical replicates) were plotted as median ±IQR. Statistical analysis was performed via GraphPad Prism software, using Mann-Whitney test, *p<0.05 vs bas.

3. IGF2R modifications: transfecting IGF2R augments ACT cell growth

To ultimately prove IGF2R relevance in the pro-mitotic behaviour of ACT, IGF2R was transiently transfected with an EGFP-tagged plasmid to increase its expression, Fig. 7A-D. Coherently with the results previously obtained, after IGF2R transfection, cell proliferation resulted significantly increased in all ACC lines tested (+27.1% (31.6) in H295R, +10.2% (23.5) in MUC-1, +58.8% (62.9) in TVBF-7, +98.0 (38.7) in JIL-2266). Interestingly, JIL-2266 which express the lowest level of IGF2R among ACC cell lines, were highly impacted by IGF2R transfection, doubling their proliferative activity (Fig.7D), thus resulting an IGF2R-inducible line.

In line with proliferation data, in Fig.7E-H a significant rise in cell viability is displayed by all 4 cell lines (+24% (16.6) in H295R, +44.4% (48.4) in MUC-1, +15.9% (29.7) in TVBF-7, +61.3% (23.6) in JIL-2266, *p<0.05 vs EMPTY-EGFP). Similarly to the previous result, JIL-2266 are the line with the greatest increase of viability after IGF2R-transfection.

The effect of the transient IGF2R transfection was also assessed on cell proliferation of primary cultures. Unfortunately, ACA and UMP cultures were not successfully transfected; however, two ACC cultures, shown in Fig. 8, were tested. Coherently with the results obtained in immortalized cells, both ACC#2 (Fig.8A) and ACC#3 (Fig.8B) had a strong rise in their proliferative activity. In particular, ACC#2 cell proliferation was increased of around 3-fold after IGF2R-transfection (*p<0.05 vs EMPTY-EGFP), and ACC#3 pro-mitotic activity rose of +50% (p=0.053 vs EMPTY-EGFP).

In combination with the data illustrated in Section 2, these findings suggest a clear IGF2R involvement in ACT, and peculiarly in ACC, proliferative mechanism, questioning for the first time the dogma of the anti-oncogenic role of this IGF2 receptor.

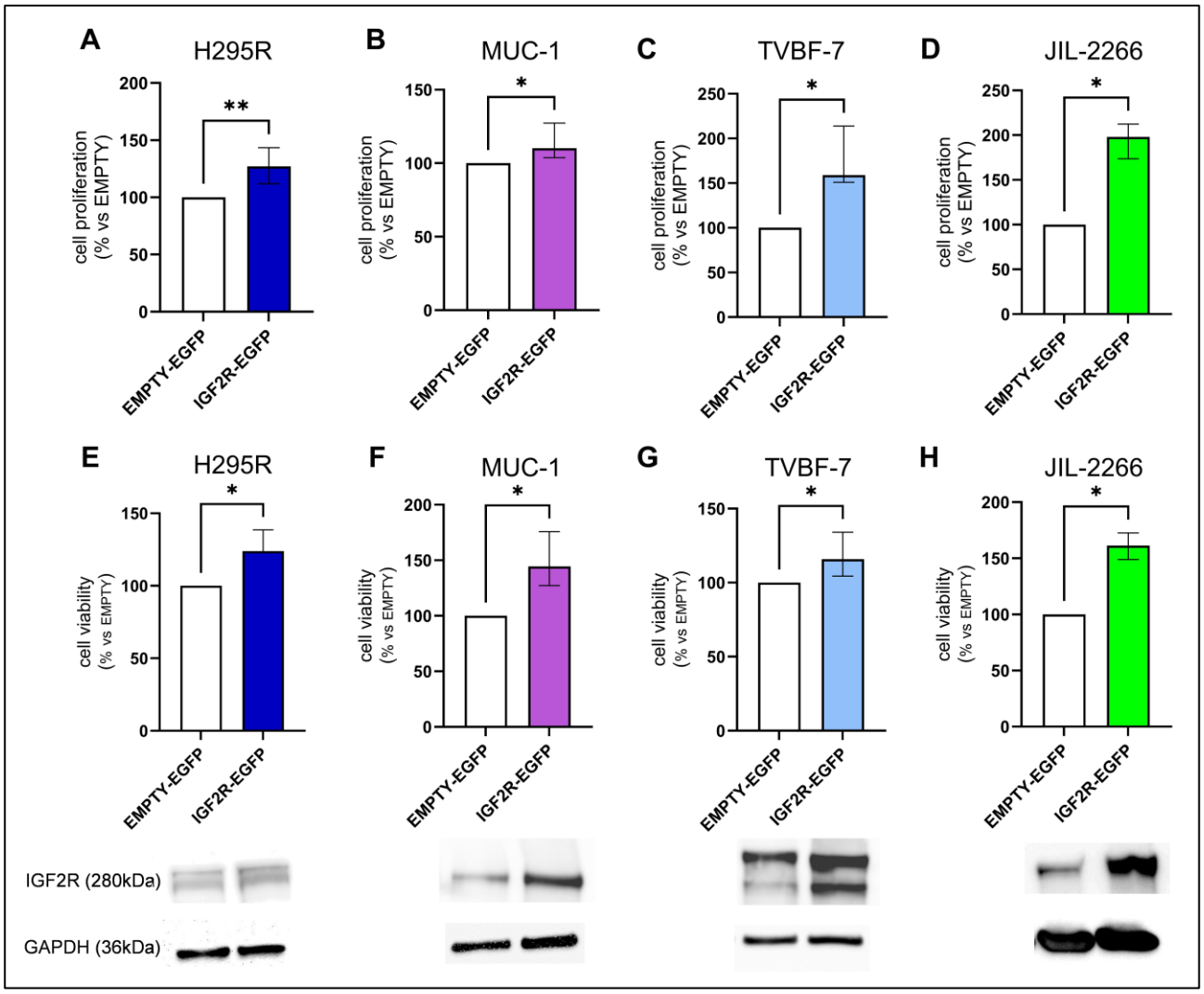

Figure 7. IGF2R transfection: effect on cell proliferation and viability of ACC cell lines. **A-D**) % of cell proliferation measured as BrdU incorporation after 48h of IGF2R-EGFP transient transfection at 1µg/µL. Successful transfection was verified via observation of EGFP fluorescent activation. Results of n>6 experiments, plotted as median ±IQR. **E-H**) % of cell viability, assessed via MTT test, after 48h of IGF2R-EGFP transient transfection at 1µg/µL. Successful transfection was observed via EGFP fluorescent activation. Results of n=6 experiments, plotted as median ±IQR. A-H) Representative immunoblots of transfection control (EMPTY-EGFP) and IGF2R (IGF2R-EGFP) samples, showing IGF2R and corresponding GAPDH bands. Statistical analysis was performed via GraphPad Prism software, using Wilcoxon test. *p<0.05, **p<0.01 vs EMPTY-EGFP.

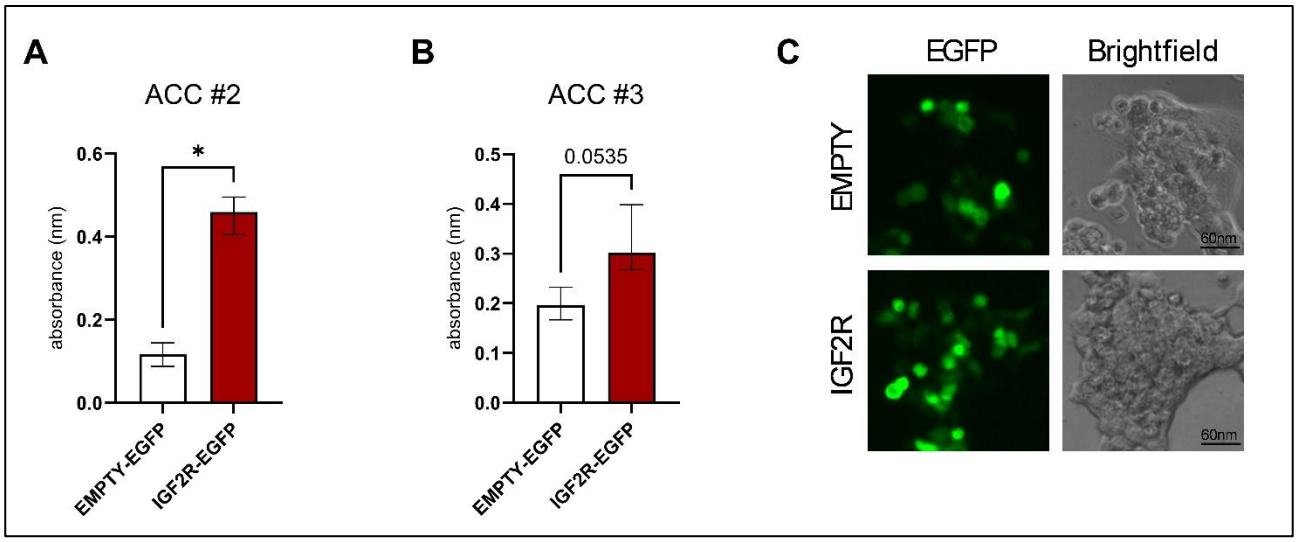

Figure 8. IGF2R transfection: effect on cell proliferation of 2 ACC primary cell cultures. **A-B**) Cell proliferation measured as BrdU incorporation after 48h of IGF2R-EGFP transient transfection at 1µg/µL. Absorbance values of a single experiment (5 technical replicates) were plotted as median ±IQR. Statistical analysis was performed via GraphPad Prism software, using Mann-Whitney test, *p<0.05 vs EMPTY-EGFP. **C**) Representative fluorescence images of ACC#2 transfection.

4. Understanding IGF2R action mechanism: IGF2-IGF2R axis and RA treatment

Since the predominant role of IGF2 in ACT and the previously demonstrated role of IGF2R in IGF2 internalization and degradation, the further step of the project was to test if IGF2 secretion, quantified as homogeneous among ACC lines (Fig. 2B), could be altered by IGF2R levels. ELISA assays shown that IGF2R silencing did not induce any change in the quantity of extracellular IGF2 (Fig.9A-C); however, only in H295R, transient IGF2R transfection determined a decrease of its extracellular levels, as shown in Fig.9D (0.58-fold (0.525), **p<0.01 vs EMPTY-EGFP).

Besides IGF2, IGF2R activity can be regulated by other ligands. Among them, retinoic acid (RA) binds IGF2R with high affinity, on a binding site distinct from those for IGF2, and it was demonstrated that it could facilitate IGF2 internalization, however, possible RA effects on IGF2 internalization rate in ACC have not been studied (93). For these reasons, the administration of retinoic acid (RA) was tested on H295R, representing the cell line which resulted most strongly affected by IGF2R alterations in terms of IGF2 extracellular levels.

In Fig. 10A, IGF2 extracellular levels of H295R resulted highly increased by 24h of 1µM RA treatment (4.41-fold (18.48), *p<0.05 vs bas). Interestingly, this was not dependent by an increased IGF2 transcription (Fig.10B), nor by a decrease of IGF2R transcription (Fig. 10C), suggesting that RA binding to IGF2R inhibited its ability to bind and internalize IGF2 in H295R.

This increase of extracellular IGF2 did not correspond to an increased cell proliferation, as expected from the mitogenic role of IGF2 in ACC cells. Indeed, RA treatment induced a dose-dependent reduction of H295R cell proliferation (Fig. 11A). This inhibitory effects was reverted in cells silenced for IGF2R, as shown in Fig.11B, where the anti-mitotic action exerted by RA on the control sample (-21.8% (35.7), *p<0.05 vs C- siRNA), was abolished after IGF2R knock-down (-16.3% (28.9)), demonstrating the need of IGF2R to promote the anti-mitotic action of RA. Furthermore, RA was able to reduce cellular proliferation on EMPTY-EGFP samples (-14.5% (22.5), **p<0.01 vs EMPTY-EGFP) and even more after IGF2R transfection (-27.5% (39.5), **p<0.01 vs IGF2R-EGFP), as displayed in Fig.11C.

Then, RA pro-apoptotic function was proved in H295R cells, where it significantly increased caspase 3 and 7 activation up to +60% (Fig.11D). Then, to strengthen the relevance of its pro-apoptotic role, the activation of the two caspases was assessed after either silencing and transfection: after IGF2R knock-down (Fig.11E), RA was still able to induce apoptosis (+139% C- siRNA+RA vs +112% IGF2R siRNA+RA), and after IGF2R transfection (Fig.11F), RA pro-apoptotic effect was similar to the control sample (+78% EMPTY-EGFP+RA vs +114.7% IGF2R-EGFP+RA, p=0.125). These observations suggest that in ACC models, the anti-proliferative RA action is IGF2R-mediated, while a different mechanism has to be searched for its pro-apoptotic effect.

To explain the finding that an increase of extracellular IGF2 did not correspond to an increase of cell proliferation, despite the well-known ability of IGF2 to promote cell growth after binding to IGF1R and IR, we tested the effect of RA on the expression of IGF binding proteins (IGFBPs), deputed to sequester IGF2 in the extracellular environment (70).

As illustrated in Fig.12A and B, the extracellular accumulation of IGF2 is accompanied by a transcriptional rise in IGFBP2 (1.14-fold (1.21), **p<0.01 vs bas) and IGFBP6 (2.85-fold (4.55), *p<0.05 vs bas), thus blocking its binding towards IGF1R or IR.

RA therapeutic potential was assessed also in several primary cell cultures, all displayed in Fig.13. Fig. 13A_1 depicts no change in cell proliferation after RA treatment, however, similarly to prior observations regarding antiIGF2R antibody, the effect of RA is partially masked by the different hormonal secretion of the analysed tumours, indeed CPA are statistically more affected by RA than APA (*p<0.05), who do not show any alteration in cell proliferation after treatment (Fig.13A_2). Analysing only RA-treated CPA, treatment induces

a trend in reducing cell proliferation, even though the difference is not statistically significant (-9.89% (37.13), p=0.0781 vs bas) (Fig. 13A_2).

Similarly, in Fig.13B, two different UMP primary cultures are displayed, and even though a trend of proliferative reduction is observable after RA treatment, no statistical significance was recorded.

Furthermore, RA was tested on ACC primary cultures both for its pro-apoptotic and anti-mitotic efficacy: in Fig. 13C ACC#2 showed a dose-dependent activation of caspase 3 and 7, which peaked at 10μM with a 35% apoptotic increase (*p<0.05 vs bas), while in Fig. 13D are displayed three different ACC cultures tested for RA inhibition of cell proliferation, which ultimately resulted in a 30% drop after treatment. Interestingly, all three ACC cultures were derived by cortisol producing tumours.

To test the role of IGF2R in mediating RA effects in ACC primary cultures, we transfected primary cultured cells with IGF2R-EGFP. As shown in Fig. 13E, RA treatment had a mild effect on control cells, but after IGF2R transient transfection it was able to strongly reduce cell proliferation (-43.7%).

Overall, our results suggest that retinoic acid can be considered a promising strategy to control the growth of ACC and of the cortisol producing subset of adrenocortical adenomas.

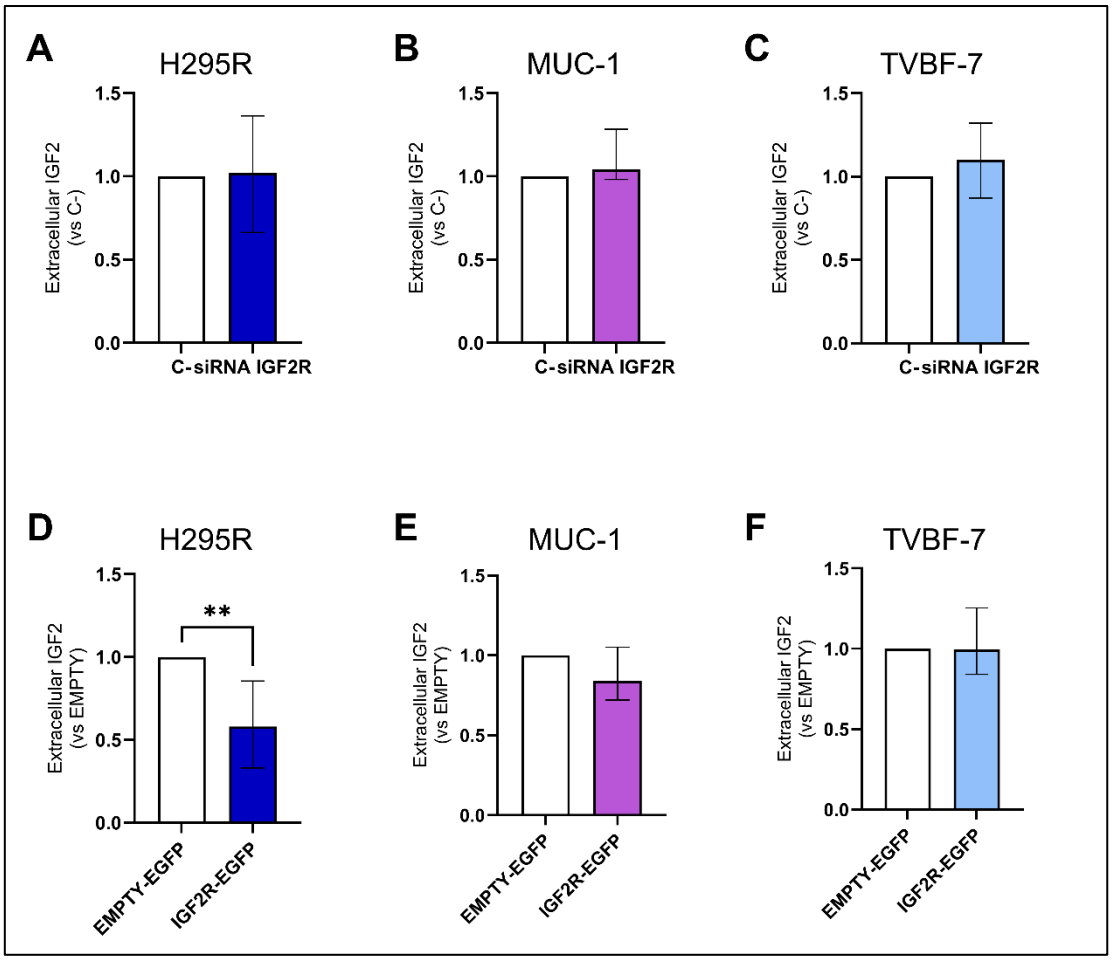

Figure 9. IGF2R silencing or transfection: effects on IGF2 extracellular levels. **A-C**) ELISA assessment of supernatant IGF2 quantities after 3 (A-B) or 6 days (C) of IGF2R genetic silencing at 25 (A) or 37.5nM (B-C). Silencing efficiency >60% was considered for further analysis. Results of n>7 experiments, plotted as median ±IQR. **D-F**) ELISA assessment of supernatant IGF2 quantities after 48h of IGF2R-EGFP transient transfection at 1µg/µL. Results of n>6 experiments, plotted as median ±IQR. Statistical analysis was performed via GraphPad Prism software, using Wilcoxon test. **p<0.01 vs EMPTY-EGFP.

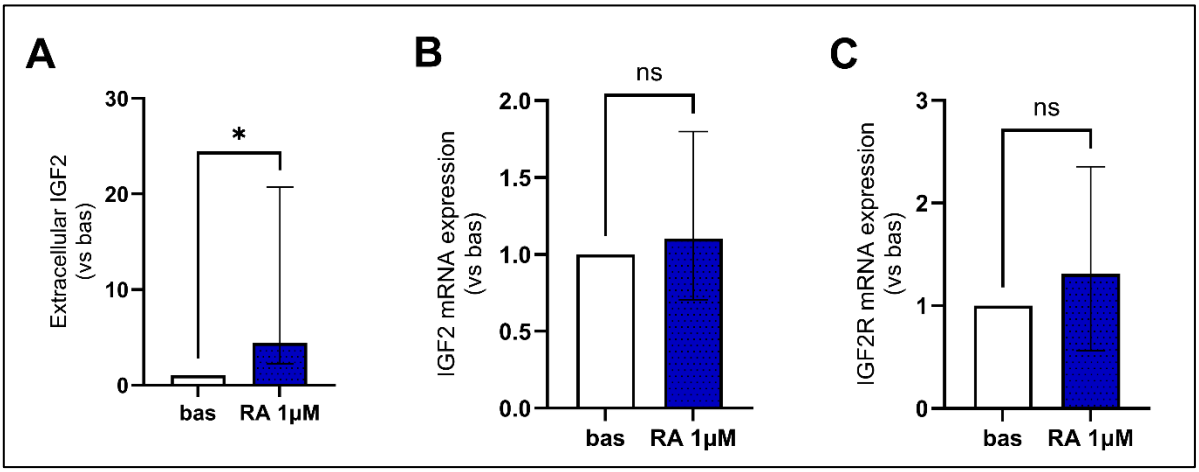

Figure 10. Retinoic acid effect on H295R: inhibition of IGF2-IGF2R. **A**) ELISA assessment of IGF2 quantity after 24h of 1µM RA treatment in starved medium. Results of n=6 experiments, plotted as median ±IQR. Statistical analysis was performed via GraphPad Prism software, using Wilcoxon test. *p<0.05 vs bas. **B-C**) IGF2 (B), IGF2R (C) mRNA relative expression, normalized on bas, evaluated through RT-qPCR after 3h of 1µM RA treatment in starved medium. Results of n>4 experiments, plotted as median ±IQR. Statistical analysis was performed via GraphPad Prism software, using Mann-Whitney test. *p<0.05, **p<0.01 vs bas.

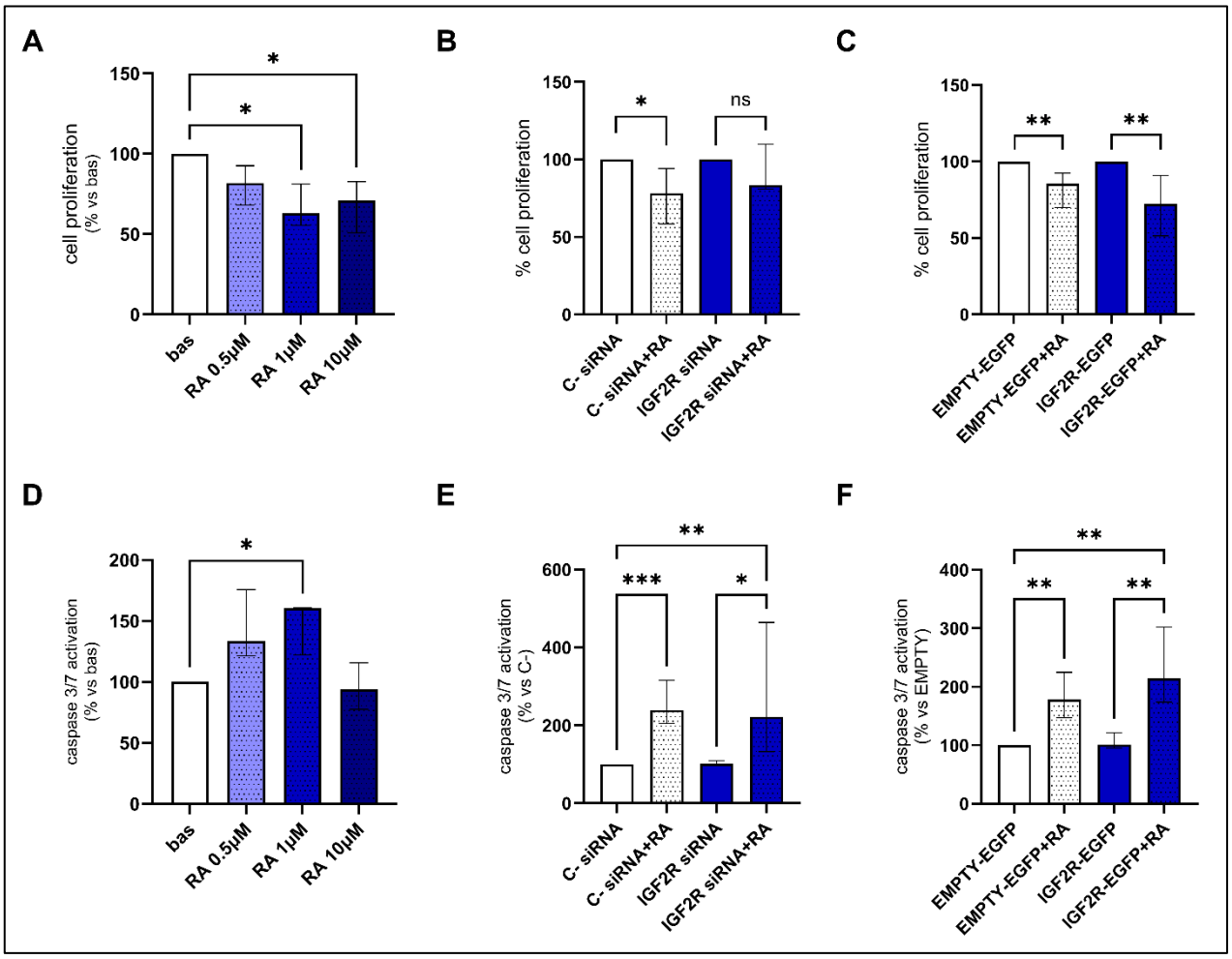

Figure 11. Retinoic acid effect on H295R: cell proliferation and apoptosis. **A**) % of cell proliferation, measured as BrdU incorporation after 24h treatment with 0.5, 1, or 10 µM RA in starved medium. Results of n=4 experiments were plotted as median ±IQR. Statistical analysis was performed via GraphPad Prism software, using Friedman test coupled with Dunn's post hoc analysis. *p<0.05 vs bas **B**) % of cell proliferation, measured as BrdU incorporation after 72h of IGF2R silencing at 25nM followed by 24h of 1µM RA treatment in starved medium. Both C-siRNA and IGF2R siRNA were set at 100%, and respective RA values were normalized consequently. Results of n=3 experiments were plotted as median ±IQR. Statistical analysis was performed via GraphPad Prism software, using Mann-Whitney test. *p<0.05 vs C- siRNA. **C**) % of cell proliferation, measured as BrdU incorporation after 48h of IGF2R-EGFP transient transfection at 1µg/µL followed by 24h of 1µM RA treatment in starved medium. Both EMPTY-EGFP and IGF2R-EGFP were set at 100%, and respective RA values were normalized consequently. Results of n=5 experiments were plotted as median ±IQR. Statistical analysis was performed via GraphPad Prism software, using Mann-Whitney test. **p<0.01 vs EMPTY-EGFP or IGF2R-EGFP. **D**) % of cell apoptosis, measured as caspase 3 and 7 activation, after 24h treatment with 0.5, 1, or 10 µM RA in starved medium. Results of n=4 experiments were plotted as median ±IQR. Statistical analysis was performed via GraphPad Prism software, using Kruskal-Wallis test coupled with Dunn's post hoc analysis. *p<0.05 vs bas. **E**) % of cell apoptosis, measured as caspase 3 and 7 activation, after 72h of IGF2R silencing at 25nM followed by 24h of 1µM RA treatment in starved medium. Results of n=4 experiments were plotted as median ±IQR. Statistical analysis was performed via GraphPad Prism software, using Kruskal-Wallis test coupled with Dunn's post hoc analysis. *p<0.05, **p<0.01, ***p<0.001. F) % of cell apoptosis, measured as caspase 3 and 7 activation, after 48h of IGF2R-EGFP transient transfection at 1µg/µL followed by 24h of 1µM RA treatment in starved medium. Results of n=4 experiments were plotted as median ±IQR. Statistical analysis was performed via GraphPad Prism software, using Kruskal-Wallis test coupled with Dunn's post hoc analysis. **p<0.01

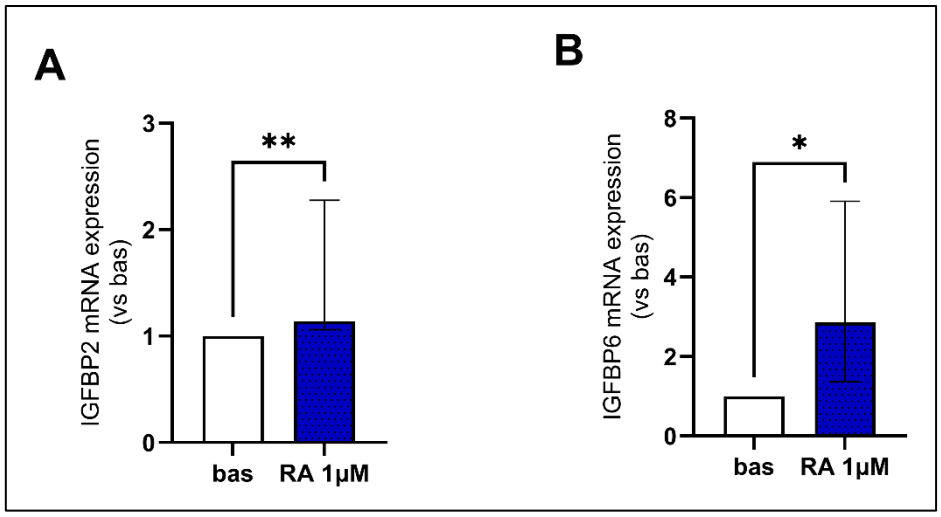

Figure 12. Retinoic Acid effect on IGFBP overexpression in H295R. IGFBP2 (A) and IGFBP6 (B) mRNA relative expression, normalized on bas, evaluated through RT-qPCR after 3h of 1µM RA treatment in starved medium. Results of n>4 experiments, plotted as median ±IQR. Statistical analysis was performed via GraphPad Prism software, using Mann-Whitney test. *p<0.05, **p<0.01 vs bas.

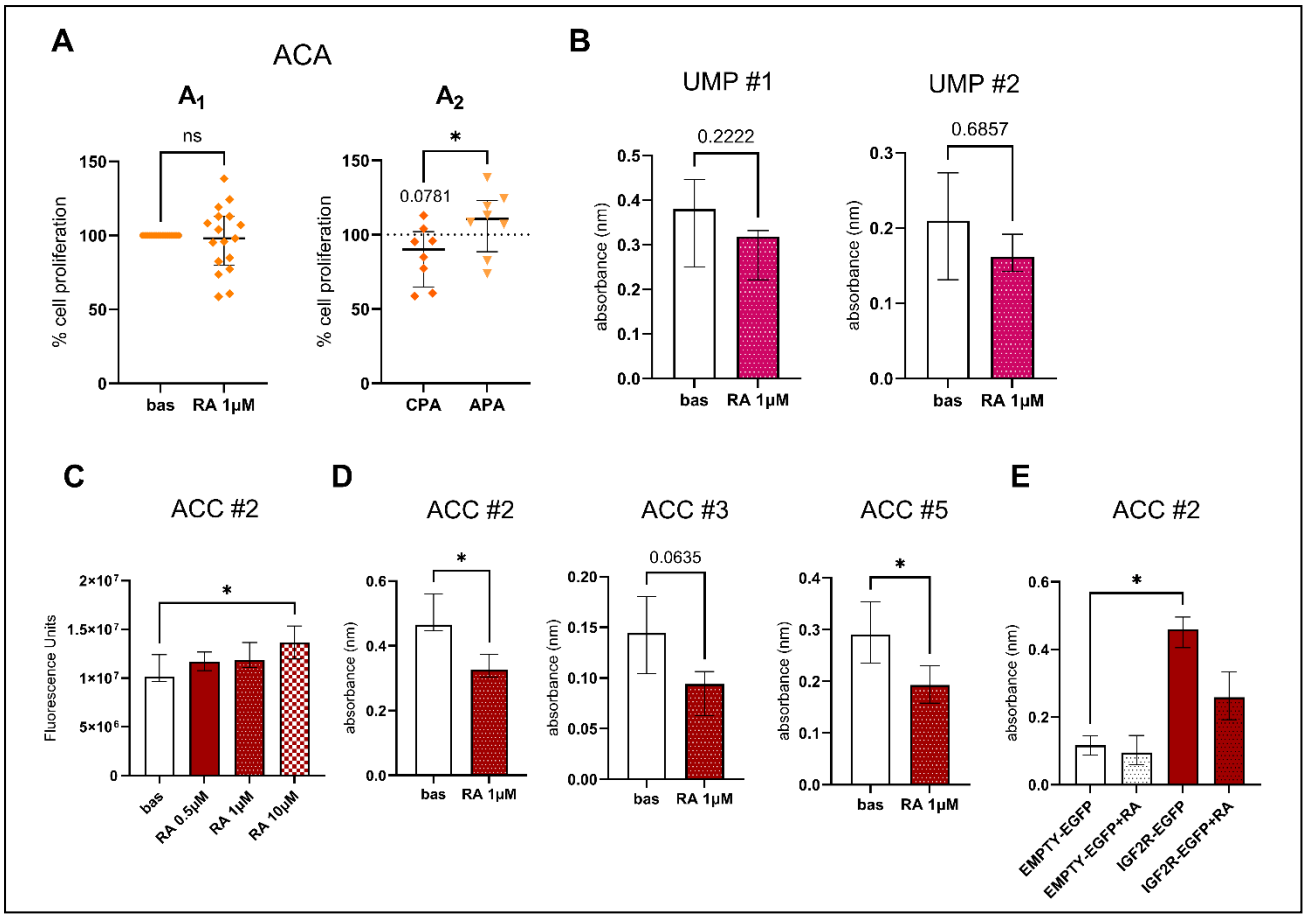

Figure 13. Retinoic acid effect on ACA, UMP, and ACC: cell apoptosis and proliferation. **A**) % of ACA cell proliferation measured as BrdU incorporation after 24h of 1µM RA in starved medium. **A_1**) Results of n=17 primary cultures plotted as individual dots with median ±IQR. **A_2**) Stratification according to hormone secretion: 8 CPA and 8 APA plotted as individual dots with median ±IQR. Statistical analysis was performed via GraphPad Prism software, using Mann-Whitney test, *p<0.05 vs APA, p=0-0781 vs bas. **B**) Cell proliferation measured as BrdU incorporation after 24h of 1µM RA in starved medium of two UMP primary cell cultures. Absorbance values of a single experiment (5 technical replicates) were plotted as median ±IQR. Statistical analysis was performed via GraphPad Prism software, using Mann-Whitney test. **C**) Cell apoptosis measured as caspase 3 and 7 activation after 24h of 0.5, 1, 10µM RA in starved medium of one ACC. Fluorescence Unit values of a single experiment (5 technical replicates) were plotted as median ±IQR. Statistical analysis

was performed via GraphPad Prism software, using Kruskal-Wallis test coupled with Dunn's post hoc analysis, *p<0.05 vs bas. **D**) Cell proliferation measured as BrdU incorporation after 24h of 1μM RA in starved medium of three ACC primary cell cultures. Absorbance values of a single experiment (5 technical replicates) were plotted as median ±IQR. Statistical analysis was performed via GraphPad Prism software, using Mann-Whitney test, *p<0.05 vs bas. **E**) Cell proliferation measured as BrdU incorporation after 48h of IGF2R-EGFP transient transfection at 1μg/μL followed by 24h of 1μM RA in starved medium of one ACC primary cell cultures. Absorbance values of a single experiment (5 technical replicates) were plotted. Statistical analysis was performed via GraphPad Prism software, using Kruskal-Wallis test coupled with Dunn's post hoc analysis. *p<0.05 vs IGF2R-EGFP.

5. Understanding IGF2R action mechanism: downstream SphK activation

Even though IGF2R has been addressed as anti-oncogenic both in ACT and in other type of tumours for a long time, lately some studies hypothesised its role as precursor in the activation of the SphK-S1P axis, possibly contributing to the increase of pro-mitotic activity and overall tumour growth. For this instance, we analysed the expression levels of both SphK isoforms, 1 and 2, in the aforementioned *in vitro* ACT models.

SphK1, the isoform most often related to pro-tumoral behaviour, was homogeneously expressed among ACC, ACA, and NA at transcription level, as illustrated in Fig. 14A. However, the protein quantification, shown in Fig. 14B and the relative immunoblots (Fig. 14C), clearly depicts a statistical difference between ACT, both ACC and ACA, and NA, with a strong overexpression of SphK1 in the tumoral populations compared to normal adrenal tissue (7.32-fold vs H295R cells (7.24) in ACC, 4.31-fold vs H295R cells (8.32) in ACA, vs 0.87-fold vs H295R cells (0.21) in NA).

In Fig. 14D, SphK2 showed a differential expression at the transcript level, with ACA bearing significantly higher levels of SphK2 compared to ACC (0.0156 (0.0062) vs 0.0019 (0.0037), ****p<0.0001). However, this was not confirmed by protein analysis, where SphK2 resulted homogeneously expressed by the three categories (Fig. 14E).

The same analysis was conducted also among the 4 ACC cell lines and presented in Fig. 15. mRNA levels of SphK1 significantly peaked in MUC-1 compared to H295R and TVBF-7 cells (**p<0.01, Fig. 15A), while SphK2 transcript expression was significantly higher in H295R and TVBF-7 compared to JIL-2266 (0.0051 (0.0013), 0.0031 (0.0011), 0.0004 (0.0003) respectively, Fig.15B). Interestingly, as shown in Fig. 15C, SphK1 protein level mimicked the transcript, with a marked overexpression in MUC-1 (1.77 (4.63)) and JIL-2266 (1.08 (2.93)) compared to H295R (0.14 (0.15)) and TVBF-7(0.06 (0.34)). Conversely, SphK2 resulted similarly expressed among the 4 cell lines (Fig. 15D).

To test the hypothesis of the IGF2R-downstream SphK activation, SphK activity was quantified after IGF2R silencing, inhibition, or transfection in different ACT models. The

results are illustrated in Fig.16. TVBF-7 were chosen as representative model for testing SphK activity after IGF2R genetic alterations, due to their higher sensitivity at IGF2R modifications, as demonstrated by the marked proliferative reduction after silencing and the corresponding elevated increase after IGF2R transfection. As expected, after silencing, Fig. 16A, SphK activity is downregulated (-14.93 (20.4), *p<0.05 vs C- siRNA), while coherently, after IGF2R transfection, Fig. 16B, SphK activity is significantly increased (+35.76 (70.7), *p<0.05 vs EMPTY-IGF2R). Moreover, also one ACC primary culture was silenced and assessed for any variation in SphK activity, which resulted reduced after IGF2R silencing, even though not significantly (-29.04% (39.22), p=0.10 vs C- siRNA, Fig. 16C). A further confirmation of the IGF2R-induced SphK activity derived from the specific treatment with the antiIGF2R neutralizing antibody: both MUC-1 cells (Fig. 16D) and ACA (Fig. 16E) showed a significant drop in SphK activity after treatment (-65.26% (64.28) and -12.01% (24.26), respectively), and the only ACC culture tested had a reduction of -11.92% (Fig. 16F).

Overall, these data suggest that the downstream mechanism of pro-mitotic IGF2R activity involves a IGF2R-dependent SphK activation. The SphK/S1P pathway has been already addressed as pro-growth and pro-survival in other tumoral models, since it can increase cell proliferation via ERK1/2, contrast apoptosis, via P13k/Akt, or stimulate migration, via Rac/PLC.

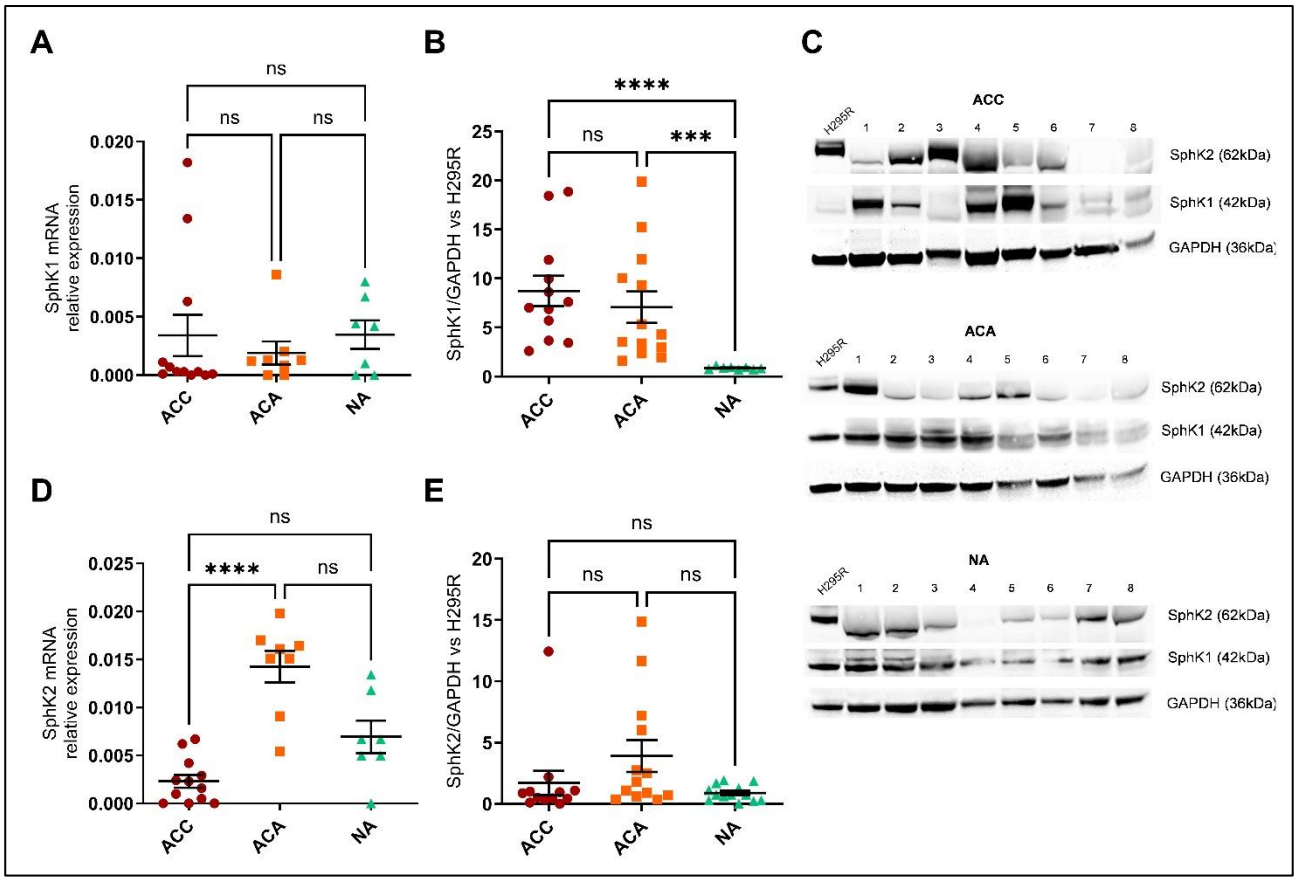

Figure 14. SphK1 and SphK2 differential expression in ACC, ACA, and NA tissues. **A-D**) SphK1 (A) and SphK2 (D) mRNA relative expression evaluated through RT-qPCR on tumoral tissue. n=12 ACC, 8 ACA, 7 NA. Results were plotted as individual dots, plus median ±IQR. Statistical analysis was performed via GraphPad Prism software, using Kruskal-Wallis test coupled with Uncorrected Dunn's post hoc analysis. ****p<0.001 vs ACA. **B-E**) Western blot analysis of SphK1 (B) and SphK2 (E) protein levels of tumoral tissue of ACC, ACA, and NA, normalized on GAPDH housekeeping levels. n=12 ACC, 13 ACA, 13 NA. Results were plotted as single dots, plus median ±IQR of SphK1/GAPDH ratio normalized on H295R expression levels. Statistical analysis was performed via GraphPad Prism software, using Kruskal-Wallis test coupled with Uncorrected Dunn's post hoc analysis. ***p<0.001, ****p<0.0001 vs NA. **C**) Representative immunoblot of H295R and 8 tumours of each type showing corresponding SphK1, SphK2, and GAPDH bands.

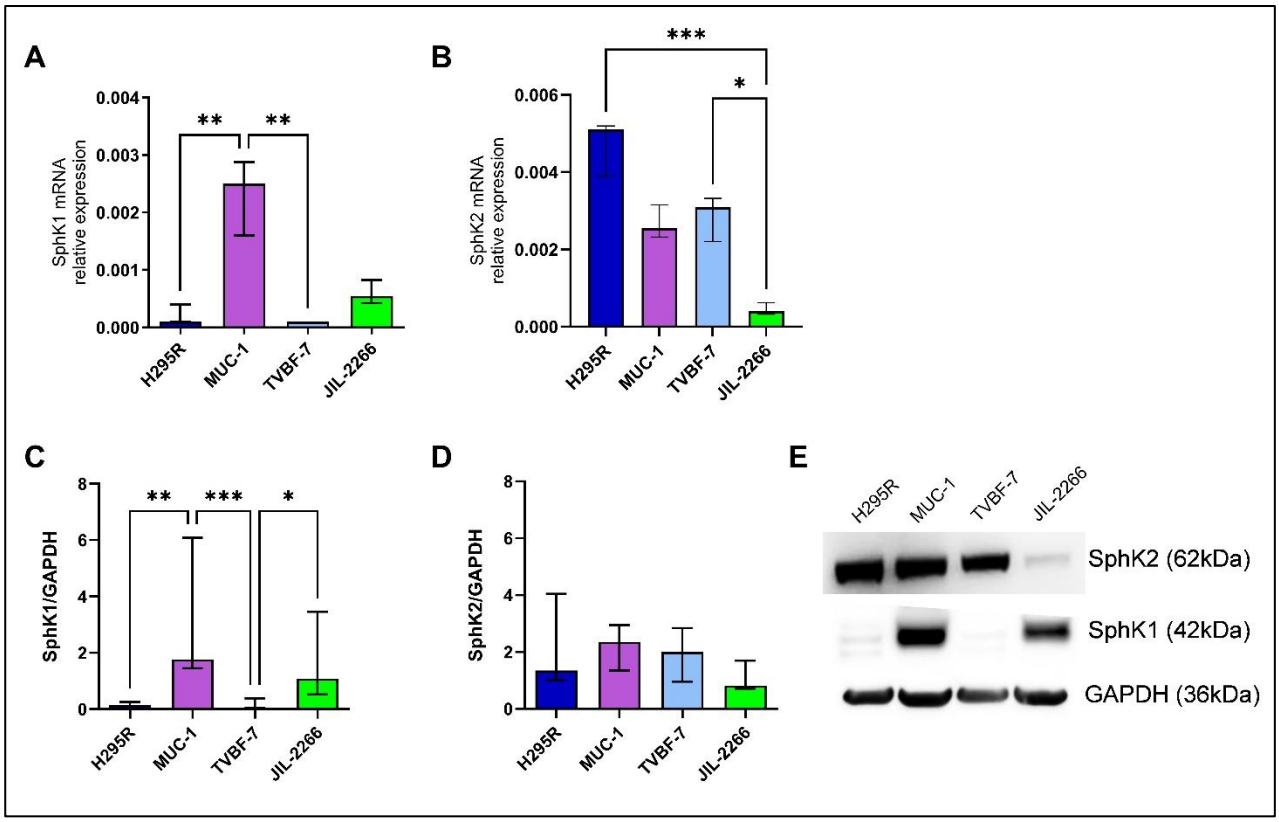

Figure 15. SphK1 and SphK2 differential expression in 4 ACC cell lines. **A-B**) SphK1 (A) and SphK2 (B) mRNA relative expression evaluated through RT-qPCR on H295R, MUC-1, TVBF-7, and JIL-2266 cells. n=4 results were plotted as median ±IQR. Statistical analysis was performed via GraphPad Prism software, using Kruskal-Wallis test coupled with Uncorrected Dunn's post hoc analysis. *p<0.05, **p<0.01, ***p<0.001. **C-D**) Western blot analysis of SphK1 (C) and SphK2 (D) protein levels of H295R, MUC-1, TVBF-7, and JIL-2266, normalized on GAPDH housekeeping levels. n=5. SphK/GAPDH ratio data were plotted as median ±IQR. Statistical analysis was performed via GraphPad Prism software, using Kruskal-Wallis test coupled with Uncorrected Dunn's post hoc analysis. *p<0.05, **p<0.01, ***p<0.001. **E**) Representative immunoblot showing SphK1, SphK2, and GAPDH levels.

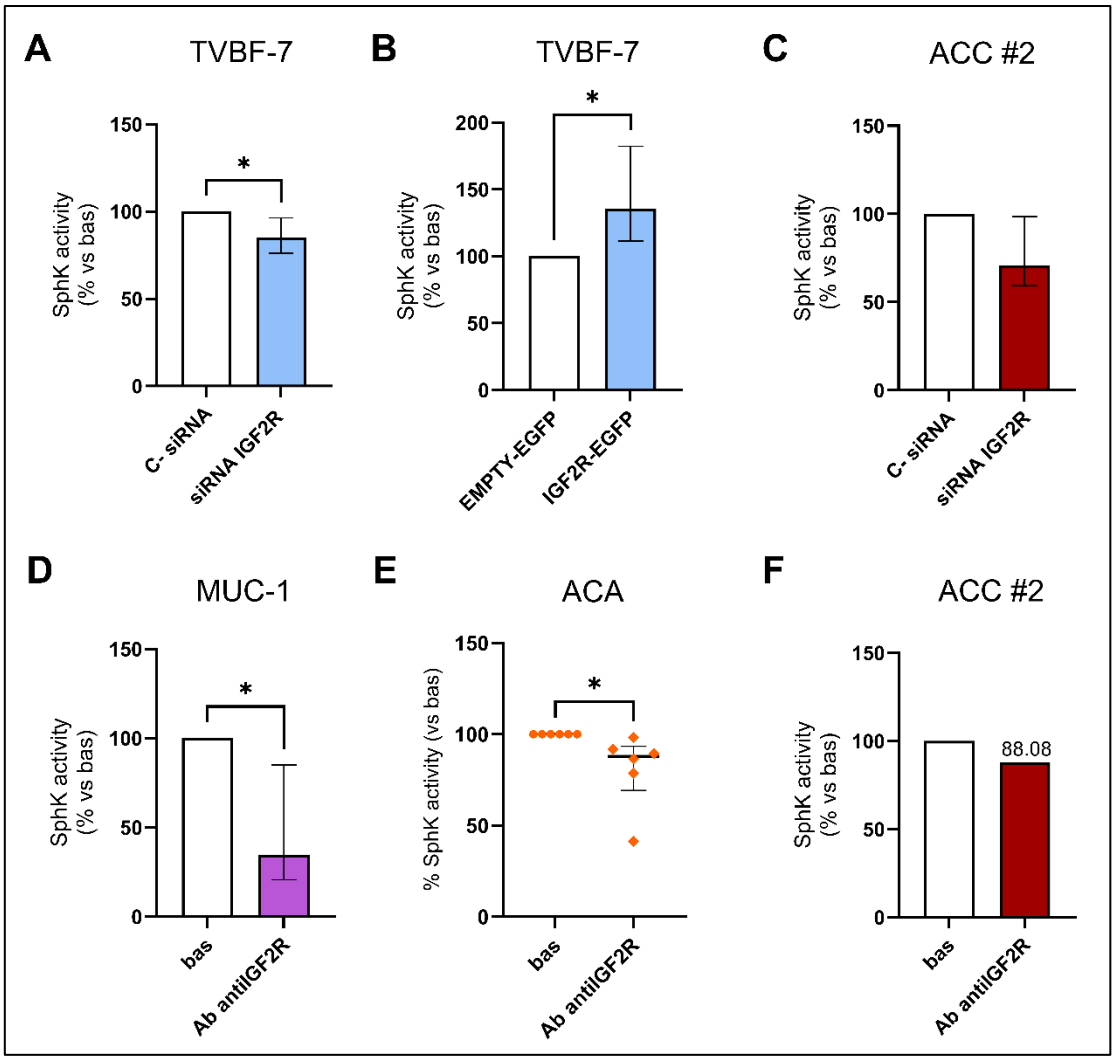

Figure 16. Evaluation of SphK activity after IGF2R silencing, inhibition or transfection in different ACT models. **A**) % of SphK activity, measured as ATP consumption in TVBF-7 cells after 6 days of IGF2R genetic silencing at 37.5nM. Results of n=7 experiments, plotted as median ±IQR. Statistical analysis was performed via GraphPad Prism software, using Wilcoxon test. *p<0.05 vs C- siRNA. **B**) % of SphK activity, measured as ATP consumption in TVBF-7 cells after 8h of IGF2R-EGFP transient transfection at 1µg/µL. Results of n=6 experiments, plotted as median ±IQR. Statistical analysis was performed via GraphPad Prism software, using Wilcoxon test. *p<0.05 vs EMPTY-IGF2R. **C**) % of SphK activity, measured as ATP consumption in one ACC primary cell culture after 3 days of IGF2R genetic silencing at 50nM. Results of n=3 experiments, plotted as median ±IQR. **D**) % of SphK activity, measured as ATP consumption in MUC-1 cells after 72h of 4µg/mL antiIGF2R antibody in starved medium. Results of n=6 experiments, plotted as median ±IQR. Statistical analysis was performed via GraphPad Prism software, using Wilcoxon test. *p<0.05 vs bas. **E**) % of SphK activity, measured as ATP consumption in ACA primary cultures after 72h of 20µg/mL antiIGF2R antibody in starved medium. Results of n=6 ACA, plotted as individual dots, with median ±IQR. Statistical analysis was performed via GraphPad Prism software, using Wilcoxon test. *p<0.05 vs bas. **F**) % of SphK activity, measured as ATP consumption in one ACC primary culture after 72h of 20µg/mL antiIGF2R antibody in starved medium.

6. SphK as novel therapeutic target in ACC

Due to the limited therapeutic options currently offered to ACT patients, particularly those suffering from advanced or metastatic ACC, there is an urgent need of new druggable targets. Since it has been demonstrated in this project that the IGF2R-SphK interconnection has a pro-mitotic and pro-survival connotation, targeted drugs against SphK can represent a novel therapeutic strategy for ACT.

Therefore, two different SphK inhibitors have been tested on several *in vitro* endpoints. Safingol (SAF) is a pan-SphK inhibitor, already used in two phase I clinical trials on solid tumours, involving also a small number of ACC patients and giving positive results as metastases regression or prolonged stabilization of the disease (84). The other inhibitor, fingolimod (FTY), mainly targeted at inhibiting SphK1, was tested in different preclinical models of ACC, showing an efficient tumour suppression (80). However, the lack of in-depth *in vitro* studies in ACT opened the possibility to fill this literature gap.

Firstly, the IC50 of the four different ACC cell lines under evaluation has been experimentally calculated, as illustrated in Fig. 17. Cell viability data, obtained via MTT assay, allowed to plot a specific curve for each cell line and obtain the relative IC50. SAF IC50 after 72h treatment, shown in Fig. 17A, correspond to 5μM for H295R, 3.8μM for MUC-1, 7μM for TVBF-7, and 4μM for JIL-2266 cells. Moreover, in Fig. 17B, FTY IC50 curves are presented, with values corresponding to 8μM for H295R, 2.7μM for MUC-1, 5μM for TVBF-7, and 4.2μM for JIL-2266 cells. It can be observed that the two cell lines featured by higher quantities of SphK1, MUC- and JIL-2266, are more sensitive towards the two inhibitors, indeed we found a trend in negative correlation between the IC50 of SAF and FTY and the protein level of SphK1 ($r=-1.0$, $p=0.0833$ for SAF, $r=-0.8$, $p=0.33$; data not shown).

To prove the anti-tumoral action of SAF and FTY, upon the quantification of the IC50 relative to cell viability, concentrations close to the IC50 were tested to evaluate alterations in cell proliferation and apoptosis. In Fig. 18A-D are displayed results obtained after SAF treatment: in each ACC line, cell proliferation after 72h of SAF was more than halved, resulting in a significant decrease (*$p<0.05$ vs bas). Furthermore, cell apoptosis (Fig. 18E-H), induced after only 24h of treatment, was strongly increased, up to 3.5-times more in TVBF-7 cells (Fig. 18G). Caspase 3 and 7 activation was promoted by SAF in all cell lines.

Fig. 19 displays the anti-proliferative and pro-apoptotic effect of the FTY treatment. Similarly to the results shown before, 72h of FTY treatment at concentrations slightly higher than IC50 induced a significant reduction of cell proliferation in all cell lines (Fig. 19A-D). Conversely to what observed for SAF, FTY was not able to increase caspase 3 and 7 activation in all cell lines, even though it determined a significant increase in MUC-1 (+79.6% (142.6), *$p<0.05$ vs bas, Fig. 19F), TVBF-7 (+360.7% (253.7), *$p<0.05$ vs bas, Fig. 19G), and JIL-2266 (+243.9% (256.5), **$p<0.01$ vs bas, Fig. 19H), H295R (Fig. 19E) were not affected by FTY treatment at either dosage.

Investigation of SAF and FTY action on primary cell cultures was conducted on several samples. Fig. 20 illustrates the data obtained after either SAF or FTY treatment on ACA primary cultures. Similarly to ACC cell lines, both SAF and FTY were able to significantly decrease cell proliferation, Fig. 20A, and stimulate apoptosis in ACA, Fig. 20B. Moreover, on CPA, cortisol secretion after treatment resulted significantly hampered by both SAF and FTY (Fig. 20C). Interestingly, as observed before, stratification according to hormonal secretion resulted in a differential cell proliferation response between APA and CPA (Fig. 20D): APA did not respond after 72h of SAF 7.5μM, while CPA proliferation was strongly reduced by the same treatment (+48.7% (123.78) vs -15.02% (39.51), **p<0.01); on the opposite, a higher anti-mitotic effect on APA vs CPA was observed after FTY 10μM treatment (-81.92% (37.81) vs -37.85% (78.04), p=0.068). A similar trend can be observed in cell apoptosis, however no significant difference was recorded (Fig. 20E).

Coherently, SAF and FTY resulted efficient in contrasting UMP and ACC *in vitro* growth, as shown in Fig. 21. Particularly, all three UMP treated with SAF had a significant rise of caspase 3 and 7 activation, determining cell apoptosis (Fig. 21A-C). SAF was also able to reduce cell proliferation in UMP#1 and #2, both hormone secreting tumours. Interestingly, FTY was able to significantly decrease cell proliferation and induce apoptosis in UMP#1 (Fig. 21A), while it had no effect on UMP#3 (Fig. 21C). In ACC primary cultures, both SAF and FTY significantly impacted on the endpoints evaluated, halving cell proliferation and doubling caspases activation (Fig. 21D-E). Moreover, in ACC#2, cortisol secretion was investigated as well, as displayed in Fig. 21D. It emerged that cortisol production was reduced more than 90% after treatment with the higher concentration of either SAF (9.24%) or FTY (8.97%).

To confirm the specific effect of SphK inhibitors on reducing SphK activity, the same kit used in Section 5 was used to quantify SphK activity after inhibitors incubation. As shown in Fig. 22A in MUC-1 cells, 72h SAF inhibition is sufficient to significantly decrease SphK activity (-52.87% (52.95), *p<0.05 vs bas). Thus, the same treatment time was used to verify the inhibition in primary cultures of ACA (Fig. 22B), UMP (Fig. 22C), and ACC (Fig. 22D-F): as expected, in ACA primary cultures, both SAF (-28.74% (72.82), *p<0.5 vs bas) and FTY (-51.64% (73.92), *p<0.05 vs bas) significantly reduced SphK activity. UMP and ACC primary cultures, due to the rarity of material were tested only once, thus no significance has been assessed, however a trend in SphK reduction after both SAF and FTY treatment is observable particularly in UMP#2 and ACC#3 after SAF 10μM treatment (-29.4%, Fig. 22C,

and -39.66%, Fig.22E, respectively). Moreover, in ACC#4 SphK activity was halved by both SAF and FTY at 10μM (-54.18% and -47.4% respectively, Fig. 22F).

Moreover, IGF2R-mediated action of SphK inhibitors was confirmed after transfection of both JIL-2266, the IGF2R-inducible cell line, and one primary culture. In both cases, SphK inhibitors treatment at concentrations below statistical significance was not efficient in reducing cell proliferation on basal cells, while after IGF2R-transfection both SAF and FTY were able to significantly decrease proliferation (Fig. 23).

To complete the evaluation of SphK inhibitors as new potential therapeutics for ACC we assessed the combinatory effect of SAF and FTY with the current therapeutic strategy, the EDP-M scheme, on cell viability.

Based on previous literature on EDP-M treatment in ACC, it was administered for 24h, alone or in combination with SAF or FTY, at 3 different concentrations, ⅛, ¼, or half of the IC50. Coherently, SAF and FTY were administered at 3 dosages: one inferior, one similar, and one superior to the 72h IC50 previously assessed (Fig. 17). Moreover, with SynergyFinder+ tool, the possible synergism between the drugs was quantified according to two mathematical models: Bliss and HSA.

Fig. 24 displays the result of combinatory treatment of SAF and EDP-M, which resulted in an additive effect (-10< Synergy Score <+10) in all the ACC cell lines evaluated; however, no synergy was observed (Synergy Score >10). High Synergy Scores were reported for MUC-1 (Bliss=+3.36, HSA=+7.51, Fig. 24B) and TVBF-7 (Bliss=+4.29, HSA=+9.65, Fig. 24C), possibly due to the fact that these two cell lines derived from patients resistant to EDP-M treatment, thus the combination with another drug has a stronger anti-proliferative effect. Coherently, the highest Synergy Scores of FTY+EDP-M treatment were obtained in the same two cell lines: confirming an additive effect in TVBF-7 (Bliss=+5.37, HSA=+6.79, Fig. 25C) and resulting in a synergic behaviour in MUC-1 cells (Bliss=+12.81, HSA=+10.10, Fig. 25B). Moreover, both H295R and JIL-2266 showed an additive effect after FTY+EDP-M treatment (Fig. 25A/D).

The same investigation was conducted on one ACC primary cell culture, as illustrated in Fig. 26. Combinatory treatment of SAF+EDP-M resulted additive, with Synergy Scores of +0.50 and +9.17 according to Bliss and HSA models respectively (Fig. 26A). Similarly, also FTY+EDP-M co-treatment resulted additive (Fig. 26B), even though Synergy Scores

resulted lower than after SAF treatment (-5.91 and +7.34 according to Bliss and HSA respectively).

These analyses demonstrate that SphK inhibitors could have a promising therapeutic role in ACT treatment, being able to reduce cell viability, proliferation, and cortisol secretion and to stimulate apoptosis by controlling the IGF2R-SphK axis.

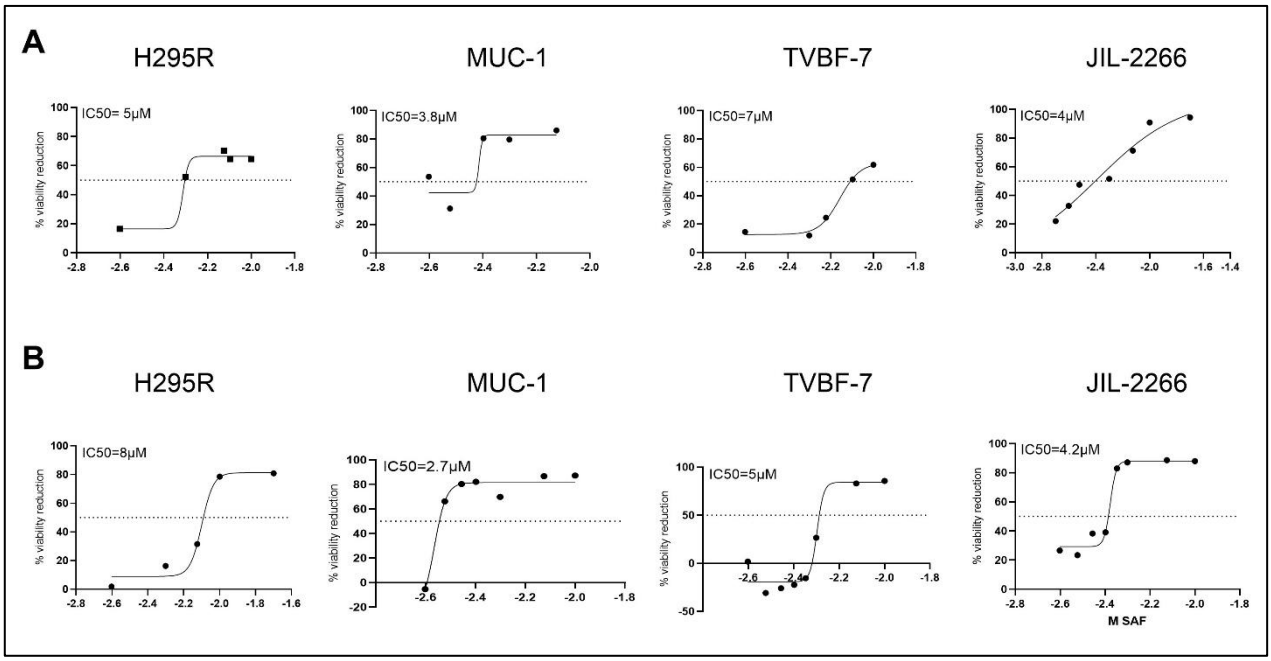

Figure 17. Determination of IC50 curves of cell viability after SAF and FTY treatment on ACC cell lines. Cell viability assessed via MTT assay, after 72h of increasing concentrations of SAF (**A**) or FTY (**B**) in starved medium. IC50 curves are built over the % of viability reduction and the logarithm of the drug concentration. 50% viability reduction is highlighted by a dotted line and each IC50 value is reported in the corresponding graph.

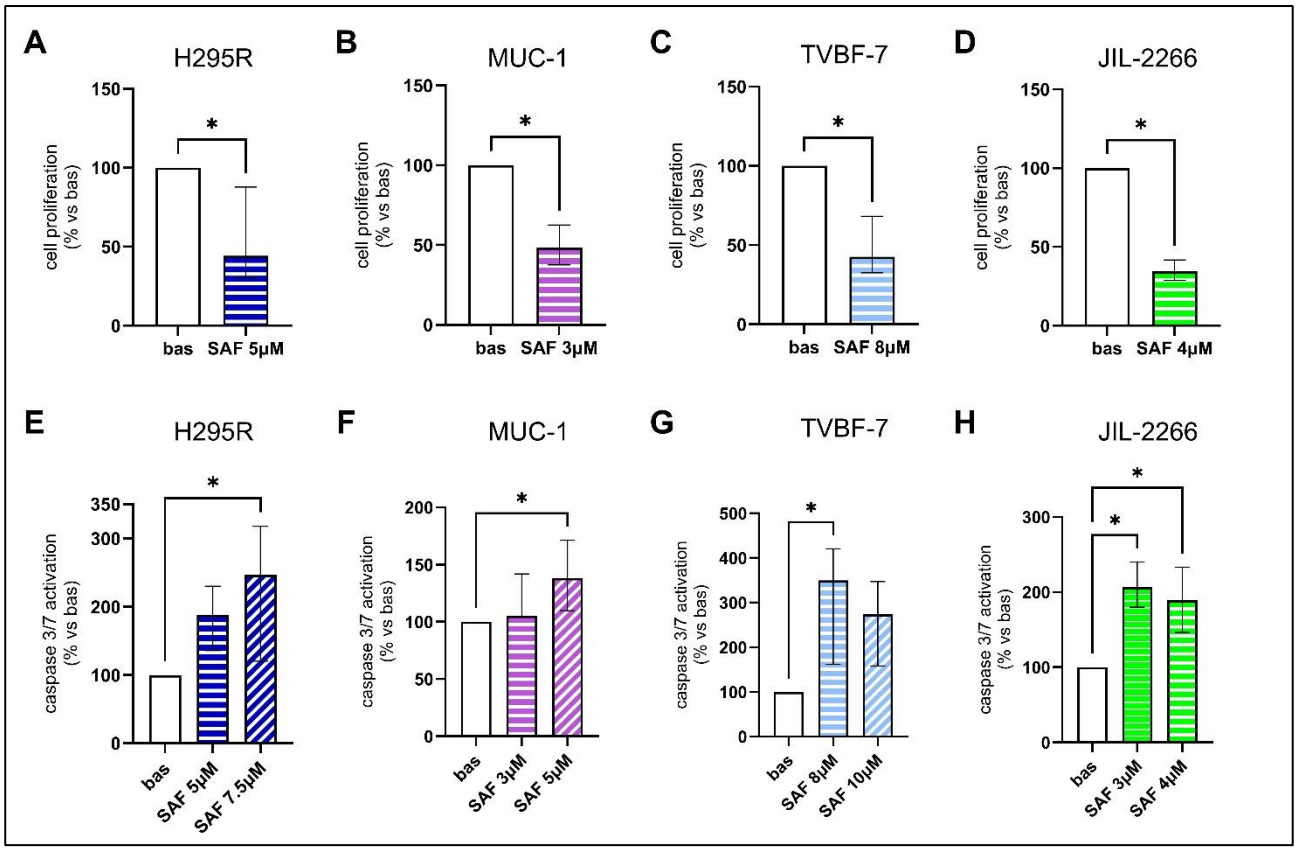

Figure 18. SAF treatment: effect on cell proliferation and apoptosis of ACC lines. **A-D**) % of cell proliferation measured as BrdU incorporation after 72h of 5µM (A), 3µM (B), 8µM (C), or 4µM (D), SAF in starved medium. Results of n>4 experiments were plotted as median ±IQR. Statistical analysis was performed via GraphPad Prism software, using Wilcoxon test. *p<0.05 vs bas. **E-H**) % of cell apoptosis, measured as caspase 3 and 7 activation, after 24h SAF treatment in starved medium. Results of n=4 experiments were plotted as median ±IQR. Statistical analysis was performed via GraphPad Prism software, using Kruskal-Wallis test coupled with Uncorrected Dunn's post hoc analysis. *p<0.05 vs bas.

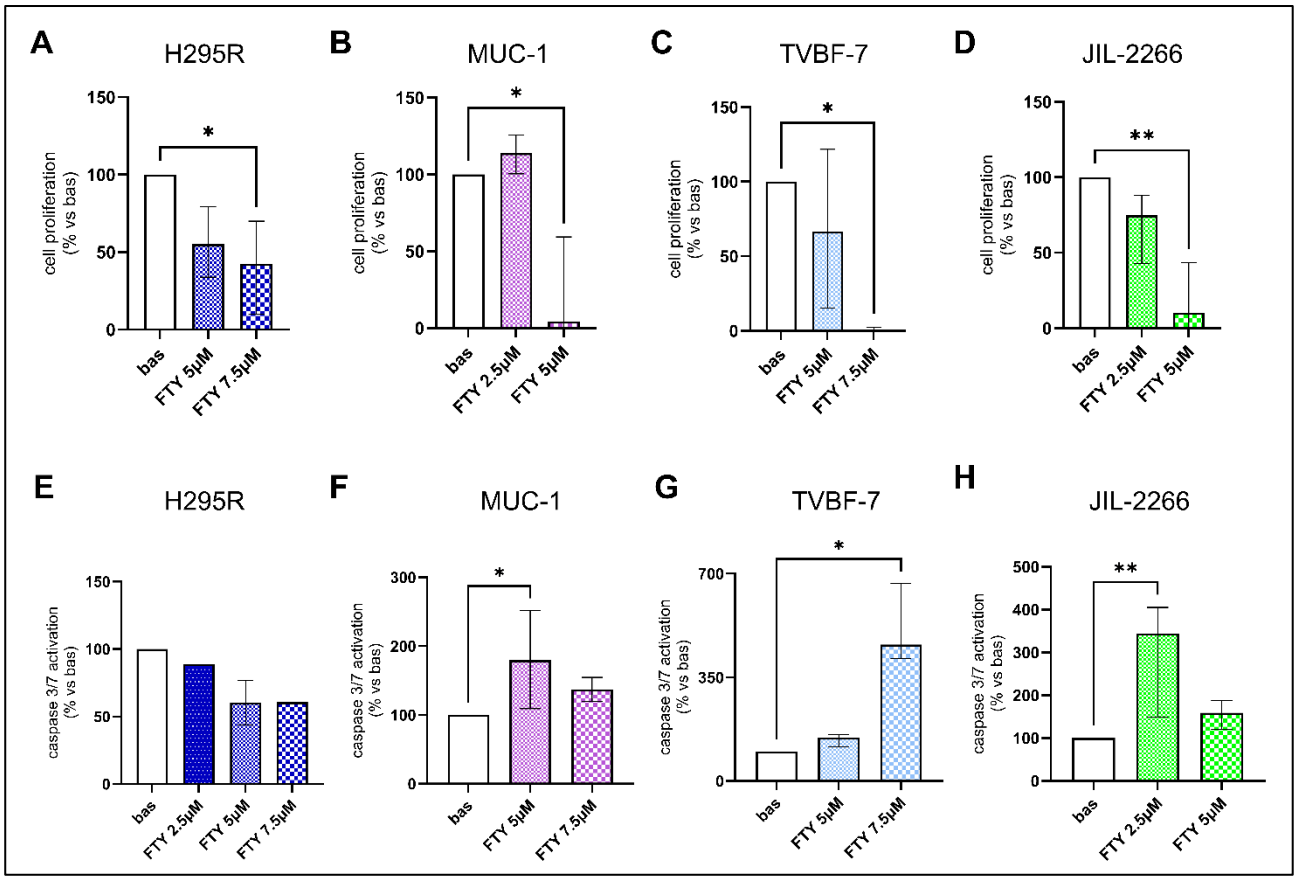

Figure 19. FTY treatment: effect on cell proliferation and apoptosis of ACC lines. **A-D**) % of cell proliferation measured as BrdU incorporation after 72h FTY treatment in starved medium. Results of n>3 experiments were plotted as median ±IQR. Statistical analysis was performed via GraphPad Prism software, using Kruskal-Wallis test coupled with Uncorrected Dunn's post hoc analysis. *p<0.05, **p<0.01 vs bas. **E-H**) % of cell apoptosis, measured as caspase 3 and 7 activation, after 24h FTY treatment in starved medium. Results of n=3 experiments were plotted as median ±IQR. Statistical analysis was performed via GraphPad Prism software, using Kruskal-Wallis test coupled with Uncorrected Dunn's post hoc analysis. *p<0.05, **p<0.01 vs bas.

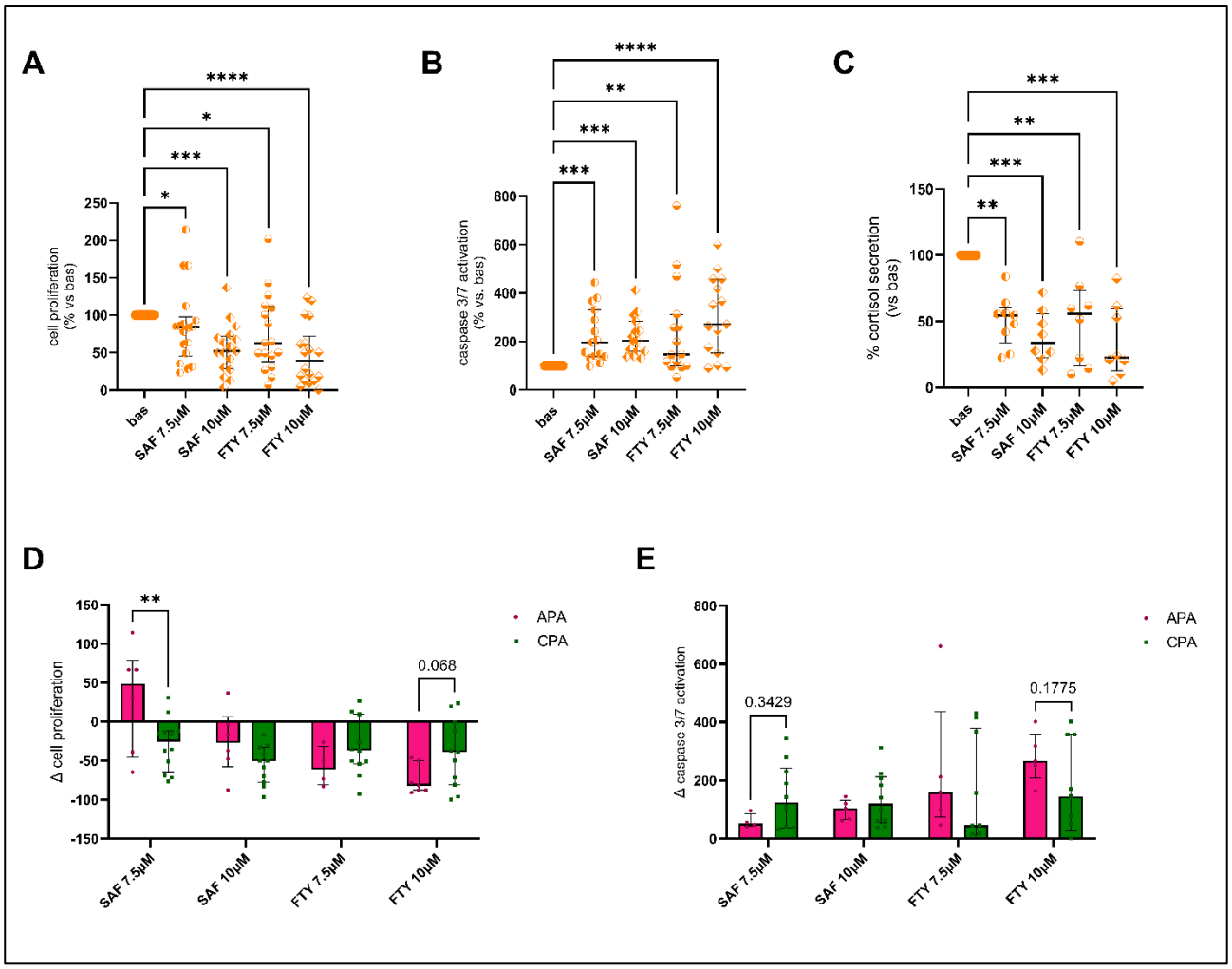

Figure 20. SAF and FTY effect on ACA: cell proliferation, apoptosis, and cortisol secretion. **A**) % of cell proliferation measured as BrdU incorporation after 72h of SAF or FTY treatment in starved medium. Results of n>17 primary cultures were plotted as single values with median ±IQR. Statistical analysis was performed via GraphPad Prism software, using Kruskal-Wallis test coupled with Uncorrected Dunn's post hoc analysis. *p<0.05, ***p<0.001 vs bas. **B**) % of cell apoptosis, measured as caspase 3 and 7 activation, after 24h of SAF or FTY treatment in starved medium. Results of n=15 primary cultures were plotted as single values with median ±IQR. Statistical analysis was performed via GraphPad Prism software, using Kruskal-Wallis test coupled with Uncorrected Dunn's post hoc analysis. **p<0.01, ***p<0.001 vs bas. **C**) % of CPA cortisol secretion after 72h of SAF or FTY treatment in starved medium. Results of n=7 primary cultures were plotted as single values with median ±IQR. Statistical analysis was performed via GraphPad Prism software, using Kruskal-Wallis test coupled with Uncorrected Dunn's post hoc analysis. **p<0.01, ***p<0.001 vs bas. **D**) Δ of cell proliferation after 72h SAF or FTY treatment divided according to hormonal secretion (APA vs CPA). Statistical analysis was performed via GraphPad Prism software, using a 2way ANOVA test, coupled with Tukey's post hoc analysis. **p<0.01 vs APA. **E**) Δ of cell apoptosis after 24h SAF or FTY treatment divided according to hormonal secretion (APA vs CPA). Statistical analysis was performed via GraphPad Prism software, using a 2way ANOVA test, coupled with Tukey's post hoc analysis.

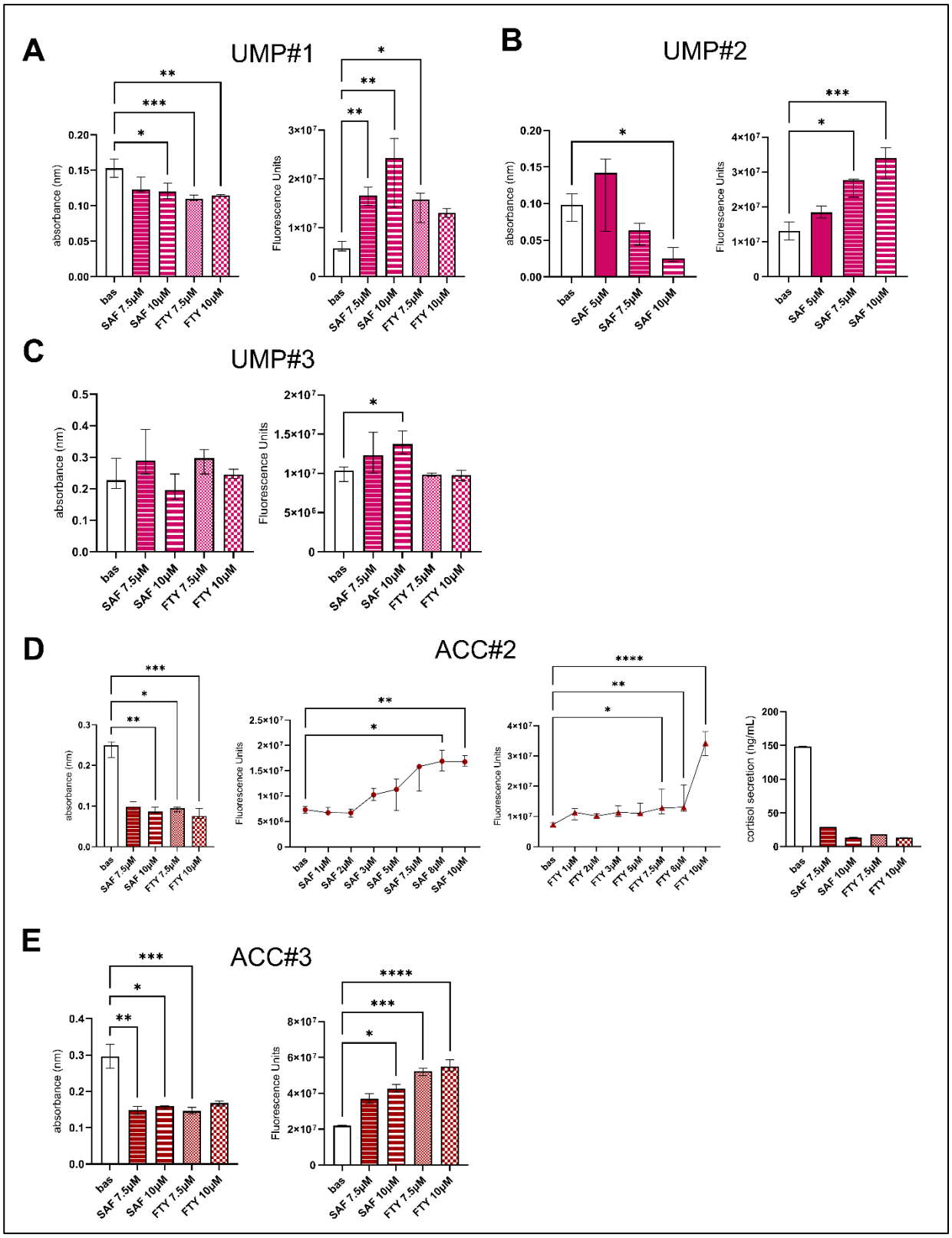

Figure 21. SAF and FTY effect on UMP and ACC: cell proliferation, apoptosis, and cortisol secretion. **A/C**) % of cell proliferation measured as BrdU incorporation or % of cell apoptosis measured as caspase 3 and 7 activation of UMP after 72 or 24h SAF and FTY treatment, respectively. Results of n=5 technical replicates for each UMP primary culture were plotted as median ±IQR. Statistical analysis was performed via GraphPad Prism software, using Kruskal-Wallis test coupled with Uncorrected Dunn's post hoc analysis. *p<0.05, **p<0.01, ***p<0.001 vs bas. **B**) % of cell proliferation measured as BrdU incorporation or % of cell apoptosis, measured as caspase 3 and 7 activation, on one UMP primary culture after 72 or 24h SAF treatment, respectively. Results of n=5 technical replicates were plotted as median ±IQR. Statistical analysis was performed via GraphPad Prism software, using Kruskal-Wallis test coupled with Dunn's post hoc analysis. *p<0.05, ***p<0.001 vs bas. **D-E**) % of cell proliferation measured as BrdU incorporation or % of cell apoptosis

measured as caspase 3 and 7 activation or ng/mL of cortisol secretion of ACC after 72 or 24h SAF and FTY treatment, respectively. Results of n=5 technical replicates for each ACC primary culture were plotted as median ±IQR. Statistical analysis was performed via GraphPad Prism software, using Kruskal-Wallis test coupled with Uncorrected Dunn's post hoc analysis. *p<0.05, **p<0.01, ***p<0.001, ****p<0.0001 vs bas.

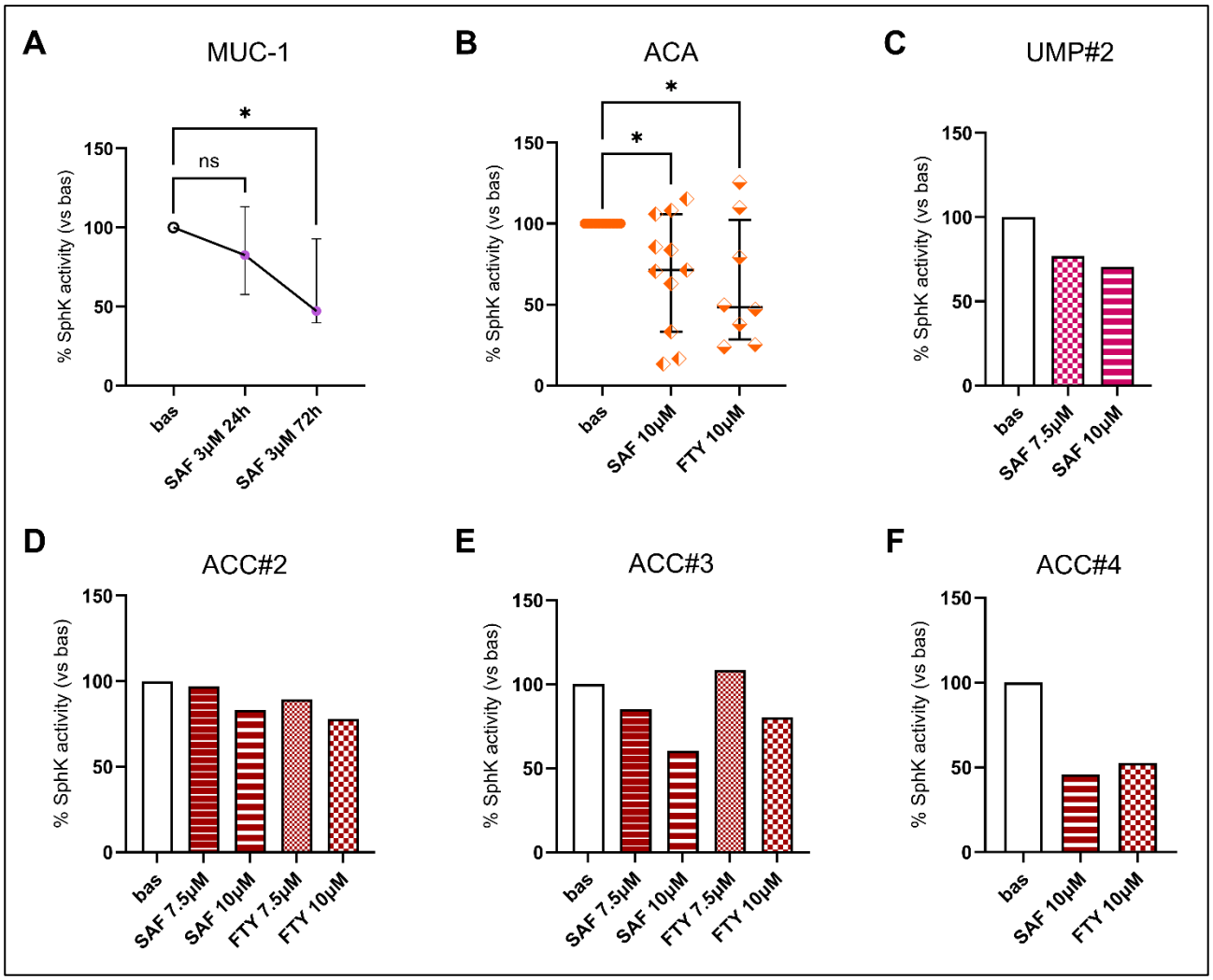

Figure 22. SAF and FTY effect on SphK activity of different in vitro models. **A**) % of SphK activity measured as ATP consumption, in MUC-1 cells after 24 or 72h of 3µM SAF treatment in starved medium. Results of 3 experiments were plotted as median ±IQR. Statistical analysis was performed via GraphPad Prism software, using Kruskal-Wallis test coupled with Dunn's post hoc analysis. *p<0.05 vs bas. **B**) % of SphK activity measured as ATP consumption, in ACA primary cell cultures after 72h of 10µM SAF or FTY treatment in starved medium. Results of ACA primary cultures were plotted as individual dots, with median ±IQR. Statistical analysis was performed via GraphPad Prism software, using Kruskal-Wallis test coupled with Uncorrected Dunn's post hoc analysis. *p<0.05 vs bas. **C**) % of SphK activity measured as ATP consumption, in UMP primary cells after 72h of 7.5µM or 10µM SAF treatment in starved medium. Results of one primary culture were plotted in the graph. **D-F**) % of SphK activity measured as ATP consumption, in ACC primary cells after 72h of 7.5µM or 10µM SAF or FTY treatment in starved medium. Results of one primary culture were plotted in each graph.

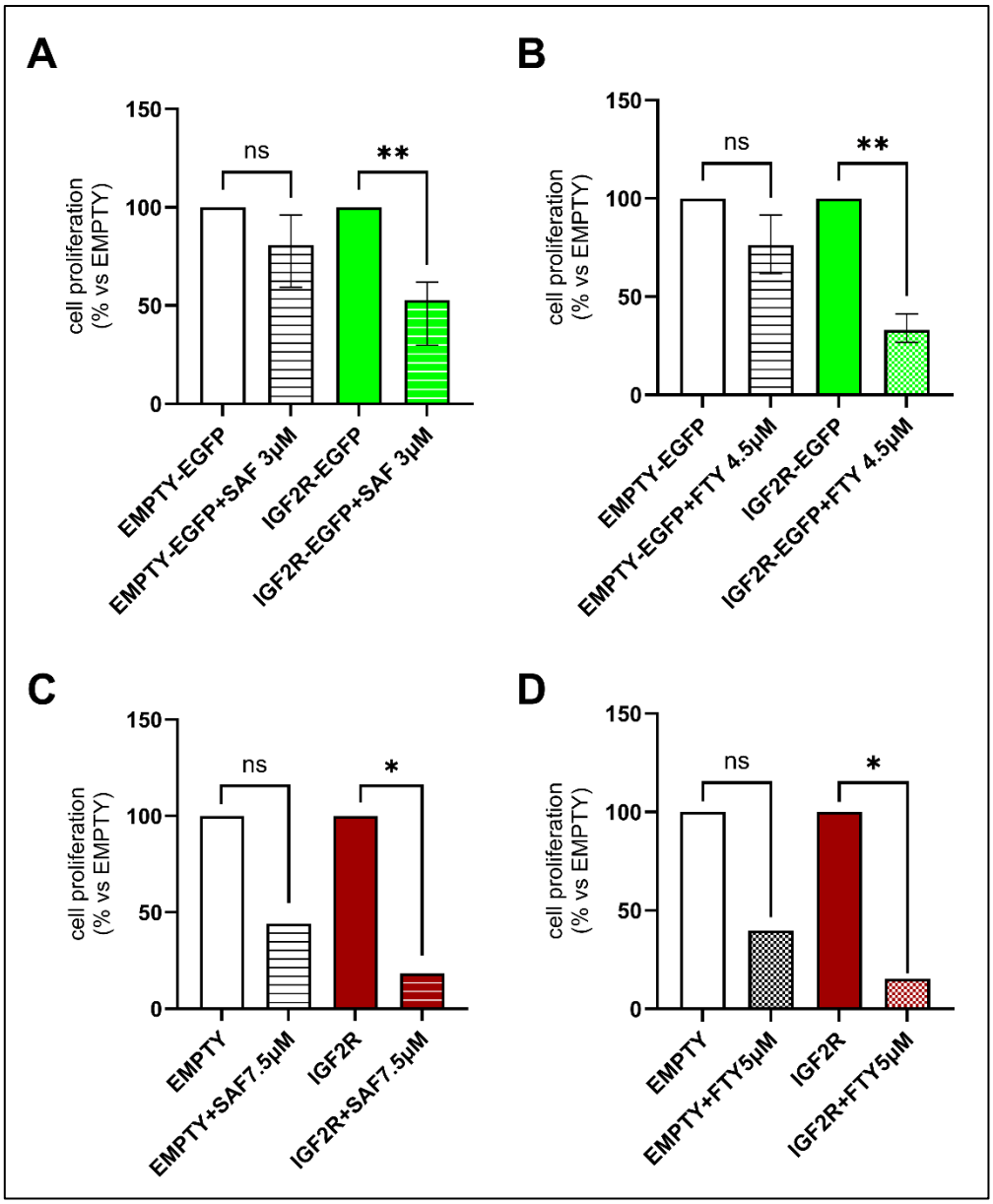

Figure 23. SAF and FTY anti-proliferative effect is IGF2R-mediated. **A-B**) % of cell proliferation, measured as BrdU incorporation after 48h of IGF2R-EGFP transient transfection at 1µg/µL followed by 72h of SAF (A) or FTY (B) treatment in starved medium in JIL-2266 cells. Both EMPTY-EGFP and IGF2R-EGFP were set at 100%, and respective SAF/FTY values were normalized consequently. Result of 4 experiments were plotted. **C-D**) % of cell proliferation, measured as BrdU incorporation after 48h of IGF2R-EGFP transient transfection at 1µg/µL followed by 72h of SAF (C) or FTY (D) treatment in starved medium in one ACC primary culture. Both EMPTY-EGFP and IGF2R-EGFP were set at 100%, and respective SAF/FTY values were normalized consequently. Result of 1 experiment (5 technical replicates) was plotted. Statistical analysis was performed via GraphPad Prism software, using Kruskal-Wallis test coupled with Dunn's post hoc analysis. *p<0.05, **p<0.01 vs IGF2R-EGFP.

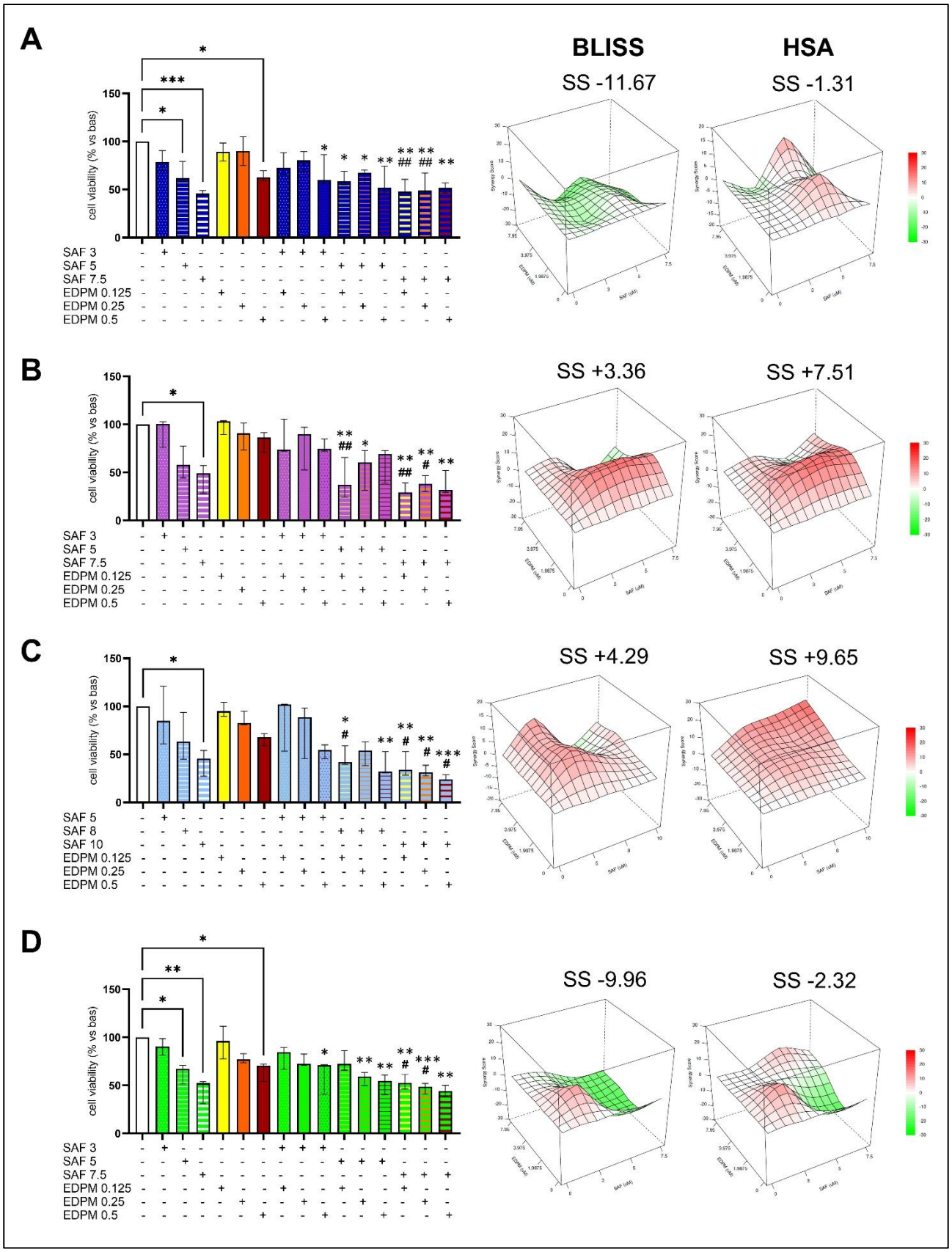

Figure 24. Combinatory effect of SAF+EDP-M on cell viability of ACC cell lines. % of cell viability assessed via MTT assay, after 24h of SAF, EDP-M, or combination treatment in complete medium on H295R (A), MUC-1 (B), TVBF-7 (C), and JIL-2266 (D). Results of 3 experiments were plotted as median ±IQR. For each cell line, the corresponding SynergyFinder+ 3D visualization report of cell viability data is presented. Synergism was confirmed in case of both Bliss and HSA synergy scores >10, additive effect of combinatory treatment was determined by -10<SynergyScore<+10. To note: each drug of the

EDP-M scheme was used at a different concentration, as stated in the Materials and Methods section. Mitotane concentrations were used to represent the whole EDP-M scheme and plotted alongside SAF. Statistical analysis was performed via GraphPad Prism software, using Kruskal-Wallis test coupled with Uncorrected Dunn's post hoc analysis. *p<0.05, **p<0.01, ***p<0.001 vs bas; #p<0.05, #p<0.01 vs corresponding EDP-M.

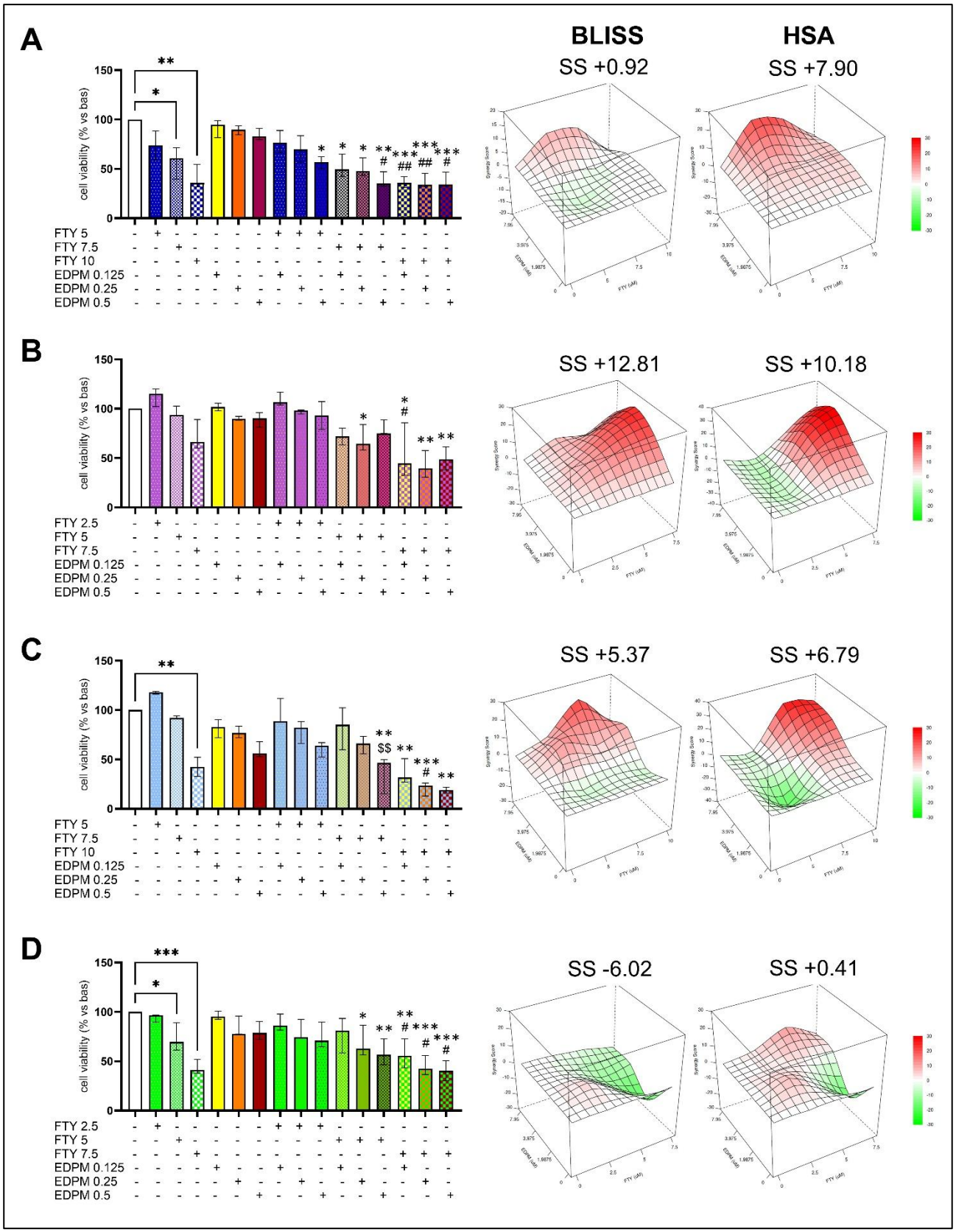

Figure 25. Combinatory effect of FTY+EDP-M on cell viability of ACC cell lines. % of cell viability assessed via MTT assay, after 24h of FTY, EDP-M, or combination treatment in complete medium on H295R (A), MUC-1 (B), TVBF-7 (C), and JIL-

2266 (D). Results of 3 experiments were plotted as median ±IQR. For each cell line, the corresponding SynergyFinder+ 3D visualization report of cell viability data is presented. Synergism was confirmed in case of both Bliss and HSA synergy scores >10, additive effect of combinatory treatment was determined by -10<SynergyScore<+10. To note: each drug of the EDP-M scheme was used at a different concentration, as stated in the Materials and Methods section. Mitotane concentrations were used to represent the whole EDP-M scheme and plotted alongside FTY. Statistical analysis was performed via GraphPad Prism software, using Kruskal-Wallis test coupled with Uncorrected Dunn's post hoc analysis. *p<0.05, **p<0.01, ***p<0.001 vs bas; #p<0.05, #p<0.01 vs corresponding EDP-M; $$p<0.01 vs corresponding FTY.

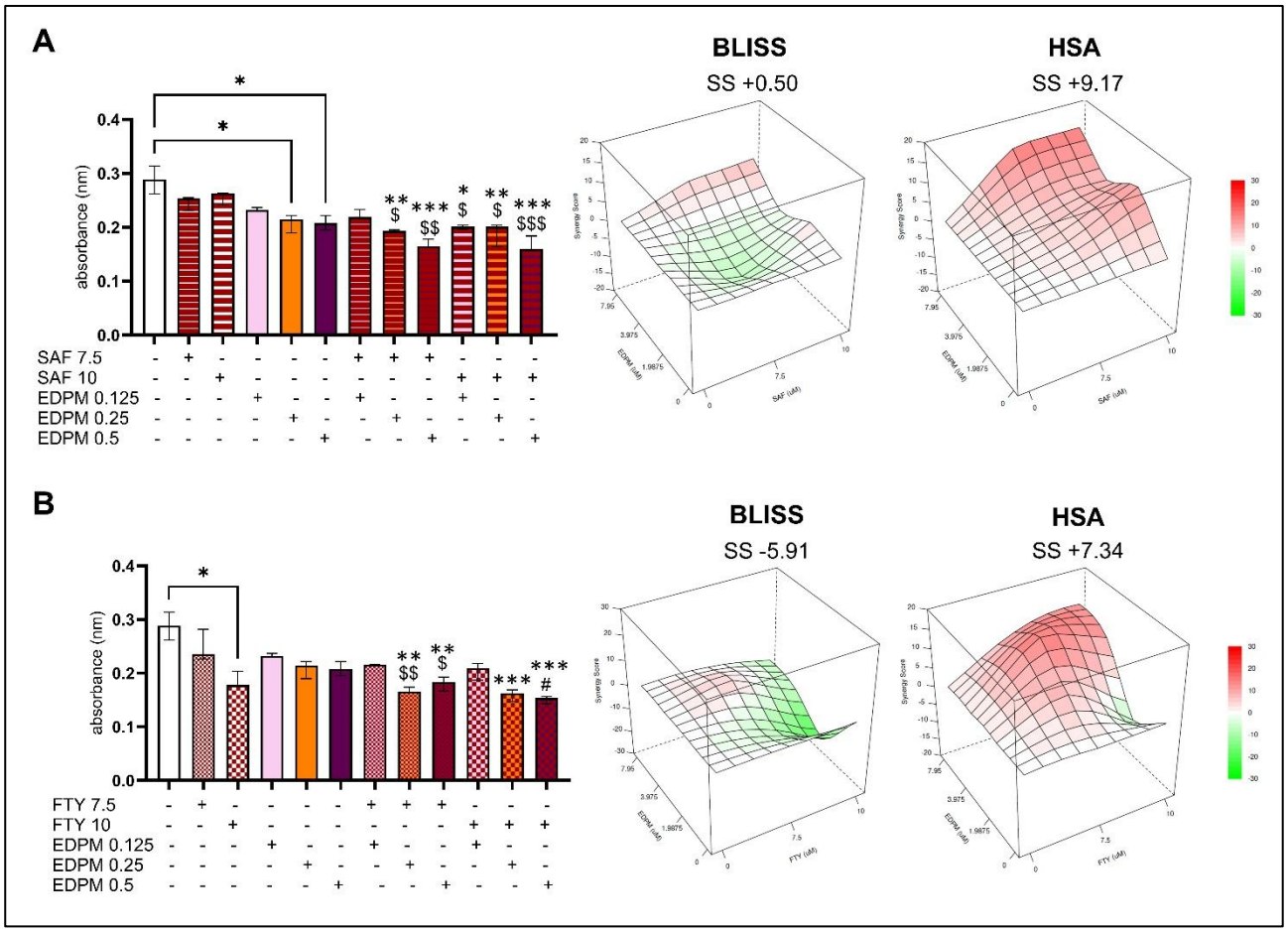

Figure 26. Combinatory effect of SAF or FTY+EDP-M on cell viability of one ACC primary culture. Absorbance of cell viability assessed via MTT assay, after 24h of SAF (A) or FTY (B), EDP-M, or combination treatment in complete medium on one ACC culture. Results of 1 experiment (5 technical replicates) were plotted as median ±IQR. For each drug combination, the corresponding SynergyFinder+ 3D visualization report of cell viability data is presented. Synergism was confirmed in case of both Bliss and HSA synergy scores >10, additive effect of combinatory treatment was determined by -10<SynergyScore<+10. To note: each drug of the EDP-M scheme was used at a different concentration, as stated in the Materials and Methods section. Mitotane concentrations were used to represent the whole EDP-M scheme and plotted alongside SAF/FTY. Statistical analysis was performed via GraphPad Prism software, using Kruskal-Wallis test coupled with Uncorrected Dunn's post hoc analysis. *p<0.05, **p<0.01, ***p<0.001 vs bas; #p<0.05 vs corresponding EDP-M; $p<0.05, $$p<0.01, $$$p<0.001 vs corresponding SAF/FTY.

DISCUSSION AND CONCLUSIONS

Heterogeneity of adrenocortical tumours has determined an ongoing challenge for clinicians to find wide and suitable therapeutic options aside from adrenalectomy. ACT include both commonly diffused adenomas and highly rare and aggressive ACC, whose altered molecular mechanisms have often constituted the core of targeted pharmacological studies. Transcriptomic analyses have cleared out a wide set of dysregulated genes and pathways that are involved in ACC tumorigenesis: while steroidogenic or metabolic effectors are downregulated, growth factors, peculiarly IGF2, DNA replication factors, as TOP2A (topoisomerase II alpha), or cell cycle regulators, as several cyclins and CDKs, result overexpressed (45).

Of particular relevance in ACC is the insulin-like growth factor 2 (IGF2), whose gene is the most overexpressed in ACC, in around 90% of patients, when compared to adenomas, where the overexpression is encountered in only 8.5% of cases (45). This discovery shed a light on the whole IGF system, whose complex ensemble is altogether involved in adrenocortical carcinogenesis. Since the late 90s, IGF2 and its RTK receptors were investigated to elucidate their pro-mitotic functioning (94): IGF2 binding with either IGF1R, the mitogenic isoform of IR (IR-A), or their heterodimer stimulates the proliferative MAPK pathway, activating Ras, Raf-1, and then ERK1/2, or the anti-apoptotic signal of PI-3K and Akt (50). This pro-tumorigenic connotation of IGF1R and IR-A has led to the development of small molecule inhibitors: linsitinib, targeted to both, or NVP-AEW541, specifically directed towards IGF1R. Of these *in vitro*-promising drugs, only linsitinib reached the phase III clinical trial stage, however it did not meet the expectations, not being able to significantly increase patients' OS (51).

Among the IGF2 system, the specific IGF2 binding receptor IGF2R has been addressed as anti-mitotic in several physio-pathological contexts. During the years, it was demonstrated that IGF2R was able to control organ and foetal overgrowth, to impair myoblast proliferation, to delay breast cancer onset, thus serving as anti-oncogenic factor, all due to its IGF2-degrading function. Controversially, IGF2R was found overexpressed in hepatocellular, gastric, and cervical cancers, giving rise to the hypothesis that the receptor could also represent a pro-tumorigenic effector (57,95).

For these instances, this project was focused on the role of IGF2R in adrenocortical tumorigenesis to assess if the receptor could bear a pro or anti-oncogenic role and whether it could represent a new therapeutic target.

First of all, IGF2R expression was assessed in either ACT tissue (ACA, ACC, and normal adrenals) and in four different ACC-derived cell lines, representing both primary (H295R and JIL-2266) and metastatic (MUC-1, from a neck metastasis, and TVBF-7, from a lymph nodal metastasis) ACC. This evaluation was needed since the scarcity of previous ACT literature on IGF2R: only two papers formerly evaluated IGF2R expression in ACC, Velázquez-Fernández et al. in 2005 and De Martino et al. in 2019, both finding IGF2R overexpressed at transcript level if either compared to ACA or to normal adrenal tissue. Even scarcer were information on IGF2R protein levels, previously assessed only by De Martino et al., who coherently retrieved a strong staining of IGF2R protein in all ACC examined (52,62). In our analysis we demonstrated similar levels of IGF2R transcript among ACA, ACC, and NA samples, while protein expression was significantly higher in both tumoral types compared to NA, suggesting an involvement in ACT tumorigenesis. Interestingly, cell line analysis revealed that H295R and MUC-1 expressed similar levels of protein IGF2R, while TVBF-7 overexpress the receptor, and JIL-2266 almost completely lack in IGF2R.

Furtherly, an in-depth *in vitro* analysis of IGF2R involvement in cell proliferation and viability was conducted, to address the role of IGF2R in ACT tumorigenesis as pro or antitumoral. In other tumour models, as in cervix cancer or in haemangioma, where IGF2R had a pro-oncogenic connotation, its silencing caused a marked cell viability or proliferation reduction (54,55). Similarly, in our ACC models IGF2R knockdown decreased the pro-mitotic activity of cells, diminishing cell proliferation, but did not impact on cell viability, suggesting that IGF2R contribution stands in the pro-mitotic but not pro-survival pathways of ACC. The proliferative role of IGF2R in ACC was confirmed by the specific inhibition of its IGF2-binding site, performed with a neutralizing antibody, that induced a decrease of cell proliferation similar to the one observed after IGF2R knockdown. Interestingly, in both cases, JIL-2266 proliferative activity was not altered by IGF2R silencing or inhibition, in agreement with the low basal expression of IGF2R in this cell type.

After having proved that IGF2R blockade was efficient in the *in vitro* control of ACC cell lines proliferative activity, the same experimental setting was proposed on primary cultures derived from adenomas, uncertain malignancies, and carcinomas. In each of the three ACT types IGF2R knockdown was efficiently anti-proliferative, regardless of their hormonal

function. However, hormonal secretion strongly influenced the response to the antiIGF2R antibody: only cortisol-secreting tumours had a significant decrease of cell proliferation after treatment. On the opposite, nor aldosterone-secreting nor inactive tumours were sensitive to IGF2R inhibition. Remarkably, to the best of our knowledge this is the first time that a relationship between cortisol-secretion and IGF2R has been established.

IGF2R-driven ACT growth was further demonstrated with transient transfection experiments. The increase of IGF2R levels determined a marked rise in cellular proliferation, and consequently of viability as well, in two primary cultures and in all ACC cell lines. Interestingly, IGF2R overexpression induced a strong increase of cell proliferation in JIL-2266, which endogenously express nearly undetectable levels of IGF2R, suggesting an IGF2R-inducible behaviour.

The investigation of IGF2R role in ACT was not supported by previous literature, since the majority of authors assumed an anti-oncogenic role for IGF2R. However, having demonstrated that IGF2R is directly involved in ACT proliferation rose many other questions on the actual mechanism of this receptor.

IGF2R is intrinsically related to the whole IGF2 pathway, thus the following step was to evaluate the role of IGF2R in regulating the amount of IGF2 secreted in the cell media. Interestingly, of the three IGF2R-expressing cell lines, despite similar basal levels of IGF2 secretion, only H295R were affected by IGF2R alterations in terms of IGF2 production. Indeed, the overexpression of IGF2R by transient transfection significantly decreased IGF2 extracellular levels in this cell model. This evidence supported an IGF2R involvement in the internalization of the ligand and suggested the modulation of this IGF2R scavenging activity as a possible novel approach to reduce the extracellular mitogenic IGF2.

Among IGF2R ligands, retinoic acid (RA) has been proved able to promote IGF2R scavenging activity. RA was of great interest in the scientific literature of the 90s, when its binding capacity to IGF2R was demonstrated. High affinity RA interaction with IGF2R, even though at an unknown binding site, facilitated IGF2 internalization and stimulated pro-apoptotic cathepsin secretion, all mediated by IGF2R (67,68,93). Since no data availability on RA action on ACT, we decided to test it in H295R cells, since in this cell line IGF2R overexpression induced a reduction of secreted IGF2, suggesting a scavenging activity of IGF2R. Unexpectedly, our data showed an increase of IGF2 extracellular levels after RA

administration. We ruled out a possible transcriptional effect of RA on IGF2 or IGF2R genes, since no variations of the respective transcripts was observed after RA incubation.

Intriguingly, the IGF2 accumulation in the extracellular environment measured after RA incubation did not promote cell proliferation, but on the contrary RA reduced cell proliferation, and this effect was mediated by IGF2R presence. This result is surprising since the increased availability of IGF2 in cell medium is expected to promote cell proliferation by binding IGF1R and IR. A possible explanation can be found in the ability of RA to induce the transcription of proteins that bind IGF2 (IGF binding proteins, IGFBPs) (96,97). Indeed, in ACT context, IGFBPs can act as anti-mitotic by controlling IGF2 availability towards the receptors, as supported by our results that demonstrated both IGFBP2 and 6 increase after RA administration.

Furthermore, RA assessment was completed by the analysis of its pro-apoptotic effect. We demonstrated that RA was able to induce a significant activation of caspases in H295R model, however we could not prove that this effect was mediated by IGF2R, since receptor alterations did not affect RA-induced apoptosis, suggesting the involvement of other pathways.

The results here described suggested a positive outcome for RA treatment in ACT, since they demonstrated how RA could represent a novel therapeutic strategy to be better explored in further ACT preclinical models. Indeed, several primary cultures were tested to uncover whether the anti-mitotic and pro-apoptotic effect of RA demonstrated in cell cultures was confirmed. RA resulted efficient in controlling proliferation of cortisol-secreting adenomas and carcinomas, and in the latter, also the pro-apoptotic stimulation was confirmed.

Overall, our data demonstrate that in ACT the hypothesized anti-oncogenic effect of IGF2R, due to a scavenging activity of IGF2 demonstrated in other cell models, not only is not present, but on the contrary, we proved that IGF2R behaves as an oncogene, promoting cell proliferation.

To date, the downstream molecular mechanism mediating the mitotic effect of IGF2R has not been investigated. Previous literature on IGF2R highlighted the interconnection of the receptor with the sphingosine kinases. Indeed, upon IGF2 binding, SphK are activated by IGF2R for converting the anti-mitotic sphingosine into the pro-survival S1P. This product is then extracellularly transferred where it can initiate a signalling cascade, beginning with its

receptors $S1P_{1-5}$ and culminating in the phosphorylation of ERK1/2 (64–66). This mechanism was confirmed in other models, while evidence of SphK and S1P involvement in adrenocortical tumorigenesis are still limited.

Interestingly, high SphK1 and 2 expression is positively correlated with reduced ACC patients' overall survival (98). Furthermore, Xu et al. demonstrated that SphK1 was responsible for sustaining ACC proliferative and invasive activity using both *in vitro* and *in vivo* preclinical models, while Lucki et al. proved S1P involvement in stimulating cortisol secretion in H295R cells (80,81).

In this study, we examined SphK1 and 2 expression and role in ACT context to test, for the first time, their possible IGF2R-dependent activation. Firstly, the transcript and protein expression of the two sphingosine kinases were evaluated across adenomas, carcinomas and normal adrenal tissues. Even though transcript expression was not correlated with protein level, a significant overexpression of SphK1 was observed in ACT, both ACA and ACC, compared to NA tissue. Conversely, our evidence was not supported by literature, since Xu et al. demonstrated a markedly higher SphK1 expression in ACC compared to ACA (80). However, this is the only published data assessing SphK1 protein quantity in ACT, and it did not evaluate SphK1 levels in NA. Moreover, we did not report any difference in SphK2 protein levels between ACT and NA, possibly suggesting a major involvement of SphK1 in adrenocortical tumorigenesis.

SphK1 expression resulted also inhomogeneous among ACC cell lines, with a strong protein expression in MUC-1 and JIL-2266 cells and low levels in H295R and TVBF-7. This pattern of expression did not correspond to the aggressiveness of the different cell lines, being MUC-1 a metastatic-deriving line and JIL-2266 originating from a primary tumour, nor to their secretory profiles, since all cell lines secrete glucocorticoids, apart from JIL-2266 (99). SphK2 had a similar expression among ACC lines, similarly to what was previously observed in ACT tissues.

To test a possible role of SphK in mediating IGF2R mitotic effects, we assessed SphK activity after IGF2R manipulation. In TVBF-7 cells, the cell line most affected by IGF2R silencing or transfection in terms of proliferative activity, SphK activity was significantly reduced by IGF2R knockdown and coherently was increased by IGF2R overexpression. Furthermore, SphK enzymatic activity was strongly hampered also by the specific inhibition

of the IGF2-IGF2R binding operated by the neutralizing antiIGF2R antibody both in MUC-1 cells and in several primary ACA cell cultures.

All this evidence combined are a novel and relevant ensemble that enlightens for the first time the predominant role of IGF2R in ACT tumorigenesis. Particularly, identifying IGF2R as a pro-mitotic receptor of the IGF2 pathway could suggest the development of new IGF2R-targeting agents or even the repurposing of therapies targeted to the IGF2-system, as linsitinib or NVP-AEW541, in combination with the IGF2R inhibition, in future studies.

Since at the present no IGF2R inhibitor was approved for the clinical practice, targeting of the sphingosine kinases could represent a more feasible and realistic way to interfere with this pathway in ACT. Indeed, plenty of previous literature aimed at identifying efficient SphK inhibitors.

SphK involvement in unbalancing the sphingosine rheostat towards S1P implies a pathogenic role in several tumours, as in breast, lung and colorectal cancers. Thus, their mechanism of action has been well established and targeted at different extents. Among the wide variety of SphK inhibiting drugs, in this project were employed SAF and FTY. SAF is a structural analogue of the sphingosine, thus it is able to competitively inhibit both SphK 1 and 2, diminishing their activity and increasing the levels of the pro-apoptotic precursor ceramide. FTY is another analogue of sphingosine, whose main target is SphK1, and that can also target PI-3K/Akt and MAPK pathways with antitumoral effects (72,85).

Both inhibitors were already widely tested on both clinical and preclinical models, even in the ACT context. FTY was employed by Xu et al. on H295R cells and xenografts, demonstrating an anti-proliferative and pro-apoptotic behaviour *in vitro*, and being able to control H295R-derived xenograft volumes (80). SAF was poorly studied in preclinical ACT settings, nevertheless several clinical trials comprising also ACC patients were concluded. The clinical trial including the highest number of ACC patients, conducted by Dickson and colleagues on advanced tumours, demonstrated a short-time stabilization of disease after combinatory treatment of SAF plus cisplatin; of the 7 ACC patients included in this trial, only two had positive outcomes, as metastases regression and disease stabilization (84).

The *in vitro* assessment of SAF and FTY efficacy on different models of ACT was the latter part of this project. Starting from plasmatic concentrations determined in the clinical trial of Boulter and colleagues, and from previous *in vitro* findings, the dosage range of both SphK inhibitors was comprised between 2 and 10μM (86). First of all, we determined the IC50 of

each drug on the four different ACC cell lines. The outcome of this viability evaluation was peculiar, since it demonstrated that MUC-1 and JIL-2266, the cell lines with higher SphK1 levels, were also the ones to respond at lower dosages of inhibitors, with IC50 of 3.8 and 4μM for SAF, and 2.7 and 4μM for FTY, respectively. Our results demonstrated the ability of SAF and FTY to exert an anti-proliferative and a pro-apoptotic action on all ACC cell lines. Controversially, FTY was able to reduce cellular proliferation while not to induce apoptosis on H295R cells.

Since the above-described findings demonstrate a great effect of both SAF and FTY on the main endpoints of tumorigenesis, both inhibitors were tested on *in vitro* established primary cell cultures. Coherently, the results obtained on ACC immortalized cells were confirmed for both SAF and FTY on both ACA, UMP, and ACC cultures. Particularly, 15 ACA were tested with high concentrations, i.e. 7.5 and 10μM of SAF and FTY, in order to evaluate the anti-proliferative and pro-apoptotic response also in these experimental models. In both cases, a strong effect was demonstrated. Similarly, UMP cultures were tested with the same dosages of SAF and FTY, proving a significant anti-mitotic and pro-apoptotic action of both drugs. Also, two ACC primary cultures, even though their greater aggressiveness compared to adenomas and uncertain malignancies, responded well to the treatment with both SAF and FTY, with no difference among the two inhibitors. Remarkably, also in ACT models SAF and FTY induced a reduction of SphK activity.

Interestingly, hormonal secretion could influence the response of adrenocortical adenomas to SphK inhibitors. Indeed, we observed a differential response to anti-proliferative and pro-apoptotic effects to these drugs between aldosterone- and cortisol-producing adenomas, with the first being better FTY-responders and the latter being more sensitive to SAF. Among the UMP tested for SphK inhibitor response, no strong secretion-driven analysis could be performed, since the three malignancies tested were all different in their hormonal production (UMP#1 cortisol secretion, UMP#2 aldosterone secretion, and UMP#3 non-secreting malignancy). However, the only cortisol-secreting malignancy tested had a stronger apoptotic activation after SAF treatment, confirming the result obtained in cortisol-producing adenomas. At last, both ACC used in this part of the project were cortisol-secreting tumours, whose response to SAF and FTY was comparable and significant both for caspases activation and for proliferative reduction.

Another endpoint evaluated after SphK inhibition is cortisol secretion, since it represents a key point in ACT tumorigenesis and could be related to the Cushing's syndrome and its

comorbidities, and is also associated with reduced OS of ACC patients (100). Moreover, recent evidence demonstrated that SphK1 activity of increasing S1P levels could stimulate cortisol secretion in H295R cells (81). Our results on primary ACT cultures proved that either SAF and FTY were similarly able to control and minimize cortisol secretion, suggesting a broad action on ACT tumorigenesis. For future research, the evaluation of aldosterone secretion after SphK inhibition could be an interesting point to assess.

After having proved the validity of SphK inhibitors as novel promising ACT drugs in our *in vitro* setting, we proceeded with testing each inhibitor in combination with the current clinical standard of therapy, the EDP-M scheme. In particular, EDP-M is a combination of chemotherapeutics plus the adrenolytic agent mitotane, whose clinical administration was already adapted in preclinical studies to compare the efficacy of new drugs (90). Both FTY and SAF were tested in comparison to well established chemotherapeutics in the context of other pathologies: SAF resulted synergic with doxorubicin, carboplatin, gemcitabine, and vincristine in reducing cell viability (101), while FTY acted synergically with doxorubicin in breast cancer (73), was able to sensitize cisplatin-resistant melanoma cells (102), and enhanced chemosensitivity to doxorubicin and etoposide of *in vitro* colon cancer cells (103). Furthermore, previous findings already promoted combinatory therapy of SphK inhibitors and singularly administered components of the EDP-M scheme in the ACC context. The preclinical study of Xu et al., compared FTY and mitotane effect on H295R growth, demonstrating a similar apoptotic stimulation and viability reduction induced by FTY alone or combined to mitotane (80). SAF was tested in two separate clinical studies in combination with either doxorubicin or cisplatin, but unfortunately the clinical activity registered was not clearly referrable to SAF or the chemotherapeutic nor specifically to their combinatory action (83,84).

The *in vitro* treatment of ACC cell lines was performed at 3 different concentrations, one under, one similar, and one above the IC50 previously calculated, while low concentrations (⅛, ¼, or ½ of the IC50) of EDP-M were administered. The effect on cell viability was registered, and the potential synergism was calculated with a dedicate software. However, while we report an additive, and non-synergic, effect of SAF+EDP-M in ACC cells, FTY+EDP-M resulted synergic in reducing cell viability of MUC-1 line and additive in the other lines. Upon both treatments, the highest synergy values were observed in MUC-1 and TVBF-7 cells, possibly due to their poor response to EDP-M alone, as their patients of origin

were resistant to clinical therapy. The same combinations were proposed also on one ACC primary culture and, similarly, resulted additive in their anti-tumorigenic effect.

Overall, our results demonstrated that both inhibitors of SphKs, SAF and FTY, are able to reduce ACT cell survival, proliferation, and cortisol secretion, thus they could represent a novel ACT therapeutic approach. Remarkably, the action of SAF and FTY is strongly linked to IGF2R quantity, as demonstrated by the increased efficiency of both drugs after IGF2R transfection, suggesting that the expression of IGF2R may represent a possible predictive biomarker useful for patients' selection.

This project was pivotal for the in-depth analysis of the role of the IGF2 receptor in adrenocortical tumours pathogenesis. Through the demonstration of IGF2R active involvement in the pro-mitotic pathways of ACC we have debunked the dogma of the IGF2R role as IGF2 scavenger and onco-suppressor in this pathology. This project proved a whole new downstream mechanism of action in the IGF2 system, with IGF2R being able to trigger the sphingosine kinase activation, which is later involved in the stimulation of cell proliferation and anti-apoptotic signalling. The strict interconnection of IGF2R and SphK was demonstrated at several extents in this project: via IGF2R knockdown, inhibition, or transfection, which resulted in a corresponding reduction or increase of SphK activity. IGF2R pro-mitotic connotation opened new possibilities in the therapeutic horizon of ACT patients, indeed different inhibitors of this target have been tested in this project. Remarkably, this newly identified IGF2R-SphK axis could be targeted at both IGF2R and SphK extents. Indeed, the specific IGF2R neutralizing antibody and retinoic acid are both able to reduce cellular proliferation by targeting the IGF2-IGF2R interaction, while the two SphK inhibitors, SAF and FTY, efficiently act on the pro-mitotic activity, apoptotic control, and cortisol secretion.

Despite the complexity of the *in vitro* work here presented, it is necessary to address two main limitations of this project. First, the small number of ACC primary cultures, only restricted to 5, cannot reflect the heterogeneity of this tumour, nor has given us the possibility to examine specific features or perform further stratifications based on hormonal hypersecretion or other variables. Second, a mere *in vitro* study is a valid tool for the investigation of cellular mechanisms, however it cannot reproduce the whole biological complexity of the tumour environment. Thus, further preclinical studies, taking advantage of 3D cultures or *in vivo* models, will be needed to support our findings.

Overall, the findings of this PhD project suggest two new druggable targets, IGF2R and SphK, for the development of novel pharmacological therapies for adrenocortical tumours.

ACKNOWLEDGEMENTS

During my PhD experience I have been able to pursue one of my childhood dreams and be an active part of the research community. For this opportunity I have to thank all those who supported me and believed in my personal and professional project. First of all, Professor Erika Peverelli and Giovanna Mantovani, who both welcomed, guided, and inspired me since I moved my first steps in the endocrinology field. Then Dr. Rosa Catalano, a mentor, a colleague, and most importantly a friend, who has been present along all the steps of my project to sustain and counsel me in the best way possible. Obviously, I have to thank also all my colleagues in the lab, each one of them has been a pivotal part of this experience. At last, I must mention the collaborators, from the Endocrinology Unit of IRCCS Policlinico Ospedale Maggiore, from the ENSAT community, and from other institutions, who helped me to complete this project.

REFERENCES

1. Lloyd R V. Endocrine Pathology. La Rosa S, Uccella S, editors. Cham: Springer International Publishing; 2022.

2. Vrezas I, Willenberg HS, Bornstein SR. Adrenal Cortex, Anatomy. In: Elsevier, editor. Encyclopedia of Endocrine Diseases. Elsevier; 2004.

3. Ross IL, Louw GJ. Embryological and molecular development of the adrenal glands. Vol. 28, Clinical Anatomy. John Wiley and Sons Inc; 2015. p. 235–42.

4. Mihai R. Physiology of the pituitary, thyroid and adrenal glands. In: Surgery. 2011. p. 419–27.

5. Shifrin AL, Raffaelli M, Randolph GW, Gimm O. Endocrine Surgery Comprehensive Board Exam Guide. Shifrin ALRMRGWGO, editor. 2022.

6. Díaz-Flores L, Gutiérrez R, Varela H, Valladares F, Alvarez-Argüelles H, Borges R. Histogenesis and morphofunctional characteristics of chromaffin cells. In: Acta Physiologica. 2008. p. 145–63.

7. Eiden LE, Jiang SZ. What's New in Endocrinology: The Chromaffin Cell. Vol. 9, Frontiers in Endocrinology. Frontiers Media S.A.; 2018.

8. Bechmann N, Berger I, Bornstein SR, Steenblock C. Adrenal medulla development and medullary-cortical interactions. Mol Cell Endocrinol. 2021 May 15;528.

9. Berends AMA, Eisenhofer G, Fishbein L, Anouk ANA, Kema IP, Links TP, et al. Intricacies of the molecular machinery of catecholamine biosynthesis and secretion by chromaffin cells of the normal adrenal medulla and in pheochromocytoma and paraganglioma. Vol. 11, Cancers. MDPI AG; 2019.

10. Xing Y, Lerario AM, Rainey W, Hammer GD. Development of Adrenal Cortex Zonation. Vol. 44, Endocrinology and Metabolism Clinics of North America. W.B. Saunders; 2015. p. 243–74.

11. Nicolaides NWHBS et al. Adrenal Cortex: Embryonic Development, Anatomy, Histology and Physiology. 2023.

12. Lotfi CFP, Kremer JL, Passaia BDS, Cavalcante IP. The human adrenal cortex: Growth control and disorders. Vol. 73, Clinics. Universidade de Sao Paulo; 2018.

13. Raff H, Sharma ST, Nieman LK. Physiological basis for the etiology, diagnosis, and treatment of adrenal disorders: Cushing's syndrome, adrenal insufficiency, and congenital adrenal hyperplasia. Compr Physiol. 2014;4(2):739–69.

14. Vinson GP. Functional zonation of the adult mammalian adrenal cortex. Vol. 10, Frontiers in Neuroscience. Frontiers Research Foundation; 2016.

15. Hu J, Zhang Z, Shen WJ, Azhar S. Cellular cholesterol delivery, intracellular processing and utilization for biosynthesis of steroid hormones. Nutr Metab (Lond). 2010;7:47. Available from: http://www.nutritionandmetabolism.com/content/7/1/47

16. Ortsater H, Sjoholm A, Rafacho A. Regulation of Glucocorticoid Receptor Signaling and the Diabetogenic Effects of Glucocorticoid Excess. In: State of the Art of Therapeutic Endocrinology. InTech; 2012.

17. Pereira SS, Lobato CB, Monteiro MP. Cell Signaling Within Endocrine Glands: Thyroid, Parathyroids and Adrenal Glands. In: Tissue-Specific Cell Signaling. Springer International Publishing; 2020. p. 63–91.

18. Belfiore A, Leroith D. Principles of Endocrinology and Hormone Action. Springer; 2018. Available from: http://www.springer.com/series/14021

19. Val P, Martinez A. Editorial: Adrenal Cortex: From Physiology to Disease. Vol. 7, Frontiers in Endocrinology. Frontiers Media S.A.; 2016.

20. K. Nigam L, V. Vanikar A, D. Patel R, V. Kanodia K, S. Suthar K. Pathology Associated with Hormones of Adrenal Cortex. In: Mitochondria and Brain Disorders. IntechOpen; 2020.

21. Pitsava G, Maria AG, Faucz FR. Disorders of the adrenal cortex: Genetic and molecular aspects. Vol. 13, Frontiers in Endocrinology. Frontiers Media S.A.; 2022.

22. Kuruba R, Gallagher SF. Current management of adrenal tumors. Curr Opin Oncol. 2008;(20):34.

23. Lenders JWM, Eisenhofer G. Pathophysiology and diagnosis of disorders of the adrenal medulla: Focus on pheochromocytoma. Compr Physiol. 2014;4(2):691–713.

24. Nölting S, Bechmann N, Taieb D, Beuschlein F, Fassnacht M, Kroiss M, et al. Personalized Management of Pheochromocytoma and Paraganglioma. Vol. 43, Endocrine Reviews. Endocrine Society; 2022. p. 199–239.

25. Fassnacht M, Tsagarakis S, Terzolo M, Tabarin A, Sahdev A, Newell-Price J, et al. European Society of Endocrinology clinical practice guidelines on the management of adrenal incidentalomas, in collaboration with the European Network for the Study of Adrenal Tumors. Eur J Endocrinol. 2023 Jul 1;189(1):G1–42.

26. Lehmann T, Wrzesinski T. The molecular basis of adrenocortical cancer. Vol. 205, Cancer Genetics. 2012. p. 131–7.

27. Thampi A, Shah E, Elshimy G, Correa R. Adrenocortical carcinoma: A literature review. Transl Cancer Res. 2020 Feb 1;9(2):1253–64.

28. Hodgson A, Pakbaz S, Mete O. A Diagnostic Approach to Adrenocortical Tumors. Vol. 12, Surgical Pathology Clinics. W.B. Saunders; 2019. p. 967–95.

29. Wang F, Liu J, Zhang R, Bai Y, Li C, Li B, et al. CT and MRI of adrenal gland pathologies. Vol. 8, Quantitative Imaging in Medicine and Surgery. AME Publishing Company; 2018. p. 853–75.

30. Libé R. Adrenocortical carcinoma (ACC): Diagnosis, prognosis, and treatment. Vol. 3, Frontiers in Cell and Developmental Biology. Frontiers Media S.A.; 2015.

31. Weiss LM. Comparative histologic study of 43 metastasizing and nonmetastasizing adrenocortical tumors. American Journal of Surgical Pathology. 1984;8(3).

32. Mete O, Erickson LA, Juhlin CC, de Krijger RR, Sasano H, Volante M, et al. Overview of the 2022 WHO Classification of Adrenal Cortical Tumors. Vol. 33, Endocrine Pathology. Springer; 2022. p. 155–96.

33. Pennanen M, Heiskanen I, Sane T, Remes S, Mustonen H, Haglund C, et al. Helsinki score - A novel model for prediction of metastases in adrenocortical carcinomas. Hum Pathol. 2015 Mar 1;46(3):404–10.

34. Viëtor CL, Creemers SG, van Kemenade FJ, van Ginhoven TM, Hofland LJ, Feelders RA. How to differentiate benign from malignant adrenocortical tumors? Vol. 13, Cancers. MDPI; 2021.

35. Lughezzani G, Sun M, Perrotte P, Jeldres C, Alasker A, Isbarn H, et al. The European Network for the Study of Adrenal Tumors staging system is prognostically superior to the international union against cancer-staging system: A North American validation. Eur J Cancer. 2010 Mar;46(4):713–9.

36. Donatini G, Caiazzo R, Do Cao C, Aubert S, Zerrweck C, El-Kathib Z, et al. Long-term survival after adrenalectomy for stage I/II adrenocortical carcinoma (ACC): A retrospective comparative cohort study of laparoscopic versus open approach. Ann Surg Oncol. 2014 Jan;21(1):284–91.

37. Elhassan YS, Altieri B, Berhane S, Cosentini D, Calabrese A, Haissaguerre M, et al. S-GRAS score for prognostic classification of adrenocortical carcinoma: an international, multicenter ENSAT study. Eur J Endocrinol. 2022 Jan 1;186(1):25–36.

38. Shariq OA, McKenzie TJ. Adrenocortical carcinoma: current state of the art, ongoing controversies, and future directions in diagnosis and treatment. Vol. 12, Therapeutic Advances in Chronic Disease. SAGE Publications Ltd; 2021.

39. Terzolo M, Fassnacht M, Perotti P, Libé R, Kastelan D, Lacroix A, et al. Adjuvant mitotane versus surveillance in low-grade, localised adrenocortical carcinoma (ADIUVO): an international, multicentre, open-label, randomised, phase 3 trial and observational study. Lancet Diabetes Endocrinol. 2023;11(10).

40. Fassnacht M, Terzolo M, Allolio B, Baudin E, Haak H, Berruti A, et al. Combination Chemotherapy in Advanced Adrenocortical Carcinoma. New England Journal of Medicine. 2012;366(23).

41. Clay MR, Pinto EM, Fishbein L, Else T, Kiseljak-Vassiliades K. Pathological and Genetic Stratification for Management of Adrenocortical Carcinoma. Journal of Clinical Endocrinology and Metabolism. 2022 Apr 1;107(4):1159–69.

42. Zennaro MC, Boulkroun S, Fernandes-Rosa F. Genetic causes of functional adrenocortical adenomas. Vol. 38, Endocrine Reviews. Oxford University Press; 2017. p. 516–37.

43. Pittaway JFH, Guasti L. Pathobiology and genetics of adrenocortical carcinoma. Vol. 62, Journal of Molecular Endocrinology. BioScientifica Ltd.; 2019. p. R105–19.

44. Lippert J, Fassnacht M, Ronchi CL. The role of molecular profiling in adrenocortical carcinoma. Vol. 97, Clinical Endocrinology. John Wiley and Sons Inc; 2022. p. 460–72.

45. Ragazzon B, Assié G, Bertherat J. Transcriptome analysis of adrenocortical cancers: From molecular classification to the identification of new treatments. Vol. 18, Endocrine-Related Cancer. 2011.

46. Chao W, D'Amore PA. IGF2: Epigenetic regulation and role in development and disease. Vol. 19, Cytokine and Growth Factor Reviews. 2008. p. 111–20.

47. Ribeiro TC, Latronico AC. Insulin-like growth factor system on adrenocortical tumorigenesis. Vol. 351, Molecular and Cellular Endocrinology. 2012. p. 96–100.

48. Livingstone C. IGF2 and cancer. Vol. 20, Endocrine-Related Cancer. 2013.

49. Guillaud-Bataille M, Ragazzon B, De Reyniès A, Chevalier C, Francillard I, Barreau O, et al. IGF2 promotes growth of adrenocortical carcinoma cells, but its overexpression does not modify phenotypic and molecular features of adrenocortical carcinoma. PLoS One. 2014 Aug 4;9(8).

50. Altieri B, Tirabassi G, Casa S Della, Ronchi CL, Balercia G, Orio F, et al. Adrenocortical tumors and insulin resistance: What is the first step? Vol. 138, International Journal of Cancer. Wiley-Liss Inc.; 2016. p. 2785–94.

51. Fassnacht M, Berruti A, Baudin E, Demeure MJ, Gilbert J, Haak H, et al. Linsitinib (OSI-906) versus placebo for patients with locally advanced or metastatic adrenocortical carcinoma: a double-blind, randomised, phase 3 study. Lancet Oncol. 2015 Apr;16(4):426–35.

52. De Martino MC, van Koetsveld PM, Feelders RA, de Herder WW, Dogan F, Janssen JAMJL, et al. IGF and mTOR pathway expression and in vitro effects of linsitinib and mTOR inhibitors in adrenocortical cancer. Endocrine. 2019 Jun 15;64(3):673–84.

53. Jones RL, Kim ES, Nava-Parada P, Alam S, Johnson FM, Stephens AW, et al. Phase I Study of Intermittent Oral Dosing of the Insulin-like Growth Factor-1 and Insulin Receptors Inhibitor OSI-906 in Patients With Advanced Solid Tumors. Clinical Cancer Research. 2015 Feb 15;21(4):693–700.

54. Ou JM, Lian WS, Qiu MK, Dai YX, Dong Q, Shen J, et al. Knockdown of IGF2R suppresses proliferation and induces apoptosis in hemangioma cells in vitro and in vivo. Int J Oncol. 2014;45(3):1241–9.

55. Takeda T, Komatsu M, Chiwaki F, Komatsuzaki R, Nakamura K, Tsuji K, et al. Upregulation of IGF2R evades lysosomal dysfunction-induced apoptosis of cervical cancer cells via transport of cathepsins. Cell Death Dis. 2019 Dec 1;10(12).

56. Martin-Kleiner I, Gall Troselj K. Mannose-6-phosphate/insulin-like growth factor 2 receptor (M6P/IGF2R) in carcinogenesis. Vol. 289, Cancer Letters. Elsevier Ireland Ltd; 2010. p. 11–22.

57. Oates AJ, Schumaker L, Jenkins S, Pearce A, DaCosta S, Arun B, et al. The mannose 6-phosphate/insulin-like growth factor 2 receptor (M6P/IGF2R), a putative breast tumor suppressor gene. Breast Cancer Res Treat. 1998;47:269–81.

58. Wang R, Qi X, Schmiege P, Coutavas E, Li X. Marked structural rearrangement of mannose 6-phosphate/IGF2 receptor at different pH environments. Vol. 6, Sci. Adv. 2020. Available from: http://advances.sciencemag.org/

59. Brown J, Delaine C, Zaccheo OJ, Siebold C, Gilbert RJ, Van Boxel G, et al. Structure and functional analysis of the IGF-II/IGF2R interaction. EMBO Journal. 2008 Jan 9;27(1):265–76.

60. Leboulleux S, Gaston V, Boulle N, Le Bouc Y, Gicquel C. Loss of heterozgosity at the mannose 6-phosphate/insulin-like growth factor 2 receptor locus: A frequent but late event in adrenocortical tumorigenesis. Eur J Endocrinol. 2001;144(2):163–8.

61. Dynkevich Y, Rother KI, Whitford I, Qureshi S, Galiveeti S, Szulc AL, et al. Tumors, Igf-2, And Hypoglycemia: Insights From The Clinic, The Laboratory, And The Historical Archive. Vol. 34, Endocrine Reviews. 2013. p. 798–826.

62. Velázquez-Fernández D, Laurell C, Geli J, Höög A, Odeberg J, Kjellman M, et al. Expression profiling of adrenocortical neoplasms suggests a molecular signature of malignancy. Surgery. 2005 Dec;138(6):1087–94.

63. Brown J, Jones EY, Forbes BE. Keeping IGF-II under control: Lessons from the IGF-II-IGF2R crystal structure. Vol. 34, Trends in Biochemical Sciences. 2009. p. 612–9.

64. El-Shewy HM, Lee MH, Obeid LM, Jaffa AA, Luttrell LM. The insulin-like growth factor type 1 and insulin-like growth factor type 2/mannose-6-phosphate receptors independently regulate ERK1/2 activity in HEK293 cells. Journal of Biological Chemistry. 2007 Sep 7;282(36):26150–7.

65. El-Shewy HM, Johnson KR, Lee MH, Jaffa AA, Obeid LM, Luttrell LM. Insulin-like growth factors mediate heterotrimeric G protein-dependent ERK1/2 activation by transactivating sphingosine 1-phosphate receptors. Journal of Biological Chemistry. 2006 Oct 20;281(42):31399–407.

66. El-Shewy HM, Abdel-Samie SA, al Qalam AM, Lee MH, Kitatani K, Anelli V, et al. Phospholipase C and protein kinase C-β 2 mediate insulin-like growth factor ii-dependent sphingosine kinase 1 activation. Molecular Endocrinology. 2011 Dec;25(12):2144–56.

67. Kang JX, Bell J, Beard RL, S Chandraratna RA. Mannose 6-Phosphate/Insulin-like Growth Factor II Receptor Mediates the Growth-Inhibitory Effects of Retinoids 1. Cell Biology. 1998;95:13687–91. Available from: http://aacrjournals.org/mcr/article-pdf/10/8/591/3169224/cw089900591p.pdf

68. Kang JX, Bell J, Leaf A, Beard RL, Chandraratna RA. Retinoic acid alters the intracellular trafficking of the mannose-6-phosphate/insulin-like growth factor II receptor and lysosomal enzymes. Vol. 95, Cell Biology. 1998. Available from: www.pnas.org.

69. Fottner C, Hoeflich A, Wolf E, Weber MM. Role of the Insulin-like Growth Factor System in Adrenocortical Growth Control and Carcinogenesis. Hormones and Metabolism Research. 2004;36:397–405.

70. Patel D, Ellis R, Howard B, Boufraqech M, Gara SK, Zhang L, et al. Analysis of IGF and IGFBP as Prognostic Serum Biomarkers for Adrenocortical Carcinoma. Ann Surg Oncol. 2014 Oct 1;21(11):3541–7.

71. Pitman MR, Costabile M, Pitson SM. Recent advances in the development of sphingosine kinase inhibitors. Vol. 28, Cellular Signalling. Elsevier Inc.; 2016. p. 1349–63.

72. Gupta P, Taiyab A, Hussain A, Alajmi MF, Islam A, Hassan MI. Targeting the sphingosine kinase/sphingosine-1-phosphate signaling axis in drug discovery for cancer therapy. Vol. 13, Cancers. MDPI AG; 2021.

73. Hii LW, Chung FFL, Mai CW, Yee ZY, Chan HH, Raja VJ, et al. Sphingosine Kinase 1 Regulates the Survival of Breast Cancer Stem Cells and Non-stem Breast Cancer Cells by Suppression of STAT1. Cells. 2020 Apr 4;9(4):886.

74. Hii LW, Chung FFL, Mai CW, Ng PY, Leong CO. Sphingosine Kinase 1 Signaling in Breast Cancer: A Potential Target to Tackle Breast Cancer Stem Cells. Vol. 8, Frontiers in Molecular Biosciences. Frontiers Media S.A.; 2021.

75. Schnute ME, McReynolds MD, Kasten T, Yates M, Jerome G, Rains JW, et al. Modulation of cellular S1P levels with a novel, potent and specific inhibitor of sphingosine kinase-1. Biochemical Journal. 2012 May 15;444(1):79–88.

76. Maceyka M, Sankala H, Hait NC, Le Stunff H, Liu H, Toman R, et al. SphK1 and SphK2, sphingosine kinase isoenzymes with opposing functions in sphingolipid metabolism. Journal of Biological Chemistry. 2005 Nov 4;280(44):37118–29.

77. Hasanifard L, Sheervalilou R, Majidinia M, Yousefi B. New insights into the roles and regulation of SphK2 as a therapeutic target in cancer chemoresistance. Vol. 234, Journal of Cellular Physiology. Wiley-Liss Inc.; 2019. p. 8162–81.

78. Neubauer HA, Pitson SM. Roles, regulation and inhibitors of sphingosine kinase 2. FEBS J. 2013 Nov 7;280(21):5317–36.

79. Wang X, Sun Y, Peng X, Naqvi SMAS, Yang Y, Zhang J, et al. The Tumorigenic Effect of Sphingosine Kinase 1 and Its Potential Therapeutic Target. Vol. 27, Cancer Control. SAGE Publications Ltd; 2020.

80. Xu Y, Dong B, Huang J, Kong W, Xue W, Zhu Y, et al. Sphingosine kinase 1 is overexpressed and promotes adrenocortical carcinoma progression. Oncotarget. 2015;7(3). Available from: www.impactjournals.com/oncotarget

81. Lucki NC, Li D, Sewer MB. Sphingosine-1-phosphate rapidly increases cortisol biosynthesis and the expression of genes involved in cholesterol uptake and transport in H295R adrenocortical cells. Mol Cell Endocrinol. 2012 Jan 2;348(1):165–75.

82. Gestaut MM, Antoon JW, Burow ME, Beckman BS. Inhibition of sphingosine kinase-2 ablates androgen resistant prostate cancer proliferation and survival. Pharmacological Reports. 2014 Feb;66(1):174–8.

83. Schwartz GK, Ward D, Saltz L, Casper ES, Spiess T, Mullen E, et al. A Pilot Clinical/Pharmacological Study of the Protein Kinase C-specific Inhibitor Safingol Alone and in Combination with Doxorubicin. Vol. 3, Clinical Cancer Research. 1997. Available from: http://aacrjournals.org/clincancerres/article-pdf/3/4/537/2068535/537.pdf?casa_token=asQnrT2jyHkAAAAA:2TjiguRklpFj8JPkDDE6yNBvqQUBn_90WoxhfNcrD7IFnAs-tgaCXVZO8jYXXeP2I4fcJIk

84. Dickson MA, Carvajal RD, Merrill AH, Gonen M, Cane LM, Schwartz GK. A phase I clinical trial of safingol in combination with cisplatin in advanced solid tumors. Clinical Cancer Research. 2011 Apr 15;17(8):2484–92.

85. Companioni O, Mir C, Garcia-Mayea Y, LLeonart ME. Targeting Sphingolipids for Cancer Therapy. Vol. 11, Frontiers in Oncology. Frontiers Media S.A.; 2021.

86. Boulter AC, Maurer BJ, Pogue M, Kang MH, Cho H, Knight A, et al. Phase I trial of intravenous fenretinide (4-HPR) plus safingol in advanced malignancies. Cancer Chemother Pharmacol. 2023 Aug 1;92(2):97–105.

87. Landwehr LS, Schreiner J, Appenzeller S, Kircher S, Herterich S, Sbiera S, et al. A novel patient-derived cell line of adrenocortical carcinoma shows a pathogenic role of germline MUTYH mutation and high tumour mutational burden. Eur J Endocrinol. 2021 Jun 1;184(6):823–35.

88. Hantel C, Shapiro I, Poli G, Chiapponi C, Bidlingmaier M, Reincke M, et al. Targeting heterogeneity of adrenocortical carcinoma: Evaluation and extension of preclinical tumor models to improve clinical translation. Oncotarget. 2016;7(48). Available from: www.impactjournals.com/oncotarget

89. Sigala S, Rossini E, Abate A, Tamburello M, Bornstein SR, Hantel C. An update on adrenocortical cell lines of human origin. Vol. 77, Endocrine. Springer; 2022. p. 432–7.

90. Hantel C, Jung S, Mussack T, Reincke M, Beuschlein F. Liposomal polychemotherapy improves adrenocortical carcinoma treatment in a preclinical rodent model. Endocr Relat Cancer. 2014;21(3):383–94.

91. Schneider CA, Rasband WS, Eliceiri KW. NIH Image to ImageJ: 25 years of image analysis. Nat Methods. 2012 Jul 28;9(7):671–5.

92. Zheng S, Wang W, Aldahdooh J, Malyutina A, Shadbahr T, Tanoli Z, et al. SynergyFinder Plus: Toward Better Interpretation and Annotation of Drug Combination Screening Datasets. Genomics Proteomics Bioinformatics. 2022 Jun 1;20(3):587–96.

93. Kang JX, Li Y, Leaf A. Mannose-6-phosphateinsulin-like growth factor-II receptor is a receptor for retinoic acid. Cell Biology. 1998;95:13671–6. Available from: www.pnas.org.

94. Logié A, Boulle N, Gaston V, Perin L, Boudou P, Le Bouc Y, et al. Autocrine role of IGF-II in proliferation of human adrenocortical carcinoma NCI H295R cell line. Vol. 23, Journal of Molecular Endocrinology. 1999. Available from: http://www.endocrinology.org

95. Bella P, Farini A, Banfi S, Parolini D, Tonna N, Meregalli M, et al. Blockade of IGF2R improves muscle regeneration and ameliorates Duchenne muscular dystrophy. EMBO Mol Med. 2020 Jan 9;12(1).

96. Choi H, Lee JY, Park NH, Nam J, Park W seok, Lee CS, et al. All-trans retinoic acid prevents oxidative stress-mediated cellular senescence via upregulation of insulin-like growth factor binding protein-6 in normal human epidermal keratinocytes. Arch Biol Sci. 2021 Sep;

97. Han GR, Dohi DF, Lee HY, Rajah R, Walsh GL, Hong WK, et al. All-trans-retinoic acid increases transforming growth factor-β2 and insulin-like growth factor binding protein-3 expression through a retinoic acid receptor-α-dependent signaling pathway. Journal of Biological Chemistry. 1997 May 23;272(21):13711–6.

98. Williams JL, Smith C, Hall C, Khaled Z, Maharaj A, Kwong R, et al. Elevated sphingosine-1-phosphate lyase leads to increased metabolism and reduced survival in adrenocortical carcinoma. Eur J Endocrinol. 2023 Jan 1;188(1).

99. Luca E, Abate A, Wang K, Bornstein S, Sigala S, Beuschlein F, et al. Human and Murine Cell Lines for Adrenocortical Carcinoma and Pheochromocytoma. Endocrines. 2024 Jul 5;5(3):261–76.

100. Sada A, Foster TR, Al-Ward R, Sawani S, Charchar HeE, Pishdad R, et al. The effect of hormonal secretion on survival in adrenocortical carcinoma: A multi-center study. Surgery (United States). 2024 Jan 1;175(1):80–9.

101. Ling LU, Tan KB, Chiu GNC. Role of reactive oxygen species in the synergistic cytotoxicity of safingol-based combination regimens with conventional chemotherapeutics. Oncol Lett. 2011 Sep;2(5):905–10.

102. White C, Alshaker H, Cooper C, Winkler M, Pchejetski D. The emerging role of FTY720 (Fingolimod) in cancer treatment. Oncotarget. 2016;7(17). Available from: www.impactjournals.com/oncotarget

103. Xing Y, Wang ZH, Ma DH, Han Y. FTY720 enhances chemosensitivity of colon cancer cells to doxorubicin and etoposide via the modulation of P-glycoprotein and multidrug resistance protein 1. J Dig Dis. 2014;15(5):246–59.

LIST OF FIGURES AND TABLES

DISSEMINATION OF RESULTS

Since the main aim of this PhD project was to identify novel therapeutic strategies for ACT management, the dissemination of results constitutes a pivotal part of the project's success. Throughout the three years I had the opportunity to share my results in several conferences both at national and international level and to be an active part of the Italian and European Endocrinology community. Local and international collaborations have allowed me to contribute to the advance of the preclinical research in the adrenocortical tumour context, by being co-author of several papers on this topic.

In the future I will continue to disseminate the results obtained in this project with the scientific and medical community engaging in:

- regular meetings and talks within university and hospital departments
- national and international conferences
- publications on peer-reviewed journals

Moreover, as I previously did, I will share and promote my project to the general public in:

- events and workshops (e.g. Meet Me Tonight -Notte Europea dei Ricercatori)
- seminars for students to teach the laboratory techniques used in biomedical research
- participation to public events organised by AIRC (e.g., AIRC nelle scuole)

Summarization of the PhD project for the general audience ENG

This PhD thesis is focused on adrenocortical tumours, a wide category of endocrine tumours that include common and indolent adenomas and also rare but aggressive carcinomas. At present, there are no markers for the early diagnosis of these tumours, and the current therapies are often limited in their efficacy, obsolete, and featured by severe collateral effects. In order to find new therapies for these tumours, is necessary to study their underlying biological mechanisms. In this project we focused on the role of a specific receptor, the IGF2R, which was demonstrated able to induce tumoral cell proliferation and growth in our *in vitro* setting. This receptor was poorly studied before and therefore no directed therapies are already available. However, we did identify its mechanism of action and find a novel and druggable target, another protein, sphingosine kinase. This protein was already studied in other cancer models; thus, we tested the efficacy of its inhibitors in adrenocortical tumours. Remarkably, we demonstrated that the two inhibitors tested are able have a strong antitumoral effect.

Riassunto del Progetto di dottorato per il pubblico ITA

Questa tesi di dottorato è focalizzata sullo studio dei tumori corticosurrenalici, un'ampia categoria di neoplasie endocrine che comprende sia gli adenomi, spesso indolenti e molto diffusi, ma anche i carcinomi corticosurrenalici, tumori rari ma estremamente aggressivi. Ad oggi, non ci sono marker specifici per diagnosticare in maniera precoce questi tumori, e le terapie che sono attualmente utilizzate sono spesso limitate, obsolete e caratterizzate da gravi effetti collaterali. Al fine di trovare nuove terapie per questi tumori è necessario studiare i loro meccanismi biologici. Lo scopo di questo progetto è stato lo studio del recettore IGF2R, che abbiamo dimostrato essere capace di stimolare la proliferazione e la crescita delle cellule tumorali *in vitro*. Questo recettore non era mai stato approfonditamente studiato pertanto al momento non sono disponibili farmaci che possano inibire la sua azione. Nonostante ciò, abbiamo identificato il suo meccanismo di azione e identificato un'altra proteina, la sfingosina chinasi, che è già stata studiata in altri tumori per il suo potenziale come target farmacologico. Pertanto, abbiamo testato l'efficacia di due suoi inibitori sui tumori corticosurrenalici e abbiamo potuto dimostrare che entrambi hanno un forte effetto antitumorale.